Chapter 3
BEHAVIOR OF CHALK AND OTHER SOFT ROCKS

MECHANICAL BEHAVIOR OF CHALK

The mechanical behavior of chalk discussed in this section was determined on the basis of results of laboratory testing of chalk. The laboratory tests performed to characterize the mechanical behavior of chalk include constitutive tests: hydrostatic compression tests, K_0 or uniaxial compression tests, drained and undrained triaxial compression tests and triaxial extension tests, true triaxial compression tests, and radial compression tests. In constitutive tests, it is assumed that uniform stress and strain fields are present throughout the tested sample; therefore, stress-strain behavior can be determined directly from the laboratory test results. Hayano et al. (2001) discuss the validity of this assumption with regards to local (*i.e.*, strain gage) and global displacement data, and conclude that local displacement data should be used. For this reason, strain gage data, where available, is always presented in this and other chapters. As part of the effort by the Joint Chalk Research (JCR) group to characterize mechanical behavior of chalk, over twenty years of laboratory test data exists. A database of laboratory test results on chalk has been compiled by the Danish Geotechnical Institute (1996a, 1996b; unpublished data, 2000, 2003). Unless otherwise specified, all laboratory results reported in this section are from the JCR database.

The mechanical behavior of chalk is quite complex. Chalk possesses material nonlinearity, meaning that stress-strain relations for chalk are non-linear. Deformation in chalk includes both elastic and inelastic, or reversible and irreversible, components. Multiple yielding and failure mechanisms have been observed experimentally. In addition, deformation in chalk occurs not only due to application of external loads, but also due to the passage of time during application of a constant external load. An additional complication specific to chalk is that chalk appears to possess significantly different characteristics (*e.g.*, strength, stiffness) when different pore fluids are present.

Since effective stresses control the mechanical behavior of geomaterials, all stresses from this point forward refer to effective stresses; the prime (') symbol normally used to denote effective stresses is omitted from stress symbols to improve clarity in the equations.

Elasticity

Elastic behavior refers to the reversible deformations which a material experiences due to application of external loads, and which are recovered upon removal of the external loads. Two aspects related to elastic behavior in chalk have been disputed in the literature. These issues are (1) symmetry in elastic behavior, and (2) dependence of elastic moduli on stress state or chalk properties.

Elastic Isotropy

Elastic stress-strain relations are described using the generalized Hooke's Law. Elastic behavior for any linear elastic material is described by elastic constants which relate various components of incremental stress to incremental strain. The number of elastic constants required to adequately describe the elastic material behavior depends on directional symmetry in elastic behavior of the material. If a material exhibits no symmetry in its elastic behavior, 21 independent elastic constants are required; if the material exhibits symmetry about each of three mutually perpendicular axes, the elastic behavior is orthotropic and 9 independent elastic constants are required; if the material exhibits symmetry within a plane and asymmetry in the direction normal to that plane, the elastic behavior is transversely isotropic and 5 independent elastic constants are required; if the material exhibits complete symmetry in all directions, the behavior is isotropic and 2 elastic constants are required (*i.e.*, any two of the elastic modulus E, shear modulus G, bulk modulus K, and Poisson's ratio ν).

Since chalk and other soft rocks are formed by sedimentation and uniaxial compaction, it may be expected that behavior is transversely isotropic with isotropy in planes parallel to bedding. Papamichos et al. (1997) stated that laboratory test results indicate that elastic behavior in Pietra Lecesse (Italy) outcrop chalk is anisotropic. Talesnick et al. (2000) showed experimentally that elastic behavior of an the Eocene-age Marasha Formation chalk (Israel) indeed appears to be transversely isotropic, as shown by the following phenomena: (1) the elastic modulus is greater in the plane of isotropy (*i.e.*, a bedding plane) than in the direction normal to this plane; and (2) the shear modulus measured experimentally in an anisotropic plane (*i.e.*, through the normal to the isotropic plane) is much greater than that which would be calculated using the experimentally measured elastic moduli measured in the plane of isotropy. Talesnick et al. determined that the ratio between the in-plane elastic modulus and the elastic modulus

perpendicular to bedding (E'/E) takes on a constant value of approximately 1.6 except at very small strains.

Hydrostatic compression test data from North Sea chalks suggest that elastic behavior in reservoir chalks is anisotropic. A suite of hydrostatic compression tests performed in triaxial cells indicates consistently that radial strain increments (within bedding planes) are less than axial strain increments (perpendicular to bedding planes) within the elastic region. This trend may be shown by examining the ratio between material compliance in the radial and axial directions.

The elastic compliance matrix for triaxial stress-strain conditions is:

$$\begin{Bmatrix} d\varepsilon_{11} \\ d\varepsilon_{33} \end{Bmatrix} = \begin{bmatrix} C_{1111} & C_{1133} \\ C_{3311} & C_{3333} \end{bmatrix} \begin{Bmatrix} d\sigma_{11} \\ d\sigma_{33} \end{Bmatrix} \tag{3.1}$$

so the sum ($C_{1111} + C_{1133}$) represents the axial compliance (*i.e.*, in the axial direction across bedding planes), while the sum ($C_{3311} + C_{3333}$) represents the radial compliance (*i.e.*, in the radial direction within bedding planes). Under hydrostatic loading conditions, $d\sigma_{11} = d\sigma_{33}$, so an isotropic material should strain equally in the axial and radial directions; that is, $d\varepsilon_{11} = d\varepsilon_{33}$. A test for elastic isotropy is to compare the calculated compliance in the axial and radial directions under hydrostatic loading conditions.

A set of 7 hydrostatic compression test results from the Valhall field, shown in Figure 3.1, indicates that the ratio between radial compliance and axial compliance is less than 1 for all tests during initial loading conditions. These results indicate that the compliance of chalk within a bedding plane is consistently less than the compliance perpendicular to bedding. However, tests conducted with repeated loading-unloading cycles indicate that effects of elastic anisotropy may vanish during repeated hydrostatic compression loading cycles. Figure 3.2 shows lab test results for hydrostatic compression tests with multiple loading-unloading cycles; it may be seen that elastic material behavior is anisotropic during initial recompression loading as indicated by unequal elastic compliances in different directions. However, the compliances become approximately equal after cyclic hydrostatic compression, which is indicative of an isotropic elastic material. Therefore, virgin hydrostatic compression appears to cause chalk to behave isotropically in the elastic zone. In the absence of cyclic hydrostatic compression, we may expect that the non-hydrostatic K_0 loading history of field chalk will cause its elastic behavior to be

anisotropic. Although transversely isotropic elastic behavior is expected in chalk, constitutive models for chalk have typically been formulated under the assumption that elastic behavior is isotropic.

Linearity of Elastic Coefficients

Elastic behavior of chalk has been described as both linear and nonlinear. For linear elastic behavior, the relationship between stress and strain is independent of the state of the material (*i.e.*, elastic moduli are constant throughout physical tests). Nonlinear elasticity occurs when the elastic moduli vary with the state of the material, typically as a function of stress or strain; often, nonlinear elasticity takes the form that the bulk modulus K increases with increasing mean stress p, or that the shear modulus G decreases with increasing deviatoric stress q. Various constitutive models for chalk have been formulated, some with linear elasticity and some with nonlinear elasticity. Constitutive models with nonlinear elasticity often incorporate this behavior using the relationship between bulk modulus K and mean stress p which is used for the Cam-Clay model:

$$K = \frac{(1+e)p}{\kappa} \tag{3.2}$$

where e is the void ratio and κ is the slope of the recompression curve in e-ln(p) space. Other nonlinear elastic models have been implemented into the framework of elastoplasticity. For example, Morrison (1995) modified Duncan and Chang's (1970) implementation of Kondner's (1963) nonlinear elastic hyperbolic model to account for elastoplastic effects, including dilatancy, within the framework of the Mohr-Coulomb model.

Talesnick et al. (2000) found experimentally that in uniaxial compression tests, radial compression tests, and torsional shear tests, the elastic modulus E and/or shear modulus G of chalk consistently decrease throughout individual tests as deviatoric strain accumulates (Figure 3.3), suggesting that elastic behavior is nonlinear. It should be noted that the apparent elastic moduli recover during the unloading phase of laboratory tests, however. While the chalk appears to become less resilient during loading cycles, the modulus increases at the start of each unloading cycle and decreases as unloading progresses. This phenomenon is observed in all types of lab tests involving loading and unloading, as shown in Figures 3.4(a) through (d) for an unconfined compression test, a hydrostatic compression test, a K_0 compression test, and a drained triaxial compression test, respectively. In each case, the average modulus for loading and

unloading cycles appears to be relatively constant at all stress levels. Therefore, the assumption of constant elastic moduli appears to be appropriate for chalk, especially if both loading and unloading are expected.

For all chalks, the elastic modulus of chalk appears to vary as a function of porosity. Gommesen and Fabricius (2001) performed static and dynamic tests to determine constrained modulus M and/or bulk modulus K for many chalk samples from the Valhall and Hod fields. Results of the tests show a very clear correlation between porosity and elastic modulus. Modulus decreases with increasing porosity, as shown in Figure 3.5. This trend is also apparent in test results contained in the JCR database. Figure 3.6 shows the best-fit line for the entire JCR database. A better fit may be obtained using test results from a single chalk field of interest. Figure 3.7 shows the average bulk modulus for many chalk samples from the Tyra, Ekofisk A, Ekofisk D, and Valhall fields. As for the data of Gommesen and Fabricius, bulk modulus decreases with increasing porosity.

Inelasticity and Yielding

Chalk behaves mechanically as a frictional material, such that the ultimate strength is described with respect to shear failure. However, it has been observed experimentally that several independent yield mechanisms occur in chalk: (1) pore collapse, (2) shear failure, and (3) tensile failure. Pore collapse is a volumetric yielding mechanism in which the rock volume is reduced irreversibly due to a reduction in pore volume; experimentally, pore collapse occurs at relatively high mean stress and low deviator stress. Shear failure is a deviatoric yielding and brittle rupture failure mechanism in which solid rock grains rotate and/or slide past each other on internal surfaces. Experimentally, shear failure occurs at relatively low mean stress and high deviator stress. Tensile failure is a material failure mechanism in which rock grains pull apart from each other when one of the normal stress components in the rock becomes sufficiently small or tensile. In addition, the magnitude of the intermediate principal stress influences the yield and failure strength of chalk. A discussion of the composite yield behavior is also included in this section.

Inelastic strains are observed when chalk activates either the shear or pore collapse yield mechanisms. The effects of inelastic strains are evident in the large unrecovered strains present after loading and unloading cycles. Figures 3.8, 3.9, and 3.10 show typical results for a

hydrostatic compression test, K_0 compression test, and drained triaxial compression test, respectively. The first two figures show test results in which the chalk activates the pore collapse yield surface; Figure 3.10 shows a test result for a chalk which activates the shear yield surface.

Pore Collapse

Pore collapse in chalk is accompanied by a sudden decrease in apparent modulus as loading continues. This change in modulus is easily seen in stress-strain plots for laboratory tests which involve volumetric loading, as in Figures 3.8 and 3.9. In stress space, the shape of the pore collapse yield surface becomes apparent by comparing the stress points at which yield occurs for compression tests performed under various lateral loading conditions. Stress path testing under various lateral stress ratios indicates that initial pore collapse yielding occurs at the stresses shown in Figure 3.11 (Loe et al., 1992). A collection of better data obtained from hydrostatic compression tests, K_0 compression tests, and triaxial compression tests performed on Lixhe outcrop chalk (Belgium) is shown in Figure 3.12 (Collin et al., 2002). The yield stress points are arranged (approximately) in a pattern matching the elliptical yield surface characteristic of Modified Cam-Clay (Roscoe and Burland, 1968).

It has been observed experimentally that the pore collapse yield surface for chalks exhibits hardening during loading. This effect is shown for the Lixhe outcrop chalk (Belgium) by Homand and Shao (2000) in Figures 3.13 and 3.14 (also in Figures 3.8 and 3.9). The volumetric strain-confining pressure curves of Figures 3.8 and 3.13 show two phenomena common for pore collapse phenomena: (1) as loading proceeds, there is a change in modulus indicative of a change from elastic to inelastic behavior, and (2) as loading continues, the stress-strain curve exhibits a concave-upward consolidation pattern typical of clays and other volumetric-hardening geomaterials under hydrostatic loading. Figure 3.14 shows results of triaxial compression tests at high mean stresses, which activates the pore collapse yield mechanism. The deviatoric stresses continue to increase as axial and lateral strains accumulate, indicating that plastic hardening occurs. The elastoplastic stress-strain behavior of chalk under hydrostatic compression or K_0 compression conditions is linear in a semilog plot, as shown in Figure 3.15.

The post-yield stress-strain behavior of chalk is of interest to determine the plastic potential surface for the pore collapse surface. Generally, plastic flow is thought to be associated for chalk when the pore collapse yield mechanism is active. Strain-controlled compression tests

on chalk samples indicate that the slope of the virgin compression stress-strain curves are approximately parallel for samples tested under hydrostatic and K_0 compression conditions, as shown in Figure 3.15 for Stevns Klint and Ekofisk D chalks. This behavior indicates that the compression coefficient λ (which is the slope of the stress-strain curve in e-log p space) of the elastoplastic stress-strain curve is unique for a given chalk which is loaded at a constant shear stress ratio.

All hardening functions incorporated into chalk models assume isotropic hardening occurs. Results from laboratory tests which probe the yield surfaces during stress reversals, and would therefore be useful in determining the appropriateness of this assumption, do not appear to exist. Isotropic hardening is easier to implement in a constitutive model than is kinematic or anisotropic hardening. Three-invariant plasticity models can only be implemented for isotropic hardening models. Anisotropic hardening models must be formulated in general three-dimensional space (R^6). Anisotropic elasticity models with plastic hardening are very difficult to implement, as described in the discussion on elasticity. Oka et al. (2003) describe an implementation procedure for a transversely isotropic soft rock.

The behavior of chalk related to pore collapse varies with the physical composition of the chalk. A convenient parameter to correlate with the initial pore collapse strength (or isotropic preconsolidation stress) of chalk is porosity. Figure 3.16 shows the apparent isotropic preconsolidation stress as a function of porosity for all hydrostatic compression tests in the JCR database. The apparent preconsolidation stress increases with decreasing porosity. Individual chalk reservoirs corroborate this trend; Figure 3.17 shows the variation of isotropic preconsolidation stress with porosity for the Valhall and Ekofisk D fields. It appears that porosity can be used as a state variable to estimate the isotropic preconsolidation stress for chalk.

The compressibility of chalk also appears to vary as a function of porosity. Such behavior is shown in Figure 3.18 for hydrostatic compression tests performed on chalks with different shear stress ratios. The compression coefficient λ appears to decrease as initial porosity increases, indicating that more porous chalks are more compressible. The correlation between compression coefficient and porosity is shown in Figure 3.19.

During pore collapse, the plastic flow direction of chalk changes throughout a lab test. Undrained triaxial compression loading of normally consolidated chalks gives rise to contractant behavior similar to that predicted by Modified Cam-Clay (Figure 3.20; see also Figures 3.23 and

3.24). The plastic flow direction changes throughout the undrained elastoplastic loading; the plastic strain increment vectors are shown in Figure 3.20. It may be seen that the plastic flow direction follows a consistent pattern in which the relative magnitude of plastic volumetric strain decreases as shear stress ratio increases.

Finally, the stress path behavior of chalk during strain-controlled K_0 compression loading also varies as a function of porosity. The shear stress ratio varies throughout K_0 compression loading but eventually approaches a steady-state value, as shown in Figure 3.21. The steady-state shear stress ratio η (= q / p) decreases with increasing porosity (Figure 3.21). Figure 3.22 shows the steady-state shear stress ratio as a function of porosity. In Figure 3.22, the attraction (a) is assumed to equal 4 MPa for deep-sea chalks, and to equal 0 for outcrop chalks.

Shear Failure

Experimental results for shear yielding of chalks appear to be interpreted differently by different researchers, and the evolution of the shear yield surface is thus incorporated differently into constitutive models. The shear strength is sometimes interpreted to increase as plastic shear strain accumulates during continued shear loading, and it is sometimes interpreted to be fixed. Figure 3.23 (Homand and Shao, 2000) and Figure 3.10 show results of triaxial compression tests at low mean stresses, which activate the shear yield surface. In these tests, deviatoric stresses reach a maximum as axial and lateral strains accumulate, suggesting that some limiting or failure surface is present. The stress-strain curves in Figures 3.23 and 3.10 show a transition between the linear elastic and perfectly plastic or nonhardening portions of the curve. The transition may be interpreted as either a nonlinear elastic portion of the stress-strain curve, or as an elastoplastic portion with hardening.

The pattern of shear failure in chalk appears to fit a straight line in triaxial stress invariant (p-q) space. The results of a suite of undrained triaxial compression tests performed on outcrop chalks show this pattern. Figure 3.12 shows shear failure points from triaxial compression tests on Lixhe chalk. Figure 3.24 shows the stress paths and failure points for undrained triaxial compression tests performed on chalk samples from the Butser-Hill (England) and Stevns Klint (Denmark) outcrops. It is clearly shown that the failure points form a straight line in p-q space. Figure 3.25 shows similar stress paths for several North Sea reservoir chalks under undrained triaxial compression. The shear stress ratio at failure varies more in the reservoir chalks than in

the outcrop chalks; this may be explained by variability in porosity of the reservoir chalks, as described in the following paragraphs.

Several properties of chalk related to shear failure vary with the physical composition of the chalk. A convenient parameter to correlate with the chalk shear strength is porosity. Matthews and Clayton (1993) indicate that uniaxial compressive strength of Cretaceous-age English outcrop chalks decreases linearly as porosity increases, as shown in Figure 3.26 (this figure also shows a strong dependence on the degree of water saturation in the chalk, as will be discussed later).

The high friction angles which have been observed for chalk during shear yielding represent excessively high dilatancy angles if flow is to be associated. Therefore, non-associated flow rules are applied to the shear yield surface. Chalk behavior during shear is generally contractant, as may be seen by the reduction in mean stress during the shearing phase of undrained triaxial compression tests (Figures 3.24 and 3.25).

The shear strength and uniaxial compressive strength of chalk indeed appears to decrease with increasing porosity. Figure 3.27(a) shows the adjusted failure shear stress ratio as a function of porosity for all triaxial compression tests in the JCR database; the adjusted shear stress ratio accounts for cohesion of the chalk as shown next to Figure 3.27. Figure 3.27(b) shows the analogous JCR data for unconfined compressive strength tests, and Figure 3.27(c) shows a combination of both data sets, since both represent the shear failure mechanism. It is clearly shown in Figure 3.27 that adjusted failure shear stress ratio in chalk decreases with increasing porosity. Individual chalk reservoirs show this same trend. Figure 3.28 shows the variation of adjusted failure shear stress ratio with porosity for the Valhall, South Arne, Tyra, and Ekofisk A fields. It appears that porosity can be used as a state variable to estimate the failure shear stress ratio for chalk.

Tensile Failure

The tensile failure surface is assumed to be non-hardening.

As for isotropic preconsolidation stress and shear strength, tensile strength also appears to decrease with increasing porosity. Figure 3.29 shows the tensile strength as a function of porosity for all Brazilian tests in the JCR database. It is clearly shown in Figure 3.29 that tensile strength decreases with increasing porosity. Data from individual chalk reservoirs show the same trend.

Figure 3.30 shows the variation of tensile strength with porosity for the Tyra and South Arne fields. It appears that porosity can be used as a state variable to estimate the tensile strength for chalk.

Third-Invariant Effects

Geomaterials typically show dependence on the third stress invariant θ, which expresses itself as a dependence on the intermediate principal stress σ_2'. It is common in geomaterials that the failure shear stress ratio is less for triaxial extension than for triaxial compression, and chalk appears to follow this trend. Risnes et al. (1998) performed triaxial extension tests on water-saturated chalk samples from the Lixhe (Belgium) and Aalborg (Denmark) outcrops; their data are shown in Figure 3.31. It may be seen by comparing the resulting shear strength profiles to the triaxial compression data for the Butser-Hill and Stevns Klint outcrops (Figure 3.24) that the shear strength is noticeably lower in triaxial extension than in triaxial compression (Figure 3.32). The best fit lines for the failure shear stress ratios give $\eta_f = 1.29$ in triaxial compression and $\eta_f = 0.92$ in triaxial extension. Analysis of these results using the Mohr-Coulomb criterion

$$\eta_f = \frac{6\sin\phi}{3-\sin\phi} \text{ in triaxial compression} \tag{3.3a}$$

$$\eta_f = \frac{6\sin\phi}{3+\sin\phi} \text{ in triaxial extension} \tag{3.3b}$$

yields a friction angle $\phi = 30^o$ for these outcrop chalks, which appears reasonable. Therefore, the Mohr-Coulomb criterion may be used to describe the third-invariant behavior of chalk in shear.

The shape of the yield surface in the π-plane, which illustrates the influence of the intermediate principal stress on failure strength, may be described by the Mohr-Coulomb, Matsuoka-Nakai (1974), and Lade-Duncan (1975) models, among others. The relative shapes of these yield surfaces in the π-plane are shown in Figure 3.33. Other "smooth" versions of the Mohr-Coulomb model were developed by William and Warnke (1975) and van Eekelen (1980). The Mohr-Coulomb model, Matsuoka-Nakai model, and William-Warnke models all can be made to coincide at points representing triaxial compression and triaxial extension.

True triaxial tests were performed on the Valhall, Tyra, Hod, and Eldfisk chalks and triaxial extension tests were performed on the Lixhe chalk. The results show scatter regarding the

behavior of chalk relative to the Lode angle, as shown in Figure 3.34(a). It is possible to correct for the variability in porosity in chalk by calculating the "expected" failure shear stress ratio for each sample if tested in triaxial compression, using the best-fit trendline shown in Figure 3.27(a). Using this method, Figure 3.34(b) shows the ratio between tested failure shear stress ratio and expected shear stress ratio for triaxial compression conditions. The effect of Lode angle may then be seen more clearly, as the chalk becomes much weaker when loading conditions move away from triaxial compression conditions. However, due to the similarity of the third-invariant models described above, all of these models appear adequate to describe the third-invariant behavior of chalk.

Composite Yield Behavior

The three yield mechanisms described above may be described by a multi-mechanism yield surface in which each component of the yield surface acts independently of the others. The pore collapse yield surface appears to take the form of an elliptical cap-type surface which appears as an ellipse in 2-dimensional stress invariant space. The shape and size of the cap yield surface may be described by the isotropic preconsolidation stress p_c, which controls the size of the ellipse along the p-axis, and by a parameter which controls the aspect ratio of the ellipse. The shear yield surface appears to be a Mohr-Coulomb-type yield surface which appears as a straight line in p-q space. The orientation of the shear yield surface may be described by a slope η_f and an intercept, either the cohesion (c) or attraction ($a = c/\eta_f$). The tensile yield surface represents a cutoff to the shear yield surface, and is described only by a tensile strength p_t. A schematic multi-mechanism yield surface is shown in Figure 3.35. A discussion of the various constitutive models which have been used to simulate chalk behavior follows in Chapter 4.

Time-Dependent Deformations

In addition to stress-induced (or time-independent) deformations, soft rock also undergoes time-dependent deformations called creep. Creep in geomaterials is characterized by continuous decrease in void space as time passes while effective stresses remain constant. In particulate media, creep is typically attributed to reorientation of solid particles. In cemented or crystalline geomaterials where the relative movements of solids are constrained, the reduction in void space is due to some other mechanism. In chalk, these time-dependent deformations are usually noted

in two types of laboratory tests: (1) creep (*i.e.*, constant-stress) tests, and (2) stress relaxation (*i.e.*, constant-deformation) tests.

Creep tests clearly show the time-dependent deformation phenomenon. Hydrostatic compression tests performed with continuous loading produces an elastoplastic stress-strain curve as described in the previous section. However, deformation continues to occur during periods of the tests in which the loading was interrupted (*i.e.*, creep phases). De Gennaro et al. (2003) performed hydrostatic compression tests with creep phases on Lixhe chalk. Their results are shown in the stress-strain curves and time-strain curves of Figure 3.36. Creep deformations under these conditions are seen to be substantial.

Much more information regarding time-dependent behavior of chalk can be obtained by examining the results of creep tests. Data from K_0 compression tests with full creep phases (*i.e.*, all stress components remain constant) on the North Sea reservoir chalks reveals that the time-strain data appear to become tangent to a linear trendline in strain-logarithmic time space, which may be termed the logarithmic creep rate. Examples of this behavior are seen in Figure 3.37 for Tyra chalk. The data of Figures 3.36(b) and 3.37 show that a time lag exists between the start of creep testing (*i.e.*, the end of mechanical loading) and the start of logarithmic creep behavior. It is also apparent that the loading rate before the creep phase influences the creep behavior; in Figure 3.36, a creep phase preceded by a faster loading rate approaches a logarithmic creep rate after approximately $1/500^{th}$ of the time lag required for the creep phases preceded by slower loading.

Other types of creep tests are available to show additional aspects of creep behavior. K_0 compression tests with σ_1'-constant creep phases were performed on chalks from the South Arne field; during these tests, the axial stress remains constant during creep loading, but the radial stress and all strains are unconstrained. During the creep phases, the radial stresses consistently increase, as shown in Figure 3.38. It is also apparent from the data of Figure 3.38 that the logarithmic creep rate varies according to stress state or other factors. In each test, creep phases were conducted at various stress levels throughout the test. In each case, the creep rate increased for the phases conducted later in the test.

Stress-relaxation tests also show that time plays a role in the behavior of chalk. If deformation is restrained, the stresses in chalk decrease to compensate for the inability to accumulate strain, as shown in Figure 3.39 for Valhall chalk. The relationship between creep

tests and stress-relaxation tests is similar to that between standard drained and undrained compression tests on geomaterials. Due to the difficulties in performing these tests, however, relatively few stress-relaxation tests have been performed on chalk.

Effect of Pore Fluid

The strength and stiffness of chalk has been shown experimentally to show significant dependence on the pore fluid present in the rock. Effects of pore fluid on mechanical behavior of chalk have been noted repeatedly in the literature, including by Matthews and Clayton (1993), Risnes et al. (1994), Risnes et al. (1996), Schroeder and Shao (1996), Papamichos et al. (1997), Risnes and Flaageng (1999), Homand and Shao (2000), Gutierrez et al. (2000), Talesnick et al. (2001), Collin et al. (2002), DeGennaro et al. (2003), and Risnes et al. (2003, 2004).

Risnes et al. (1994) indicate that chalks subjected to increased degree of shear deformation exhibit decreased stability (*i.e.*, greater potential for dissolution) when saturated with water. This behavior indicates a dependence of the apparent yield stress on the pore fluid for the pore collapse mechanism and possibly for the shear yield mechanism. A direct comparison of the stress-strain curves generated by Papamichos et al. (1997) for hydrostatic compression tests on Pietra Lecesse (Italy) outcrop chalks with different water contents shows that yield stress and elastic modulus both decrease as degree of water saturation increases (Figure 3.40). Papamichos et al. concluded that the elastic modulus and yield stress vary continuously as water saturation changes, but the Poisson's ratio remains constant. A comparison of the stress-strain curves of Homand and Shao (2000) for water-saturated chalks and oil-saturated chalks is also revealing. Figures 3.14 and 3.23 show behavior of oil-saturated chalks during pore collapse and shear failure, respectively. Analogous figures for the same chalk when water-saturated are shown in Figures 3.41 and 3.42 for pore collapse and shear failure, respectively. For both yield mechanisms, the yield stress and elastic stiffness is reduced substantially in water-saturated chalk from the higher values exhibited by oil-saturated chalks. In the literature, it has been reported consistently that the strength of oil-saturated chalk is greater than that of water-saturated chalk. Such results were reported by Risnes et al. (1996) for Lixhe chalk in pore collapse, shear failure, and tensile failure; Schroeder and Shao (1996) on Haubourdin (France) outcrop chalk in pore collapse and shear; Gutierrez et al. (2000) for Lagerdorf (Germany) outcrop chalk in direct shear

on fractured surfaces; Homand and Shao (2000) for Lixhe chalk in pore collapse and shear; and Collin et al. (2002) on Lixhe chalk in pore collapse in shear.

The yield envelopes for chalks with different pore fluids are shown in Figures 3.43 to 3.45 for Shroeder and Shao (1996), Gutierrez et al. (2000), and Homand and Shao (2000), respectively. The behavior of chalk is that the yield stress is greatest for dry (or air-saturated) chalks, is less for oil-saturated chalks, and is the least for water-saturated chalks, as shown schematically in Figure 3.46.

The apparent yield stress decreases as water saturation increases. Schroeder and Shao reported that the threshold water saturation between "oil-like" behavior and "water-like" behavior occurs at approximately 2.5 %. Risnes et al. (2004) indicate that the relative strength of chalk in all failure modes, as shown in hydrostatic compression, triaxial compression, and Brazilian tests, increases as water activity decreases for both organic and inorganic solutes. Water activity decreases as concentration of dissolved solids or liquids in the water increases, and so reflects the tendency for water to react when in contact with liquids or solids. Risnes et al. report that the influences of water activity are seen such that elastic modulus decreases, Poisson's ratio increases, and relative cohesion decreases as water activity increases. Selected results of Risnes et al. (2004) are shown in Figure 3.47. Schroeder et al. (1998) showed during waterflooding of a chalk sample that pore collapse and a sudden increase in volumetric strain accompany the waterfront as it passes through the chalk. Results of Schroeder et al. are shown in Figure 3.48.

Time-dependent behavior of chalk is also influenced by the pore fluid. Schroeder and Shao showed that the creep rate of water-saturated chalk is greater than that of oil-saturated chalk, as seen by comparing independent creep test results shown in Figure 3.49. This result may also be seen during individual creep tests in which an initially oil-saturated chalk becomes water-saturated due to waterflooding. In such tests, the creep rate immediately increases as the pore fluid composition changes. Typical results for a waterflooding test are shown in Figure 3.50 for Stevns Klint chalk.

SIMILARITY OF CHALK BEHAVIOR TO OTHER SOFT ROCKS

Many of the aspects of chalk mechanical behavior discussed in the previous section apply to other soft rocks as well. A discussion of various aspects of soft rock behavior reported in the literature follows.

Most soft rocks appear to behave anisotropically. Niandou et al. (1997) reported that the behavior of Tournemire shale (France) in shear was very different depending on the direction of triaxial compression relative to bedding. Stress-strain curves for shale samples with three different compression orientations have different patterns and are shown in Figure 3.51. Plastic straining is also apparent during triaxial loading-unloading cycles seen in Figure 3.51. However, as shown in Figure 3.52, the shear strength is relatively independent of bedding direction under high confining stresses.

Papamichos et al. (2000) tested the shear behavior of Red Wildmoor sandstone (England) under a variety of stress conditions, including unconfined compression, triaxial compression, triaxial extension, and biaxial plane strain compression. Repeated loading-unloading cycles in compression indicate that inelastic strains accumulate long before shear failure as shown in Figure 3.53(a). Shown in Figure 3.53(b) is a composite strength envelope for a suite of compression loading tests. These test results indicate that the magnitude of the intermediate principal stress influences the strength of the sandstone. Papamichos et al. suggest that the three-dimensional failure criterion lies between that of Mohr-Coulomb and Drucker-Prager (*i.e.*, it is similar to one of the rounded models described earlier).

Jeng et al. (2002) tested the Mushan sandstone (Taiwan) under triaxial compression and pure shear conditions. It was observed that, like the Red Wildmoor sandstone, plastic straining occurred before shear failure. The plastic strain increments are initially strongly contractant, but become less contractant and eventually dilatant as shearing continues, as shown in Figure 3.54.

Time- and rate-dependent deformations occur in other soft rocks in addition to chalk. Ngwenya et al. (2001) tested four North Sea oil reservoir sandstones under creep conditions to try to find the creep law for these rocks. The creep behavior was found to be best described by a power law, but also to be strongly dependent on confining pressure and cohesion, which acts as an indicator of brittle behavior.

Hayano et al. (2001) tested silt-sandstone and mudstone members of the Kazusa group (Japan) in drained triaxial compression at various strain rates, including creep phases. It was

found that creep occurs in these sedimentary rocks, and that the shearing rate strongly influences the strain behavior of soft rock. In fact, as shown in Figure 3.55, it appears that a "backbone" stress-strain curve exists for each independent loading rate. Upon changing the loading rate, the stress-strain behavior quickly approaches the backbone curve corresponding to the new loading rate.

Also, it appears that the pore fluid influences the mechanical behavior of some other soft rocks in the same way as is observed for chalk. Papamichos et al. (2000) observed that oil-saturated Red Wildmoor sandstone exhibits higher shear strength than water-saturated sandstone in unconfined compression and triaxial compression. Results are shown in Figure 3.56.

REFERENCES

Borja, R.I., Lin, C-.H., and Montans, F.J. (2001). Cam-clay plasticity, part IV: Implicit integration of anisotropic bounding surface model with nonlinear hyperelasticity and ellipsoidal loading function. Computer Methods in Applied Mechanics and Engineering, 190, 3293-3323.

Collin, F., Cui, Y.-J., Schroeder, C., and Charlier, R. (2002). Mechanical behavior of Lixhe chalk partly saturated by oil and water: experiment and modeling. International Journal for Numerical and Analytical Methods in Geomechanics, 26, 897-924.

Dafalias, Y.F. (1986). Bounding surface plasticity I: Mathematical foundation and hypoplasticity. ASCE Journal of Engineering Mechanics, 112(9), 966-987.

Danish Geotechnical Institute (1996a). JCR IV – Review of Rock Mechanical Data, Confidential Final Report.

Danish Geotechnical Institute (1996b). JCR IV – Constitutive Modeling of Chalk, Final Report.

Danish Geotechnical Institute (2000). JCR Database of Chalk Mechanical Data (Unpublished electronic media).

Danish Geotechnical Institute (2003). New chalk mechanical data (Unpublished electronic media).

Datcheva, M., Charlier, R., and Collin, F. (2001). Constitutive equations and numerical modeling of time effects in soft porous rocks. Lecture Notes in Computer Science, 1988, 222-229.

DeGennaro, V., Delage, P., Cui, Y.-J., Schroeder, C., and Collin, F. (2003). Time-dependent behaviour of oil reservoir chalk: a multiphase approach. Soils and Foundations, 43(4), 131-147.

Duncan, J.M. and Chang, C.-Y. (1970). Nonlinear analysis of stress and strain in soils. ASCE Journal of the Soil Mechanics and Foundations Division, 96(SM5), 1629-1653.

Gommesen, L. and Fabricius, I.L. (2001). Dynamic and static elastic moduli of North Sea and deep sea chalk. Physics and Chemistry of the Earth Part A, 26(1-2), 63-68.

Gutierrez, M., Oino, L.E., and Hoeg, K. (2000). The effect of fluid content on the mechanical behavior of fractures in chalk. Rock Mechanics and Rock Engineering, 22(2), 93-117.

Hayano, K., Matsumoto, M., Tatsuoka, F., and Koseki, J. (2001). Evaluation of the time-dependent properties of soft rock and their constitutive modeling. Soils and Foundations, 41(2), 21-38.

Homand, S., and Shao, J.F. (2000). Mechanical behavior of a porous chalk and effect of saturating fluid. Mechanics of Cohesive-Frictional Materials, 5, 583-606.

Jeng, F.-S., Weng, M.-C., Huang, T.-H., and Line, M.-L. (2002). Deformational characteristics of weak sandstone and impact to tunnel deformation. Tunnelling and Underground Space Technology, 17, 263-274.

Kondner, R.L. (1963). Hyperbolic stress-strain response: cohesive soils. ASCE Journal of the Soil Mechanics and Foundations Division, 89(SM1), 115-143.

Lade, P.V. and Duncan, J.M. (1975). Elastoplastic stress-strain theory for cohesionless soil. ASCE Journal of Geotechnical Engineering Division, 101, 1037-1053.

Loe, N.M., Leddra, M.J., and Jones, M.E. (1992). Strain states during stress path testing of the chalk, In: Proceedings of the 33rd Symposium of Rock Mechanics (Tilerson, J.R. and Wawersik, W.R., Eds.), Santa Fe, June 3-5, 927-936.

Matsuoka, H. and Nakai, T. (1974). Stress-deformation and strength characteristics of soil under three different principal stresses. Proceedings of Japanese Society of Civil Engineers, 232, 59-70.

Matthews, M.C. and Clayton, C.R.I. (1993). Influence of intact porosity on the engineering properties of a weak rock. In: Proceedings of Geotechnical Engineering of Hard Soils-Soft Rocks (Anagnostopoulos et al., eds.), 693-702.

Morrison, C.S. (1995). The Development of a Modular Finite Element Program for Analysis of Soil-Structure Interaction. Ph.D. thesis, Virginia Tech.

Ngwenya, B.T., Main, I.G., Elphick, S.C., Crawford, B.R., and Smart, B.G.D. (2001). A constitutive law for low-temperature creep of water-saturated sandstones. Journal of Geophysical Research, 106(B10), 21811-21826.

Niandou, H., Shao, J.F., Henry, J.P., and Fourmaintraux, D. (1997). Laboratory investigation of the mechanical behavior of Tournemire shale. International Journal of Rock Mechanics and Mining Sciences, 34(1), 3-16.

Oka, F., Kimoto, S., Kobayashi, H., and Adachi, T. (2003). An elasto-plastic constitutive model for soft sedimentary rock. Proceedings of ASCE 16th Engineering Mechanics Conference, Seattle, July 16-18, 12 p.

Papamichos, E., Brignoli, M., and Santarelli, F.J. (1997). An experimental and theoretical study of a partially saturated collapsible rock. Mechanics of Cohesive-Frictional Materials, 2, 251-278.

Papamichos, E., Tronvoll, J., Vardoulakis, I., Labuz, J.F., Skjaerstein, A., Unander, T.E., and Sulem, J. (2000). Constitutive testing of Red Wildmoor sandstone. Mechanics of Cohesive-Frictional Materials, 5, 1-40.

Risnes, R. and Flaageng, O.F. (1999). Mechanical properties of chalk with emphasis on chalk-fluid interactions and micromechanical aspects. Oil and Gas Science and Technology, 54(6) 751-758.

Risnes, R., Garpestad, O.J., Gilje, M., Oland, L.T., Ovesen, M., and Vargervik, E. (1998). Strain hardening and extensional failure in high porosity chalk. Proceedings of EUROCK '98, Trondheim, Norway, 475-484.

Risnes, R., Gjesdal, S.A., Landaas, T.L., and Madland, I. (1994). Changes in mechanical properties of chalk caused by deformation and by pore pressure. Proceedings of EUROCK '94, Delft, The Netherlands, 853-860.

Risnes, R., Haghighi, H., Korsnes, R.I., and Natvik, O. (2003). Chalk-fluid interactions with glycol and brines. Tectonophysics, 370, 213-226.

Risnes, R., Hole, M., and Kwabiah, N.K. (2004). Chalk-fluid interactions with water-glycol mixtures. Proceedings of Workshop on Chalk Mechanical Behavior, Stavanger, Norway, Feb. 3-4, 33 p.

Risnes, R., Kristensen, C.N., and Andersen, M.A. (1996). Triaxial tests on high porosity chalk with different saturating fluids. Proceedings of the 5th North Sea Chalk Symposium, Riems, France, 12 p.

Roscoe, K.H. and Burland, J.B. (1968). On the generalized stress-strain behaviour of 'wet' clay. In: (Heyman, J. and Leckie, F.A., Eds.), Engineering Plasticity, Cambridge University Press, 535-609.

Schroeder, C. and Shao, J.F. (1996). Plastic deformation and capillary effects in chalks. Proceedings of the 5th North Sea Chalk Symposium, Reims, France, 14 p.

Schroeder, C., Bois, A.-P., Maury, V., and Halle, G. (1998). Water/chalk (or collapsible soil) interaction: part II. Results of tests performed in laboratory on Lixhe chalk to calibrate water/chalk models. Proceedings of EUROCK '98, Trondheim, Norway, 505-514.

Talesnick, M.L., Hatzor, Y.H., and Tsesarsky, M. (2001). The elastic deformability and strength of a high porosity, anisotropic chalk. International Journal of Rock Mechanics and Mining Sciences, 38, 543-555.

Van Eekelen, H.A.M. (1980). Isotropic yield surfaces in three dimensions for use in soil mechanics. International Journal for Numerical and Analytical Methods in Geomechanics, 4, 98-101.

William, K.J. and Warnke, E.P. (1975). Constitutive model for the triaxial behavior of concrete, ISMES Seminar on Concrete Structures Subjected to Triaxial Stress, Bergamo, Italy, 1-30.

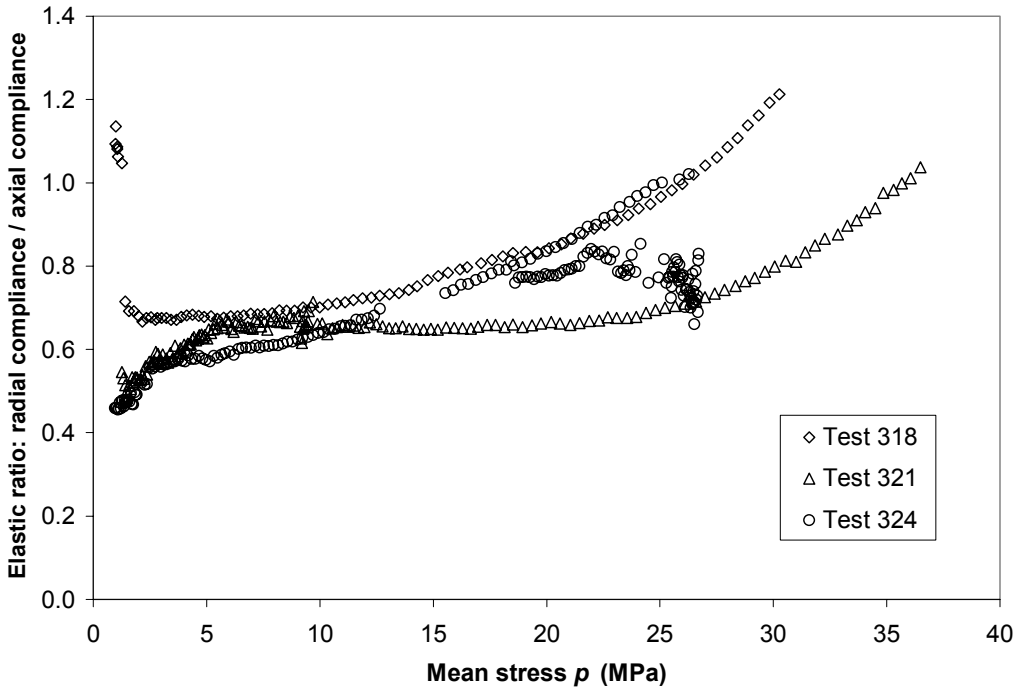

(a)

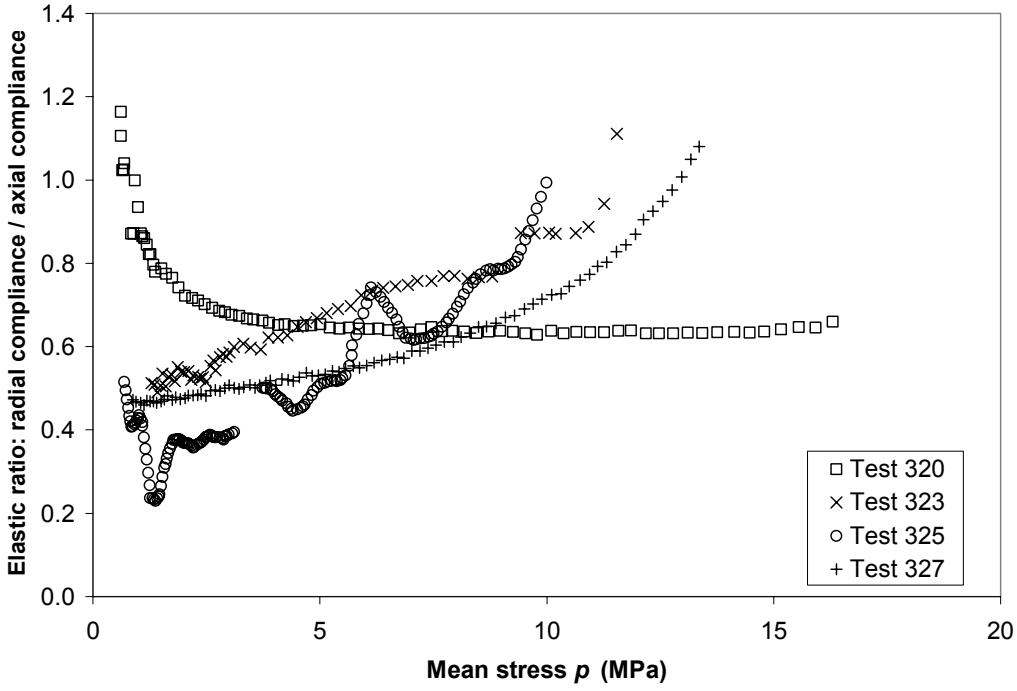

(b)

Figure 3.1 (a,b). Ratio between calculated elastic compliances in the radial and axial directions during hydrostatic compression tests on Valhall field chalk. Ratio is consistently less than 1 during initial loading phase of test, indicating that chalk initially behaves anisotropically during recompression. Data shown is from DGI (2000).

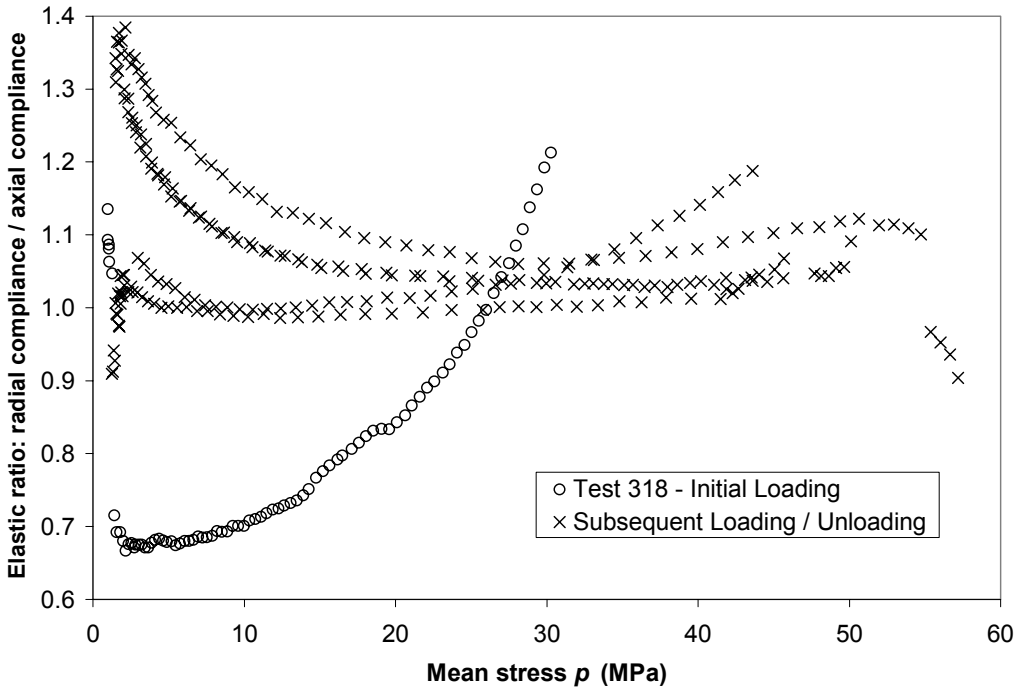

(a)

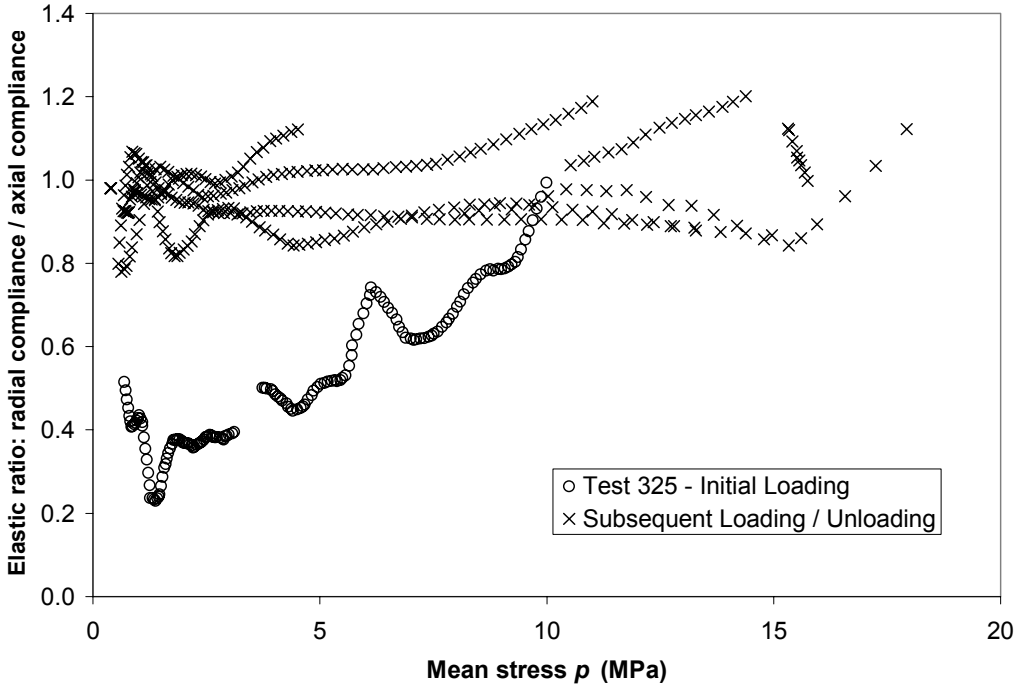

(b)

Figure 3.2 (a,b). Ratio between calculated elastic compliances in the radial and axial directions during hydrostatic compression tests on Valhall field chalk. Ratio increases to a value of approximately 1 during repeated cycles of loading and unloading, indicating that elastic chalk behavior becomes isotropic as hydrostatic loading continues. Data shown is from DGI (2000).

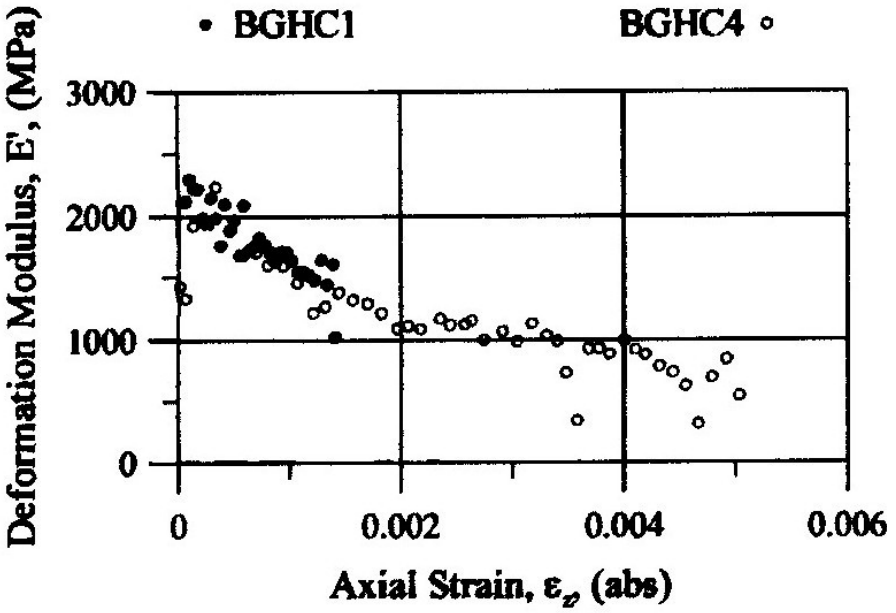

(a)

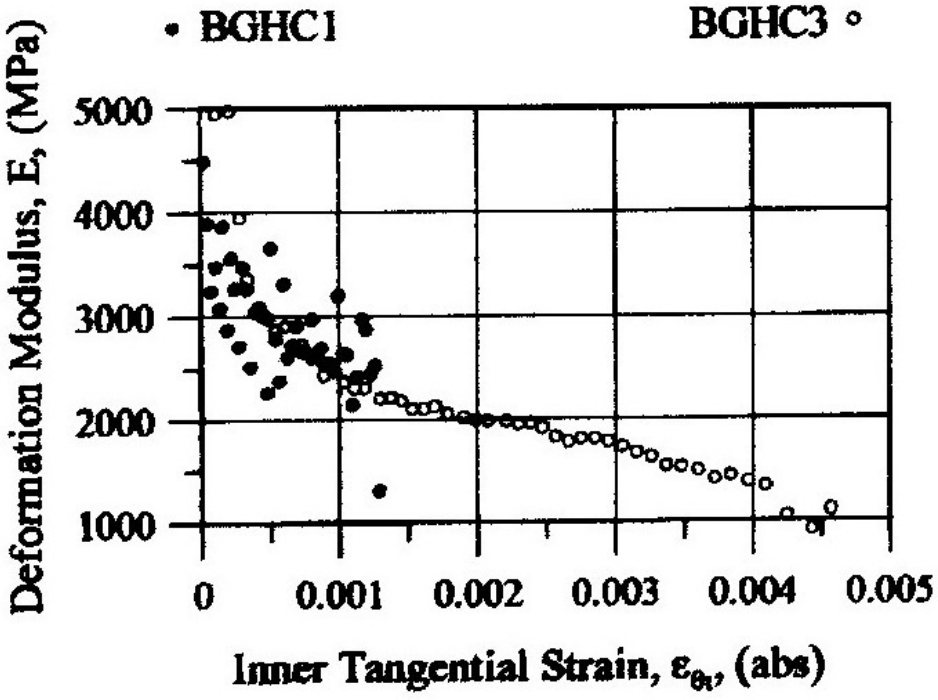

(b)

Figure 3.3. Elastic modulus *E* decreases as elastic strain accumulates for (a) uniaxial compression tests; (b) radial compression tests (Talesnick et al., 2001).

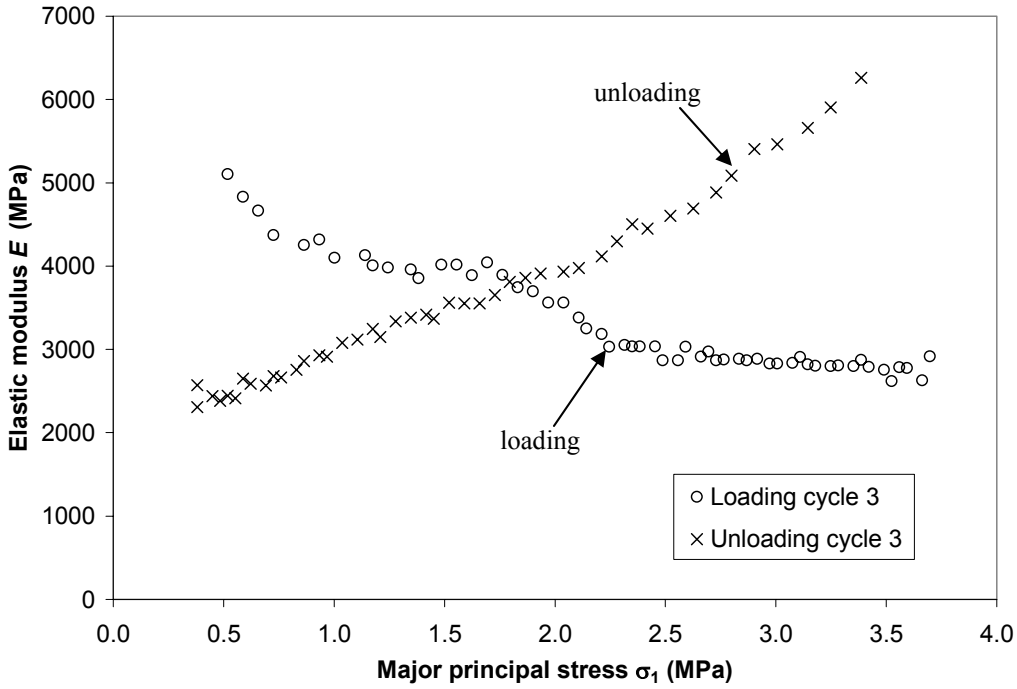

(a)

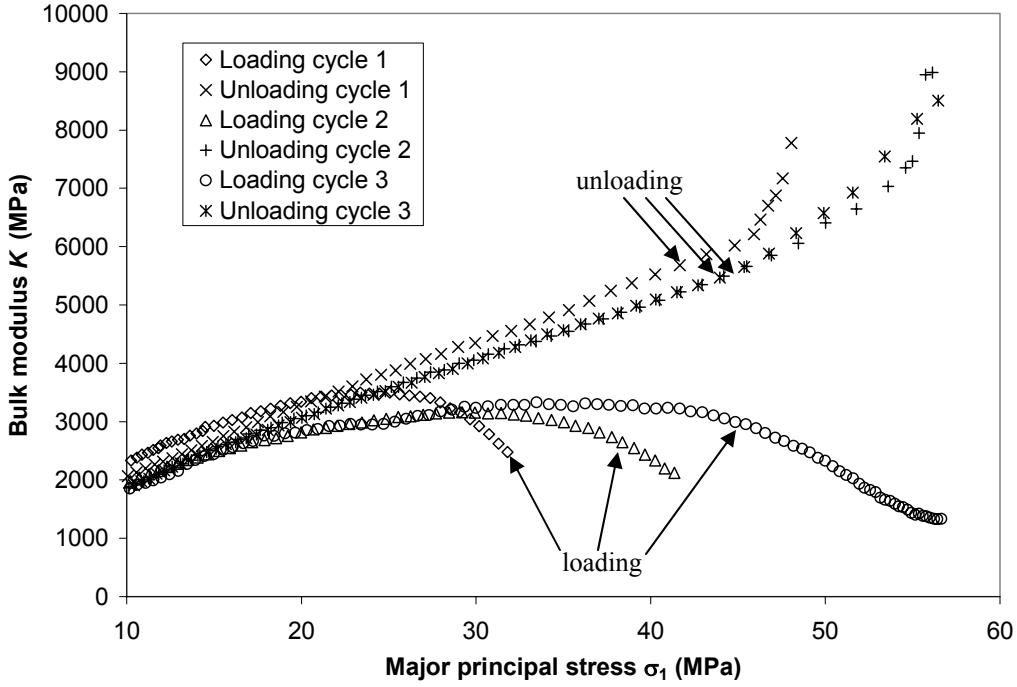

(b)

Figure 3.4. Elastic modulus *E* (bulk modulus *K* in Figure 3.4b) decreases during loading cycles but recovers during unloading cycles. Data shown is for (a) unconfined compression test on Dan chalk (File 309); (b) hydrostatic compression test on Dan chalk (File 310). Data shown is from DGI (2000).

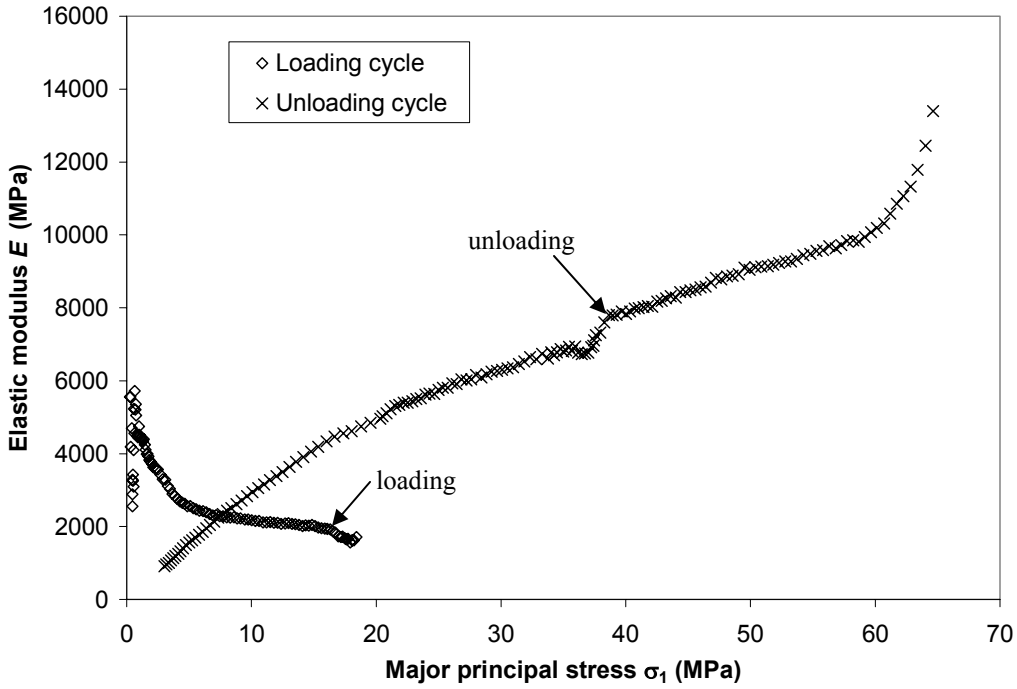

(c)

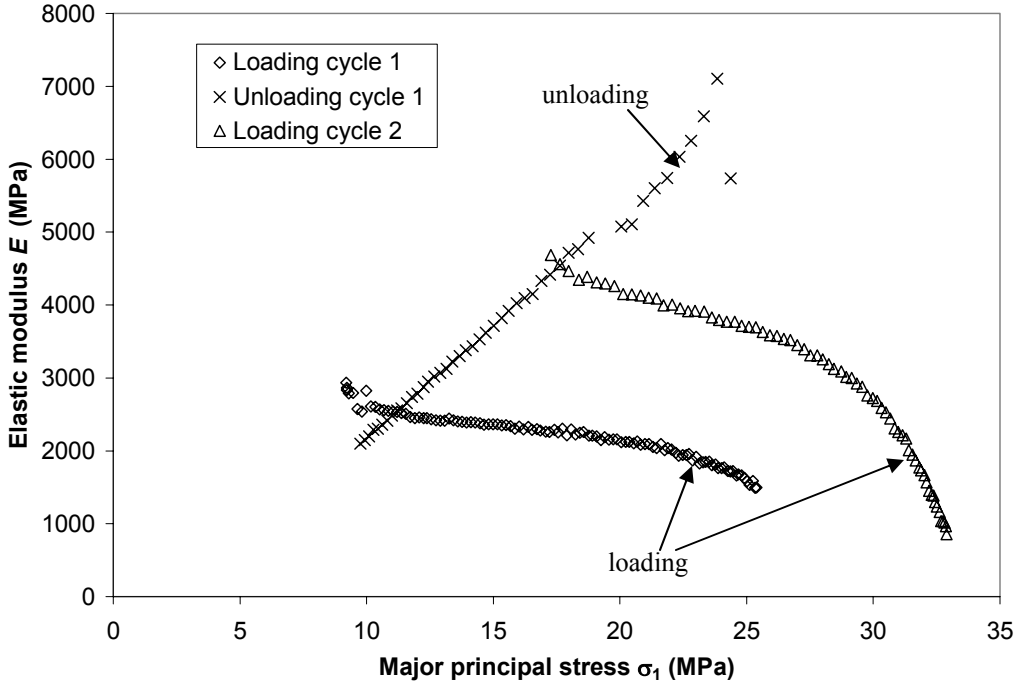

(d)

Figure 3.4 (continued). Elastic modulus *E* decreases during loading cycles but recovers during unloading cycles. Data shown is for (c) K_0 compression test on Tyra chalk (File 453); (d) triaxial compression test on Ekofisk chalk (File 331). Data shown is from DGI (2000).

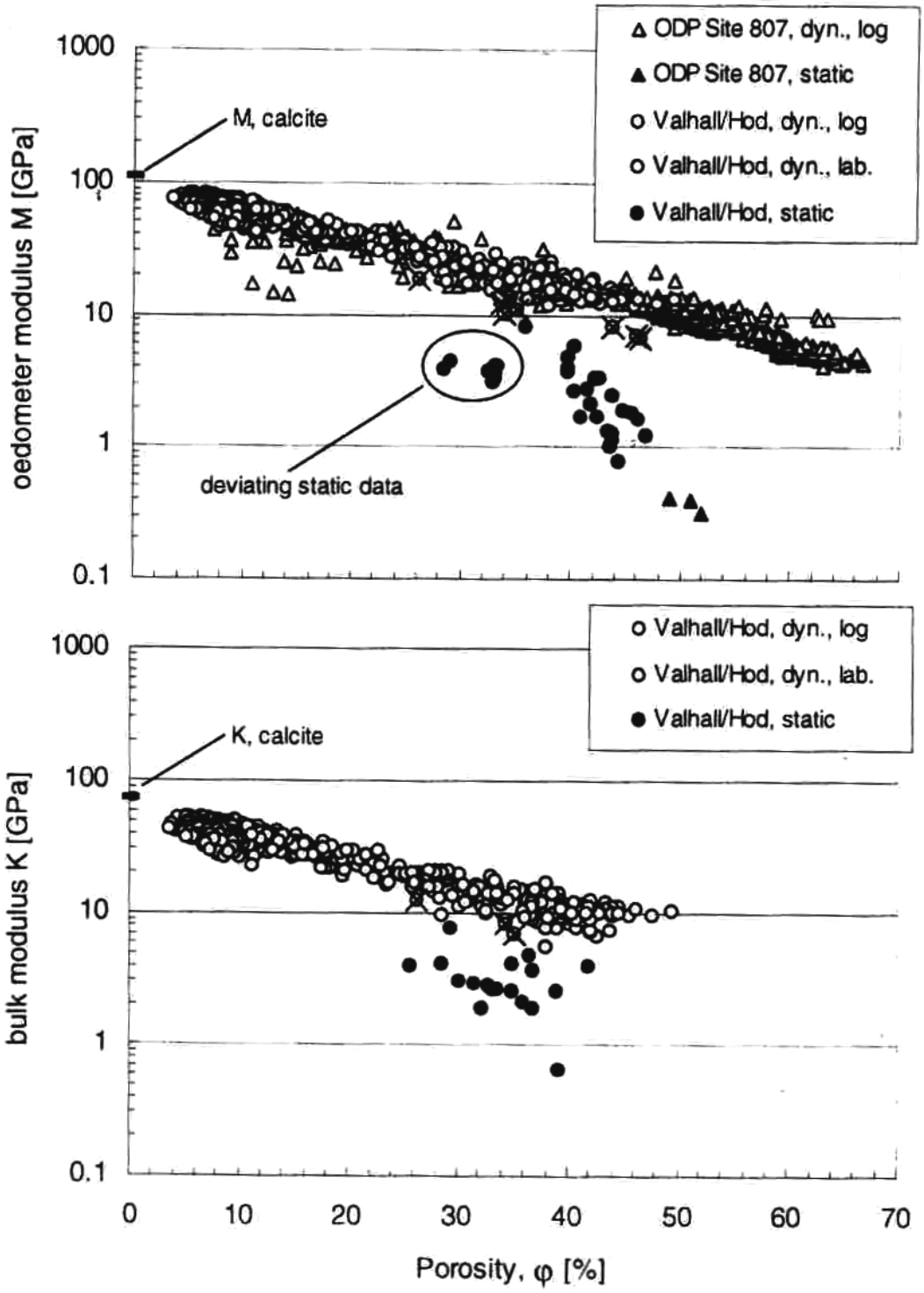

Figure 3.5. Static and dynamic test data from the Valhall and Hod fields show that constrained modulus *M* and bulk modulus *K* decrease with increasing porosity (Gommesen and Fabricius, 2001).

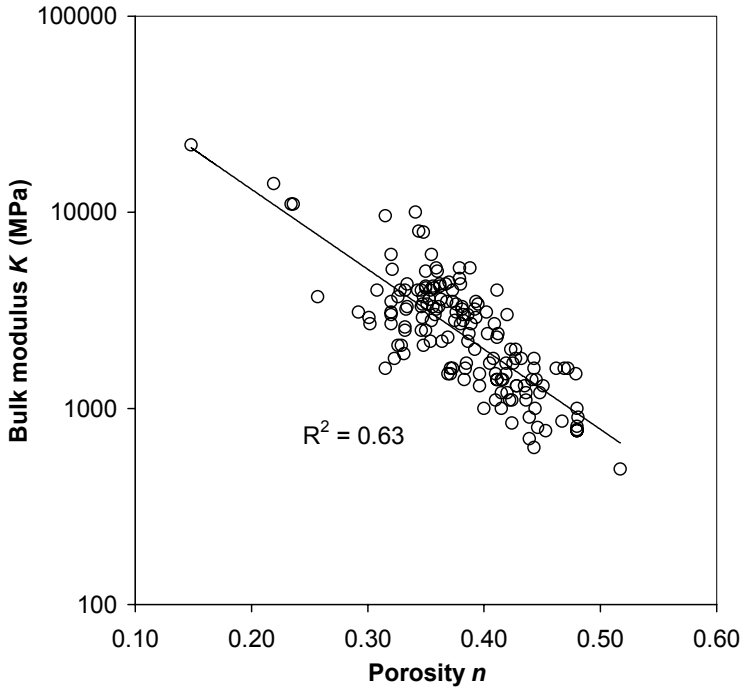

Figure 3.6. Test results for chalk indicate that bulk modulus *K* decreases as a function of porosity. Data shown is for all tests on oil- and gas-saturated chalks in the JCR database (DGI, 2000).

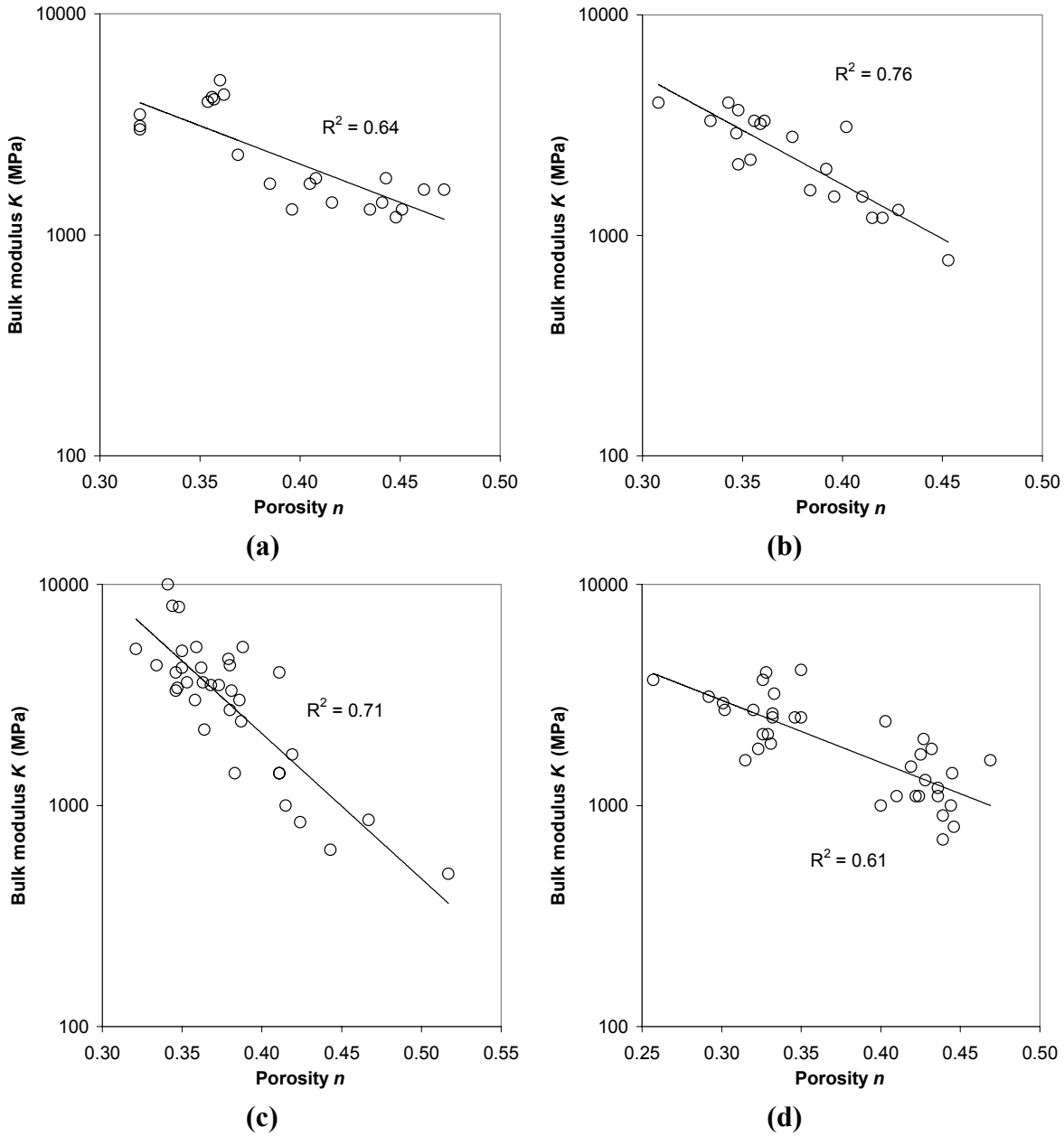

Figure 3.7. Test results from individual chalk fields indicate that bulk modulus *K* decreases as a function of porosity. Data shown is for (a) Tyra, (b) Ekofisk A, (c) Ekofisk D, and (d) Valhall fields. Data shown is from DGI (2000).

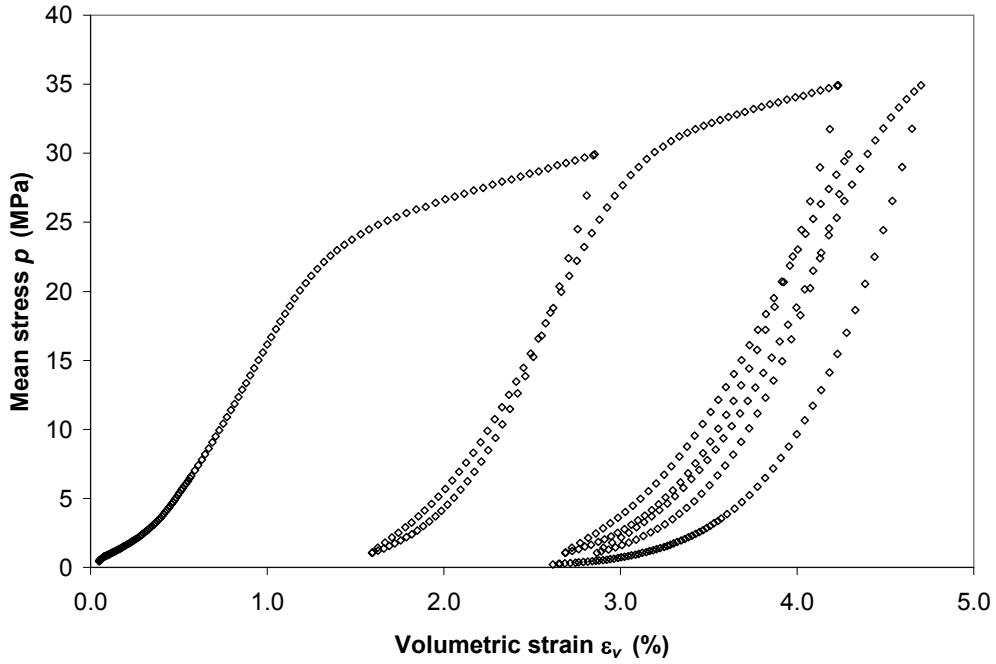

Figure 3.8. Hydrostatic compression test data shows the large irrecoverable strains remaining after sample unloading. Data shown is for Ekofisk A field (File 329). Data shown is from DGI (2000).

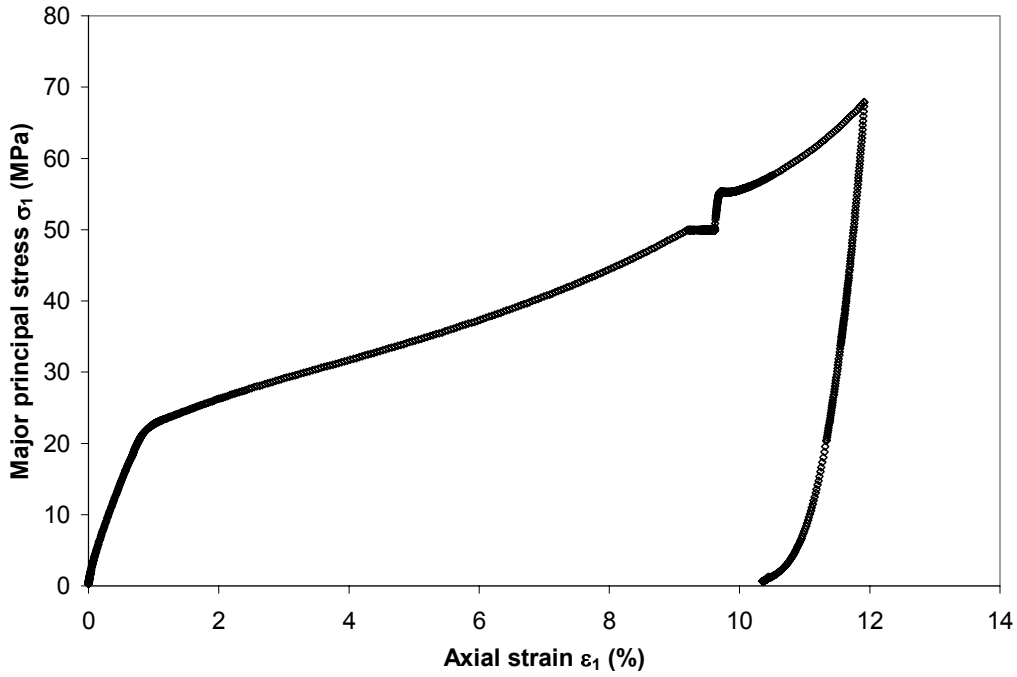

Figure 3.9. K_0 compression test data shows the large irrecoverable strains remaining after sample unloading. Data shown is for Tyra field (File 453). Data shown is from DGI (2000).

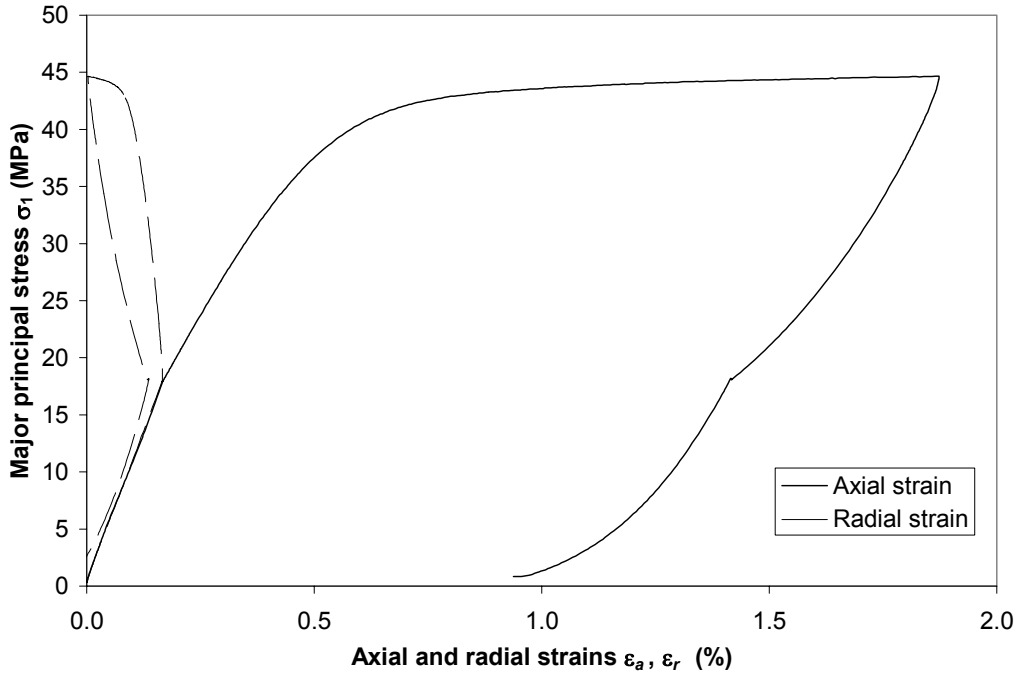

Figure 3.10. Drained triaxial compression test data shows the large irrecoverable strains remaining after sample unloading. Data shown is for Dan field (File 312). Data shown is from DGI (2000).

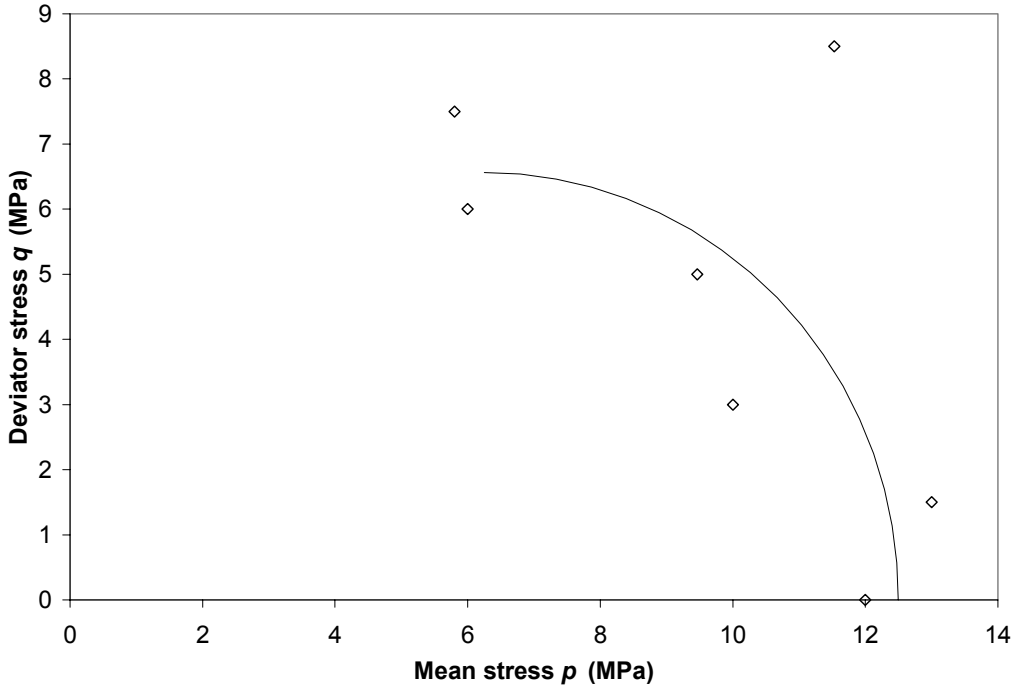

Figure 3.11. Stress path testing under various lateral stress ratios indicates that initial pore collapse yielding occurred at the stresses shown. These yield stress points appear to fit an elliptical yield surface. Data shown is for Butser Hill outcrop chalk (Loe et al., 1992).

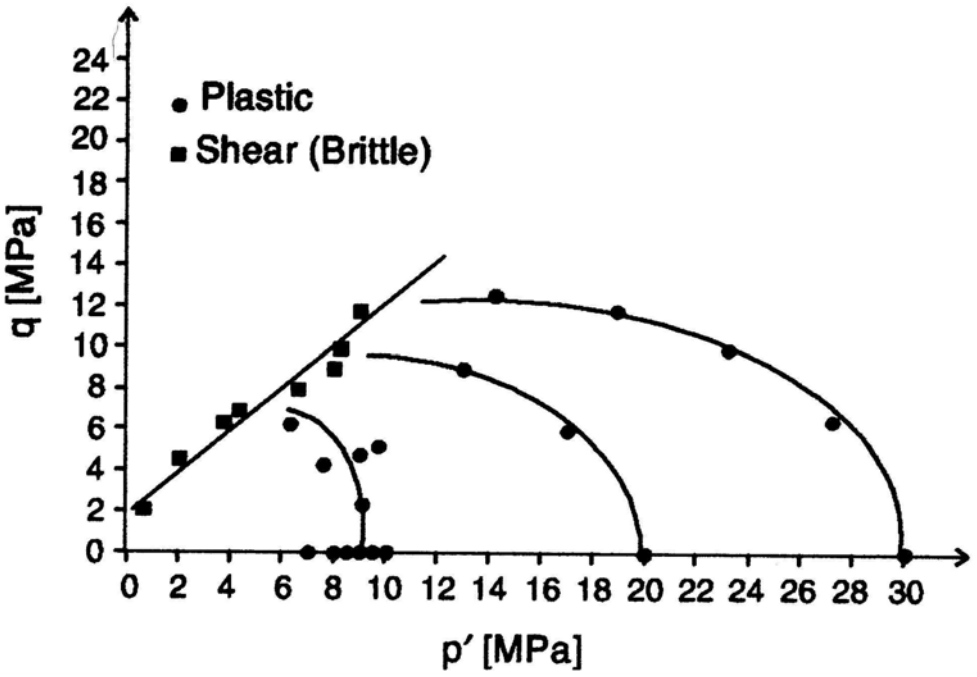

Figure 3.12. Hydrostatic compression test, K_0 compression test, and triaxial compression test results indicate that initial pore collapse yielding and shear failure occurred at the stresses shown for Lixhe outcrop chalk (Collin et al., 2002). As in Figure 3.11, yield stress points fit an elliptical yield surface.

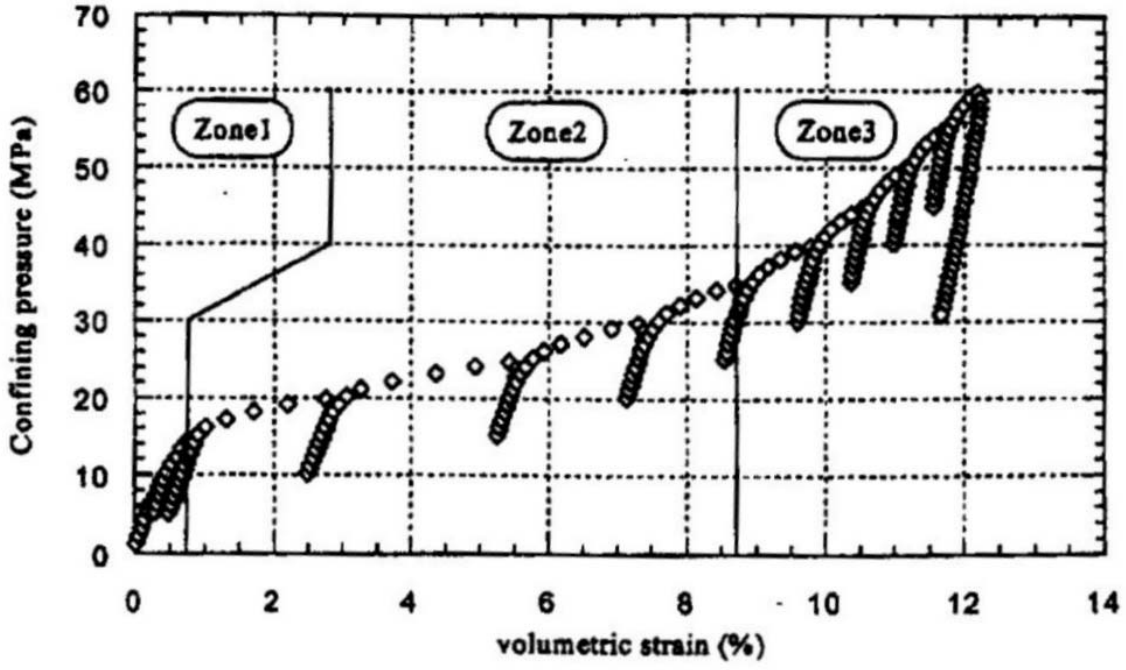

Figure 3.13. Stress-strain curves for a hydrostatic compression test show the concave-upward shape characteristic of compressible geomaterials (Homand and Shao, 2000).

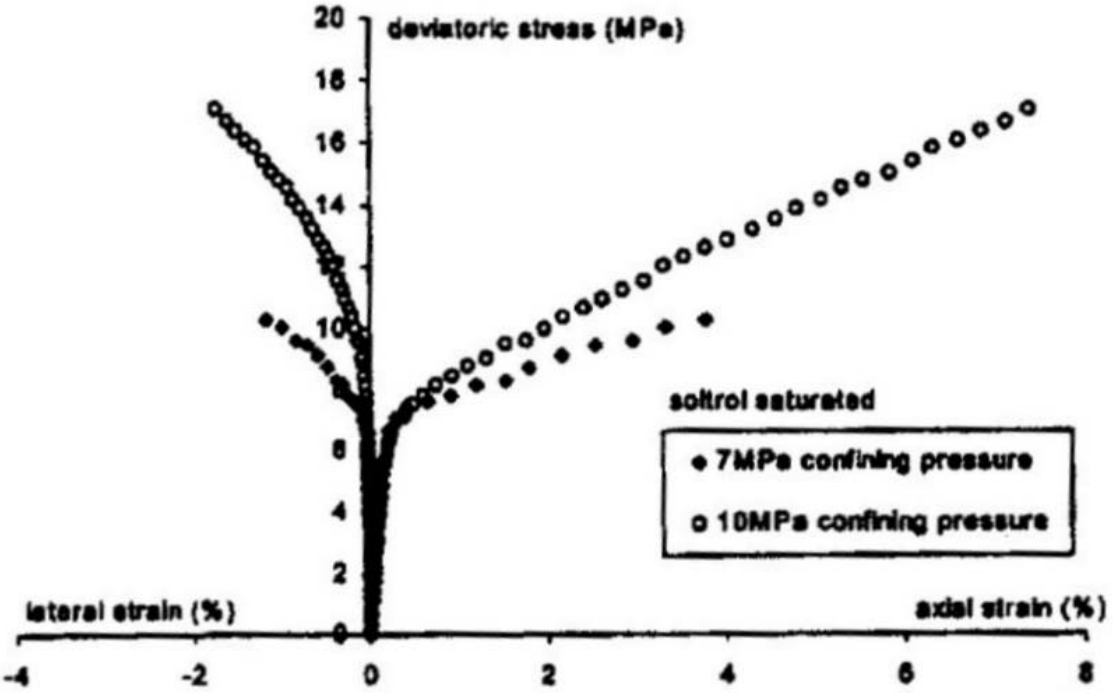

Figure 3.14. Stress-strain curves for oil-saturated samples subjected to triaxial compression tests at relatively high mean stress *p* indicate that the yielding mechanism exhibits plastic hardening (Homand and Shao, 2000).

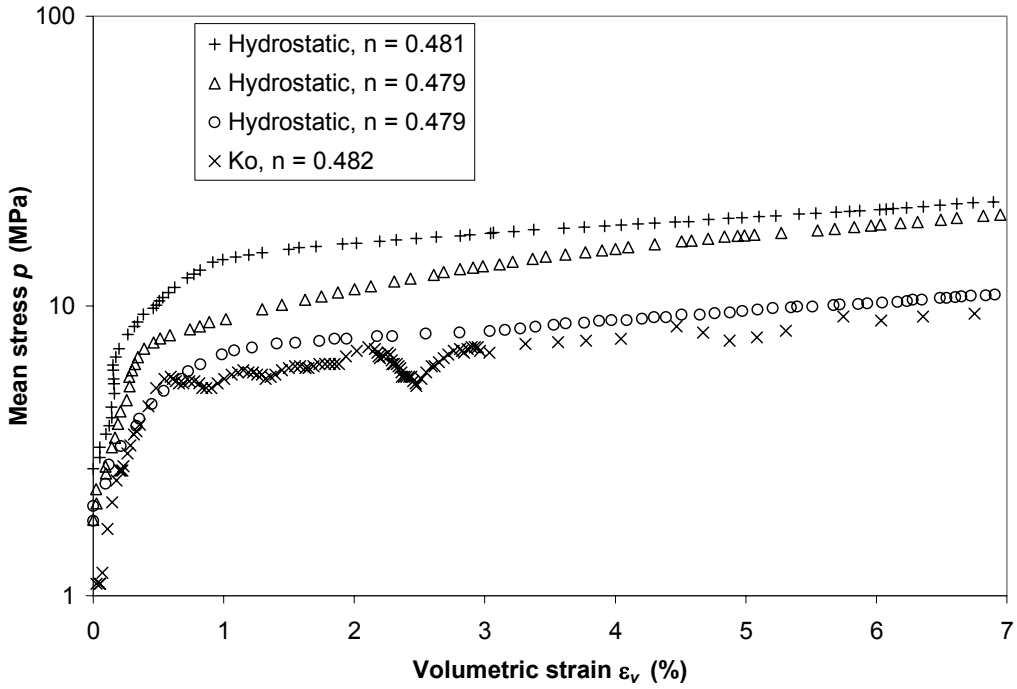

(a)

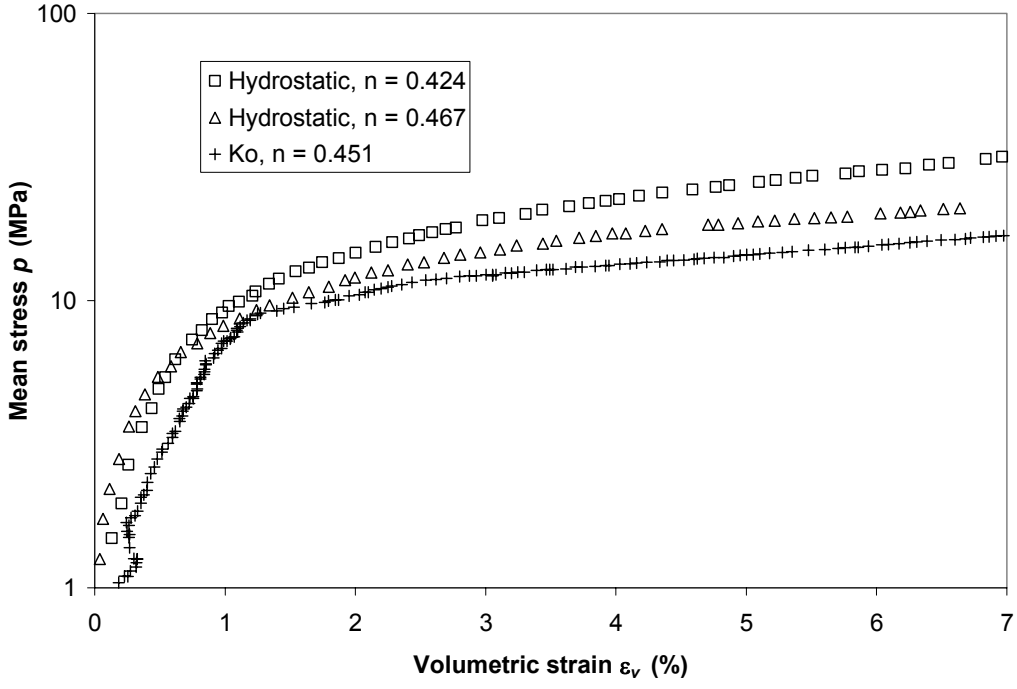

(b)

Figure 3.15. The slope of the virgin compression stress-strain curves are approximately parallel for samples tested under hydrostatic and K_0 compression conditions. Data shown is for (a) Stevns Klint; (b) Ekofisk D chalks. Data shown is from DGI (2000).

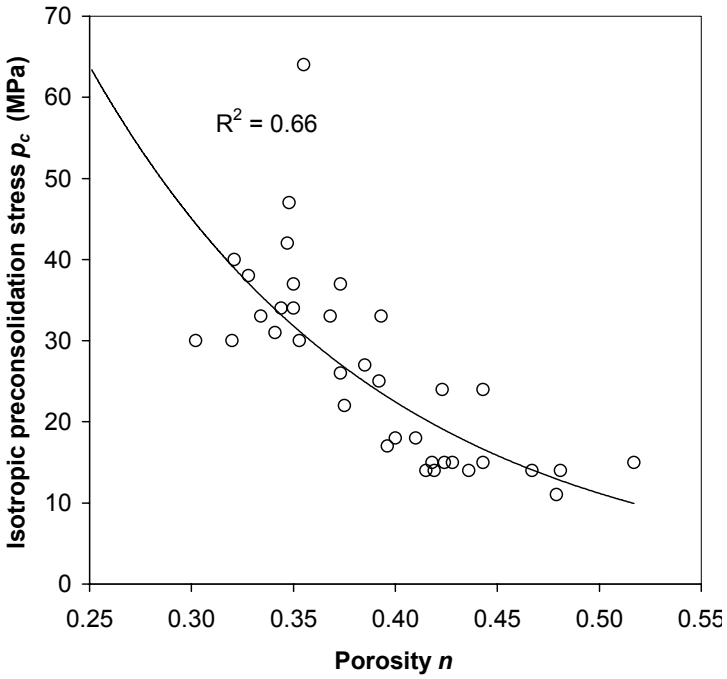

Figure 3.16. Isotropic preconsolidation stress decreases with increasing porosity. Data shown is for all hydrostatic compression tests on oil-saturated chalks in the JCR database (DGI, 2000), and includes both deep sea chalks and outcrop chalks.

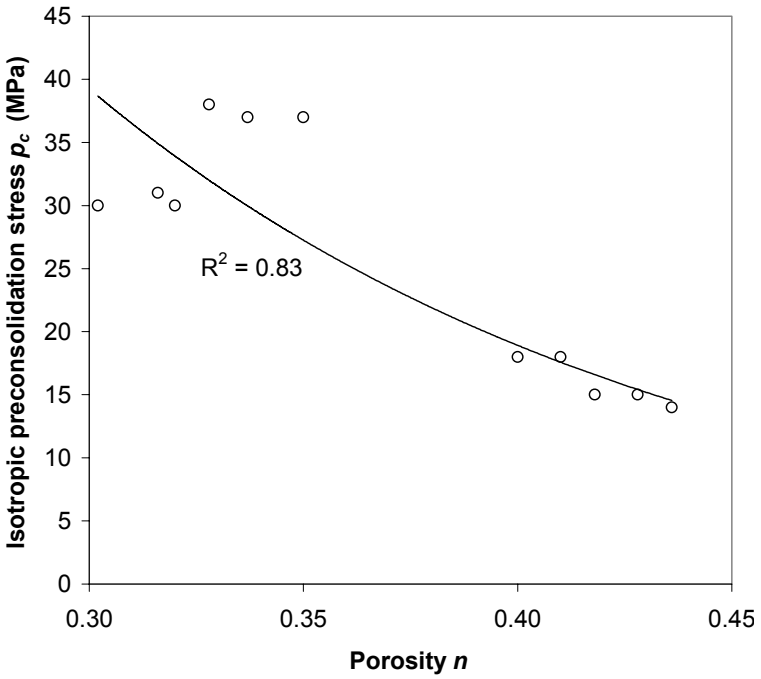

(a)

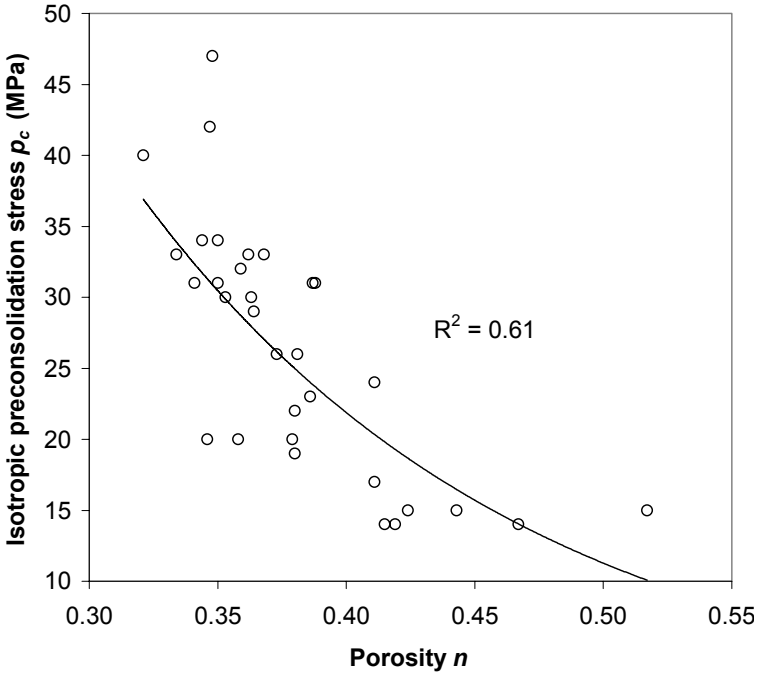

(b)

Figure 3.17. Isotropic preconsolidation stress decreases with increasing porosity. Data shown is for (a) Valhall field; (b) Ekofisk D field. Data shown is from DGI (2000).

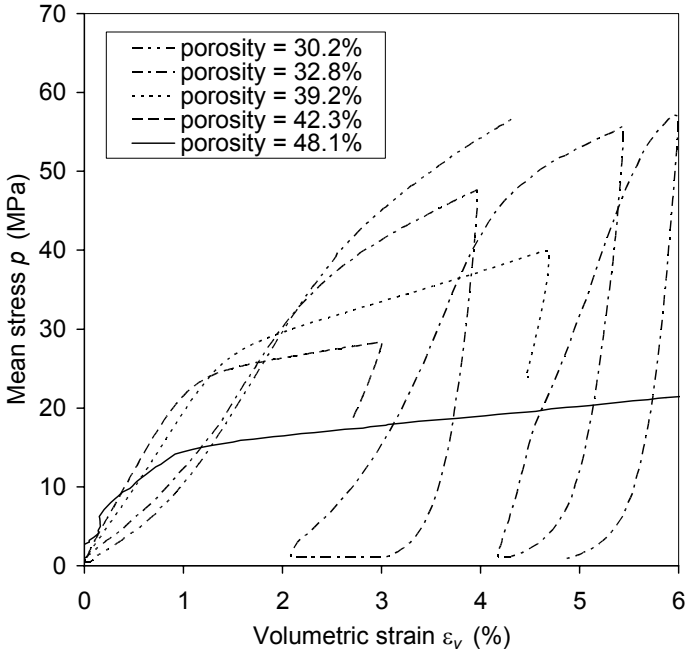

Figure 3.18. Chalk compressibility increases with increasing porosity, as observed in hydrostatic compression tests. Data shown is from DGI (2000).

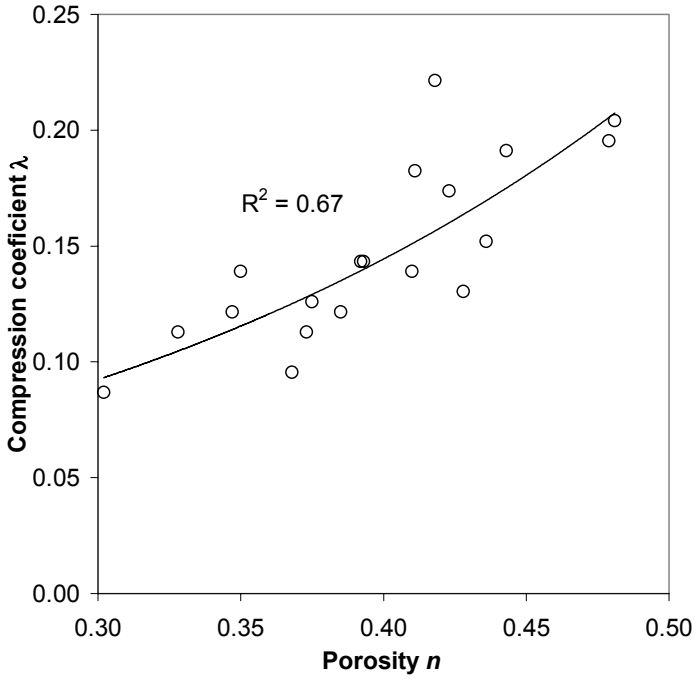

Figure 3.19. Compression coefficient λ increases with increasing porosity. Data shown is for all hydrostatic compression tests on oil-saturated chalks in the JCR database (DGI, 2000).

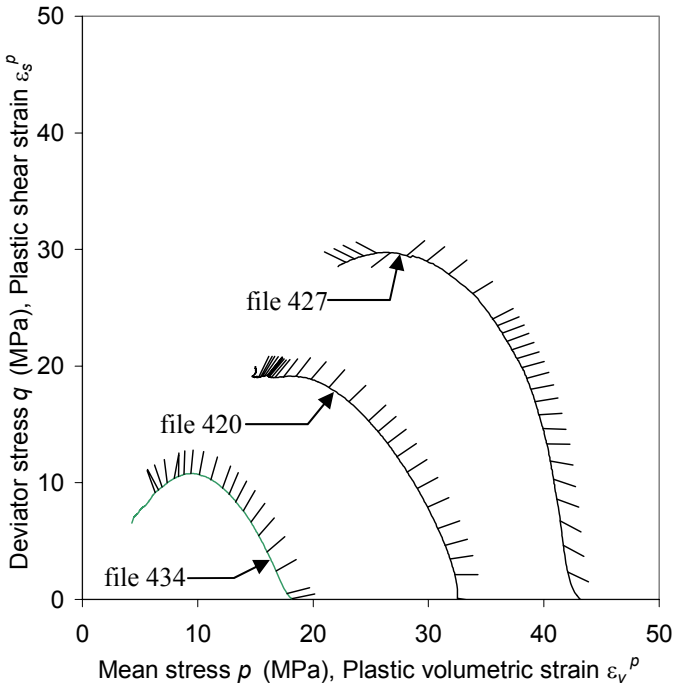

Figure 3.20. Mean stress decreases and plastic flow direction changes consistently as shear stress ratio changes during undrained triaxial compression loading. Data shown is from DGI (2000).

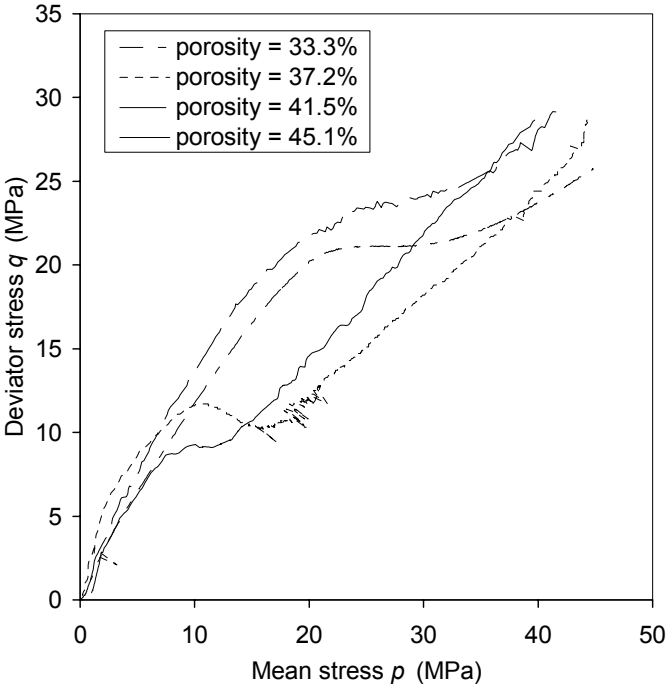

Figure 3.21. The steady-state shear stress ratio η (= *q*/*p*) decreases with increasing porosity during K_0 compression loading. Data shown is from DGI (2000).

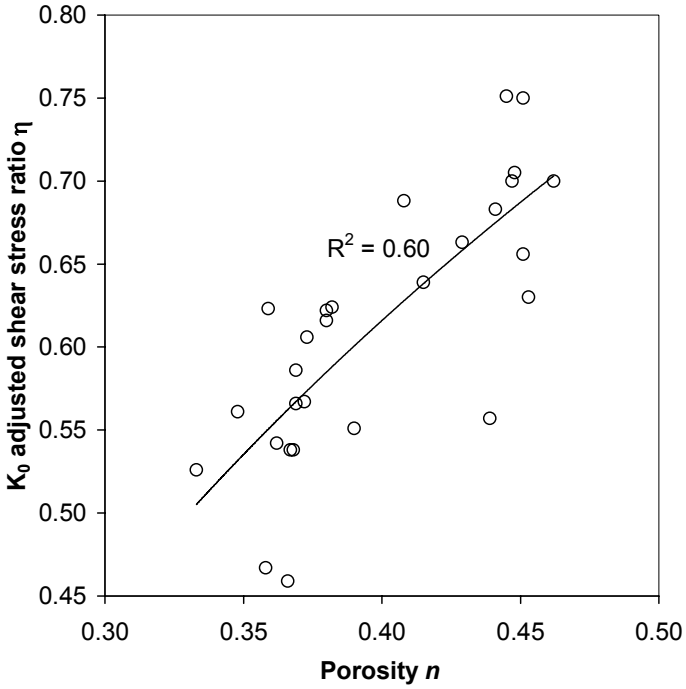

Figure 3.22. The steady-state shear stress ratio decreases with increasing porosity during K_0 compression loading. Data shown is for all K_0 compression tests in the JCR database (DGI, 2000). For deep-sea chalks, attraction (a) = 4 MPa; for outcrop chalks, a = 0.

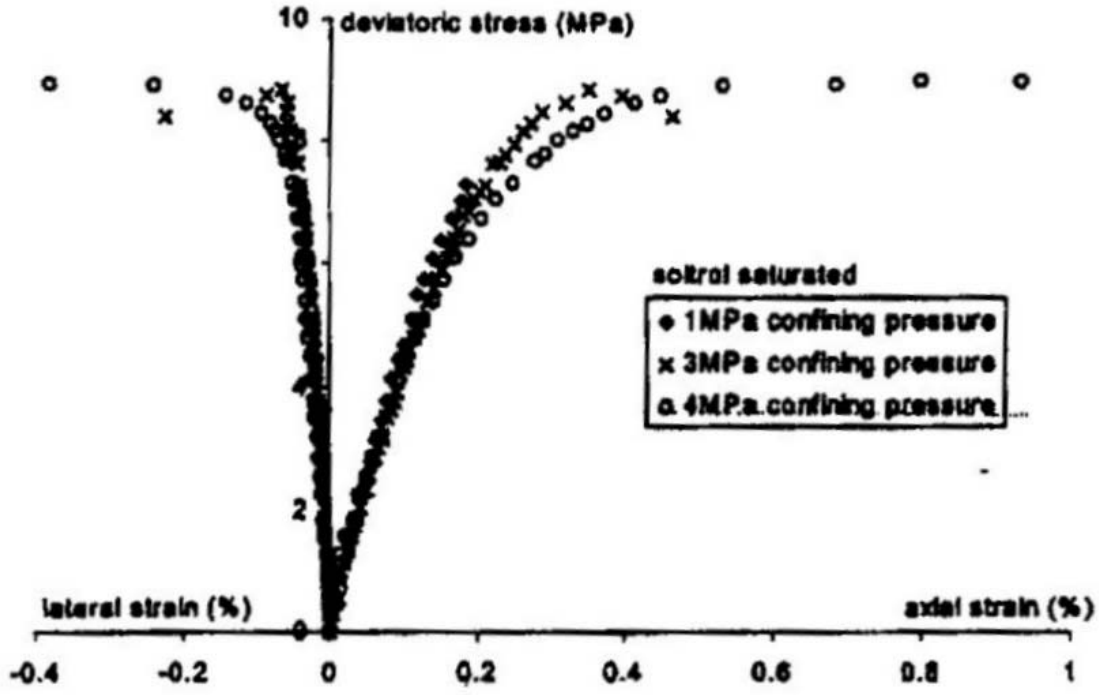

Figure 3.23. Stress-strain curves for oil-saturated samples subjected to triaxial compression tests at relatively low mean stress p indicate that an ultimate strength exists but that some hardening may occur before failure (Homand and Shao, 2000).

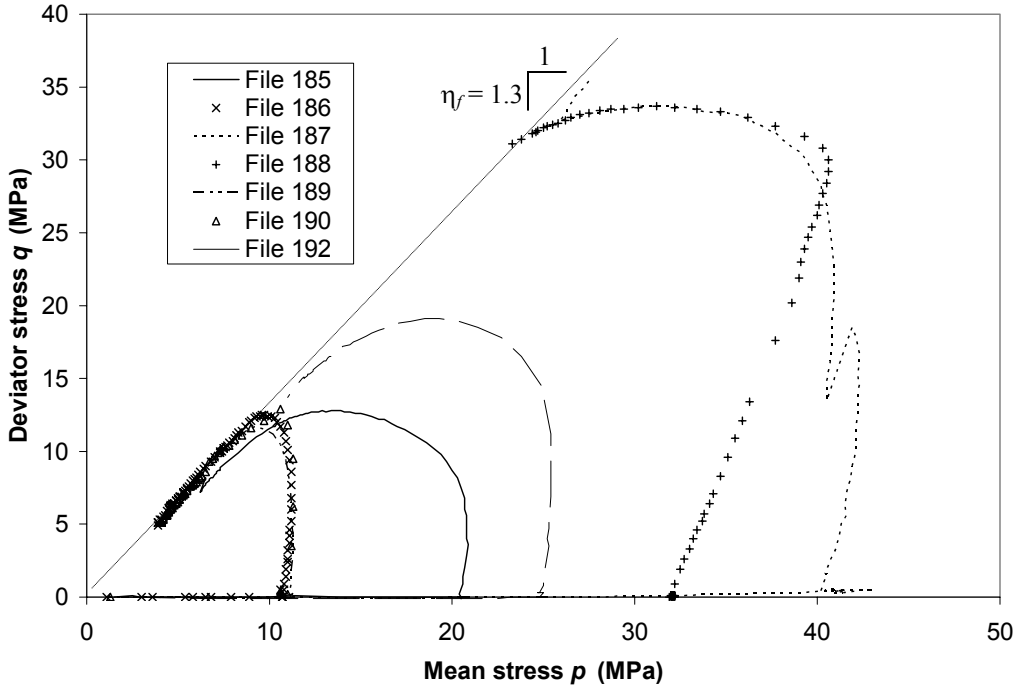

(a)

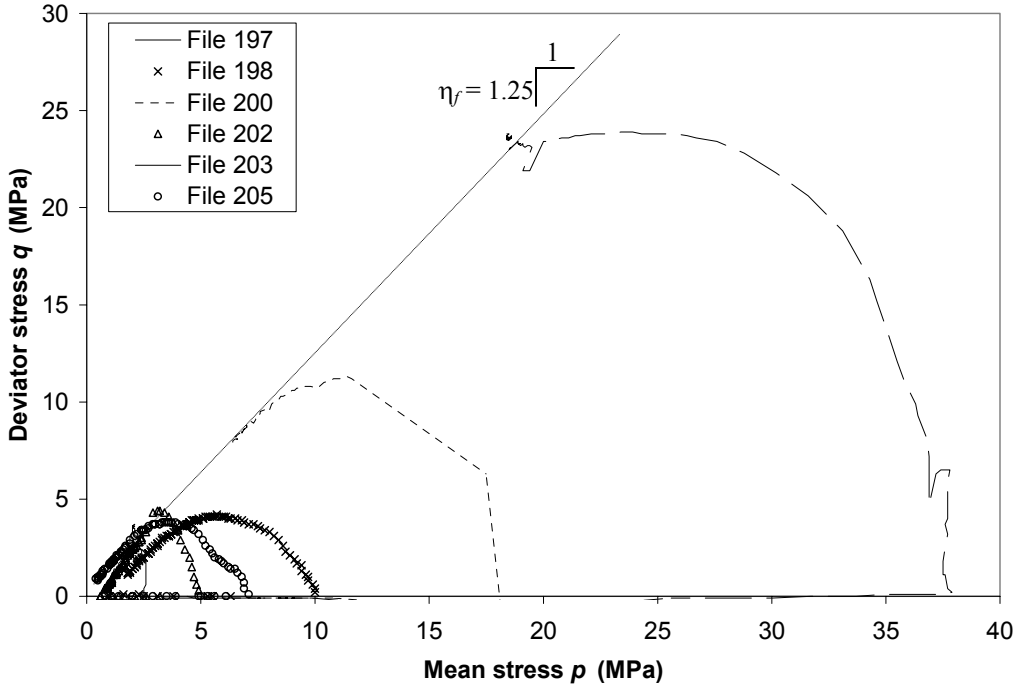

(b)

Figure 3.24. Stress paths for undrained triaxial compression tests on chalk outcrop samples shows that the failure shear stress ratio is approximately constant for a single chalk type. Data shown is for (a) Butser Hill outcrop; (b) Stevns Klint outcrop. Data shown is from DGI (2000).

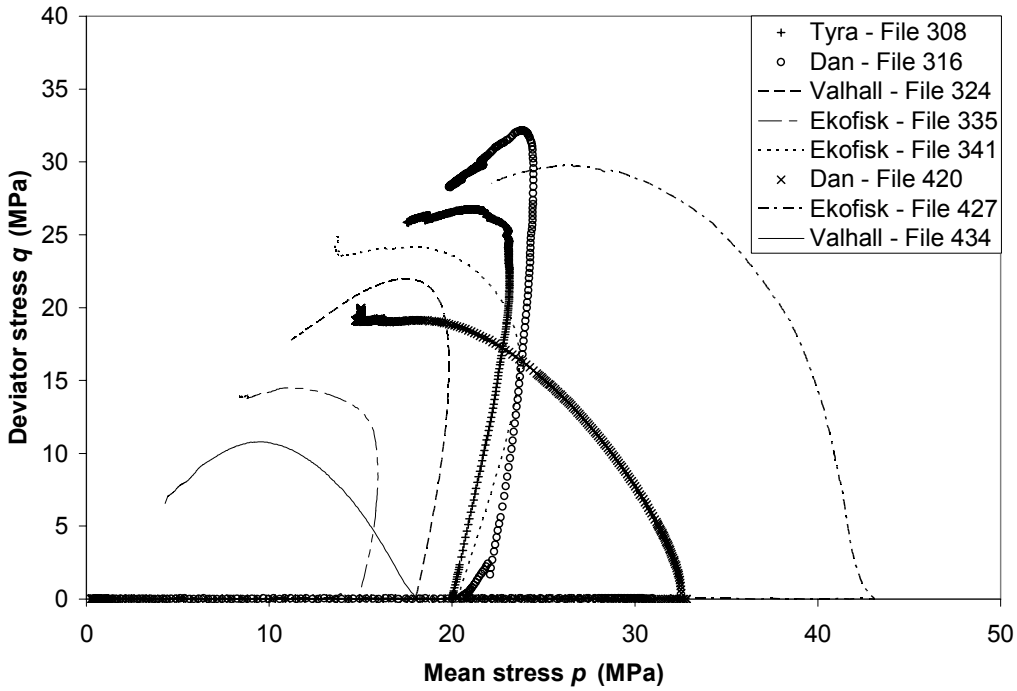

Figure 3.25. Stress paths for undrained triaxial compression tests on chalk reservoir samples shows that the failure shear stress ratio is nearly constant for all chalks. Data shown is for Tyra, Dan, Ekofisk, and Valhall fields. Data shown is from DGI (2000).

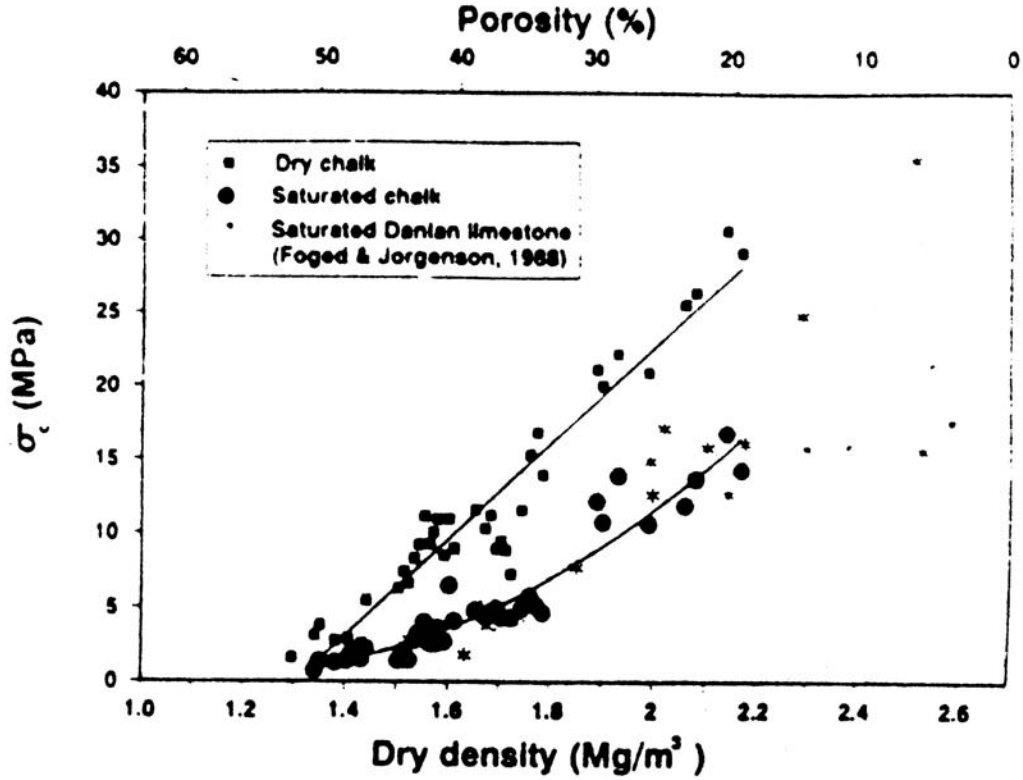

Figure 3.26. The uniaxial compressive strength of Cretaceous-age English outcrop chalks decreases linearly as porosity increases (Matthews and Clayton, 1993).

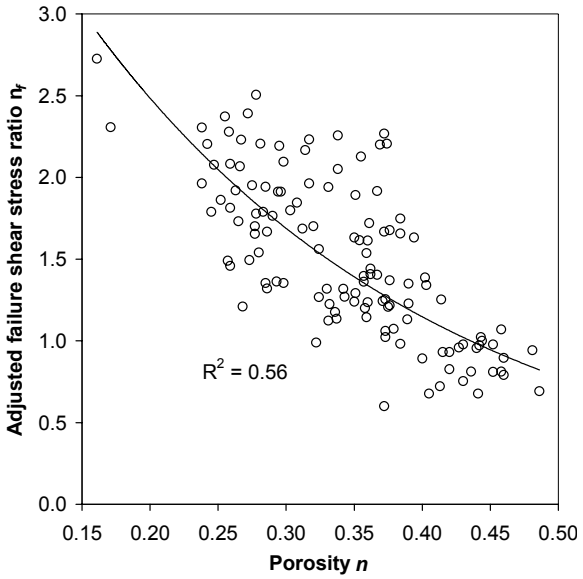

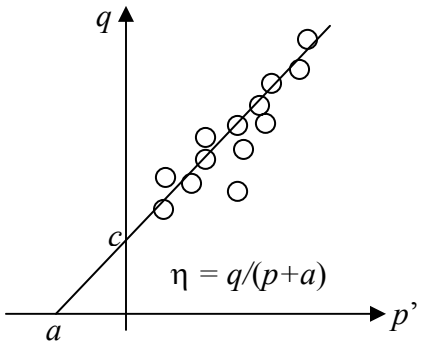

Adjusted failure shear stress ratio η accounts for cohesion c or attraction a

(a)

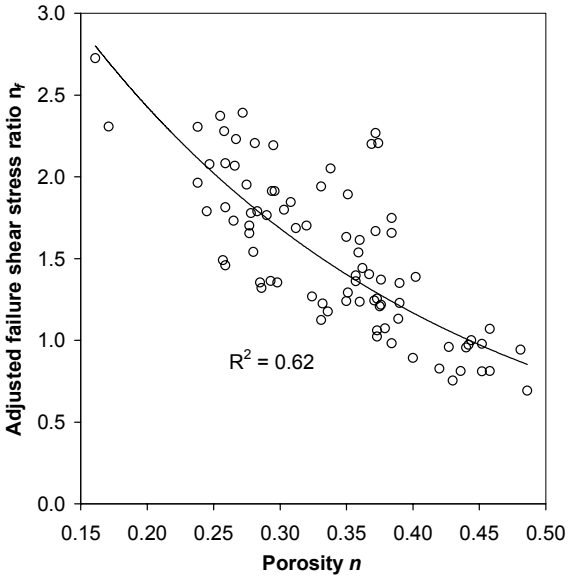

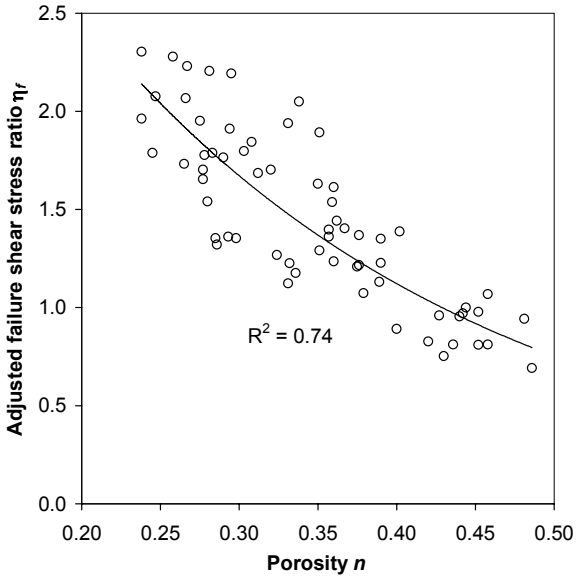

(b) **(c)**

Figure 3.27. Adjusted failure shear stress ratio decreases with increasing porosity. Data shown includes all results from JCR database on oil- and gas-saturated chalks (DGI, 2000) for (a) triaxial compression tests and unconfined compression tests on deep-sea chalks and outcrop chalks; (b) triaxial compression tests on deep-sea chalks and outcrop chalks; (c) triaxial compression tests on deep-sea chalks only. The adjusted failure shear stress ratio accounts for cohesion of the chalk as shown. For deep-sea chalks, attraction (*a*) = 4 MPa; for outcrop chalks, *a* = 0.

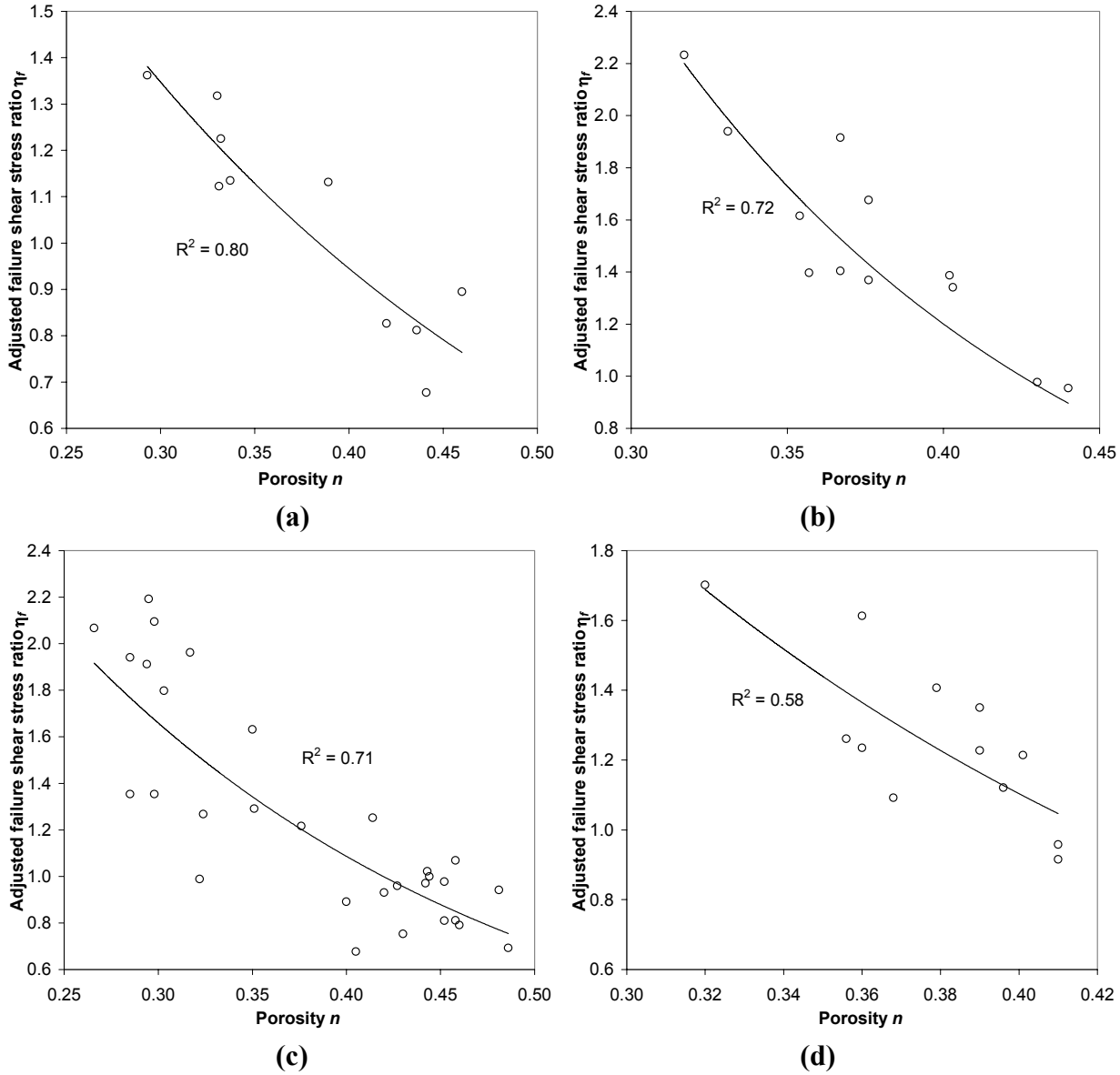

Figure 3.28. Adjusted failure shear stress ratio decreases with increasing porosity. Data shown is for oil- and gas-saturated chalks of (a) Valhall field; (b) South Arne field; (c) Tyra field; (d) Ekofisk A field. Data shown is from DGI (2000).

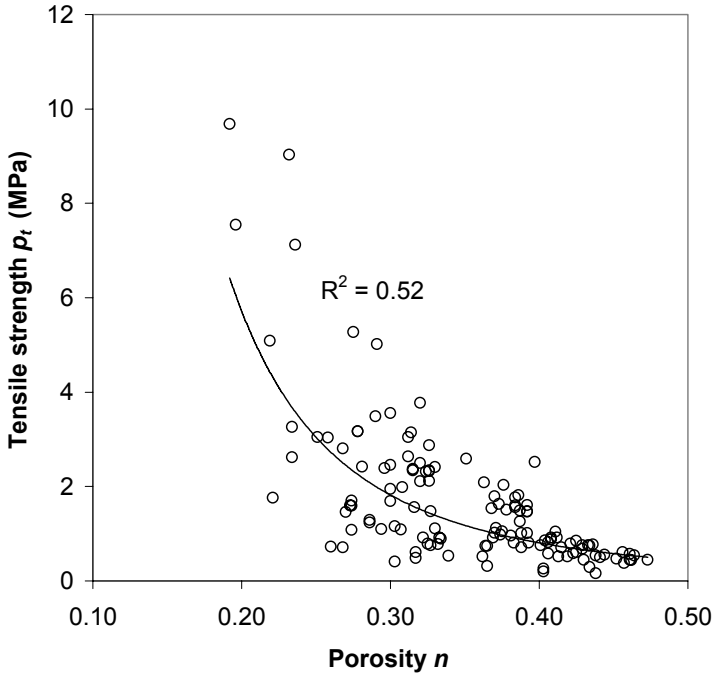

Figure 3.29. Tensile strength decreases with increasing porosity. Data shown is for all Brazilian tests in the JCR database (DGI, 2000).

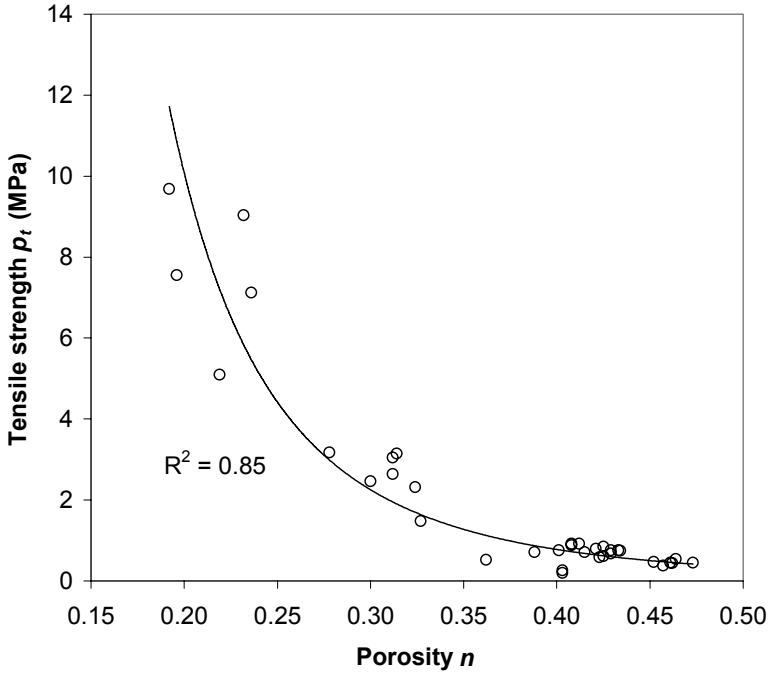

(a)

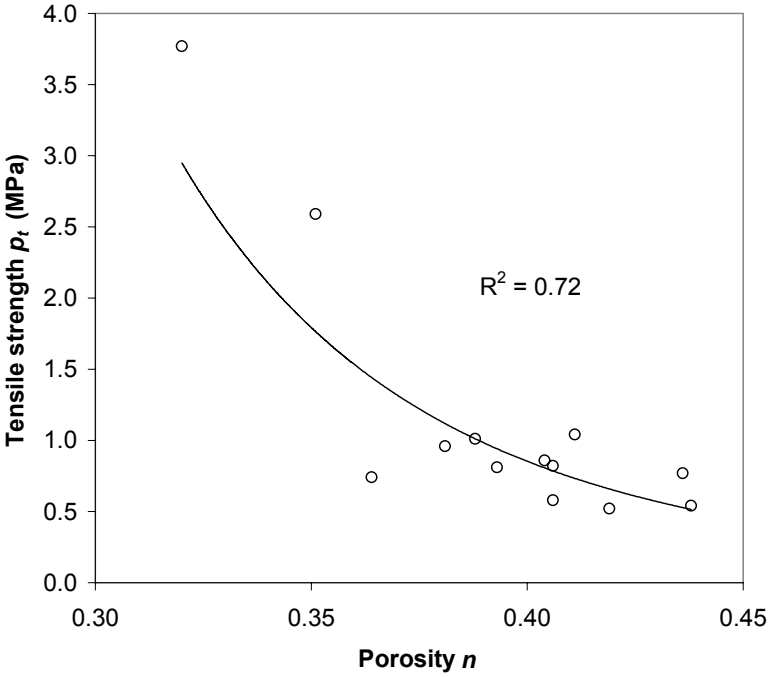

(b)

Figure 3.30. Tensile strength decreases with increasing porosity. Data shown is for oil- and gas-saturated chalks of (a) Tyra field; (b) South Arne field. Data shown is from DGI (2000).

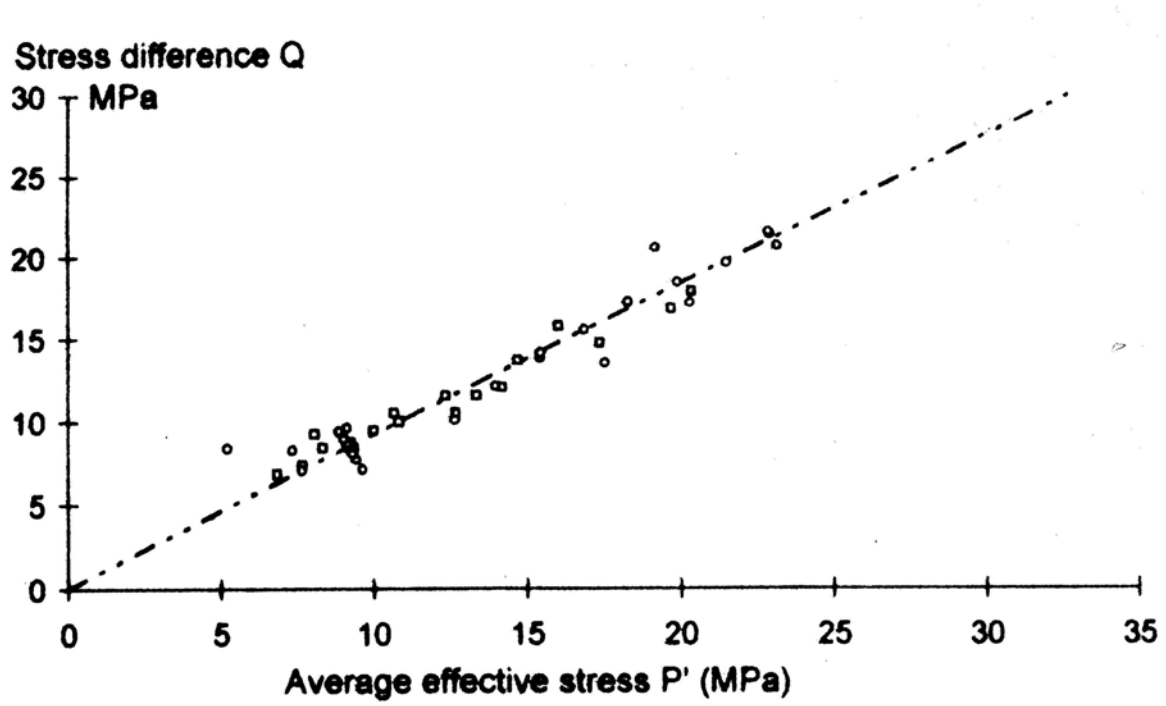

Figure 3.31. Failure shear stress ratio of Lixhe and Aalborg outcrop chalks in triaxial extension appears to be constant in *p-q* space (Risnes et al., 1998).

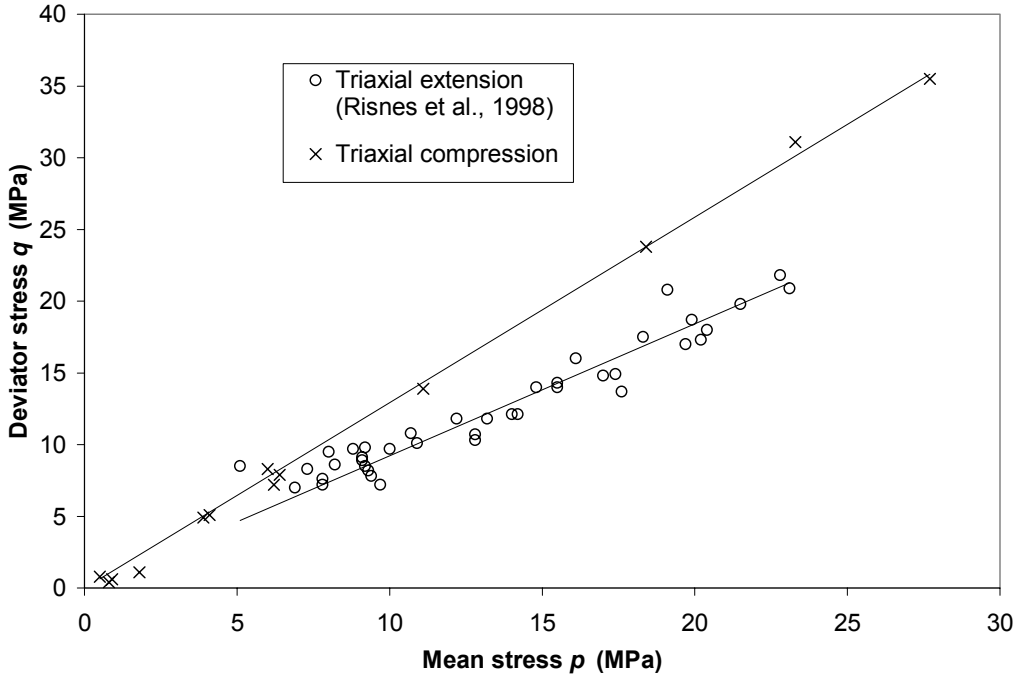

Figure 3.32. Failure shear stress ratio of Lixhe and Aalborg outcrop chalks in triaxial extension is less than that of Butser-Hill and Stevns Klint outcrop chalks in triaxial compression, suggesting that Mohr-Coulomb third-invariant model may apply. Butser-Hill and Stevns Klint data is from DGI (2000).

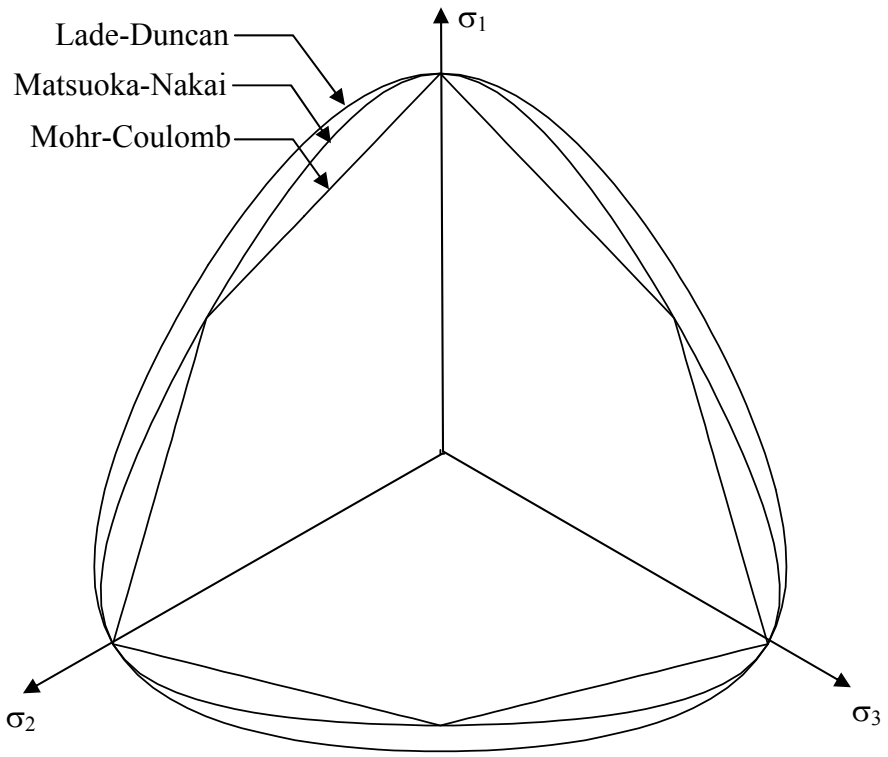

Figure 3.33. Relative shapes of various 3rd-invariant constitutive models in the π–plane.

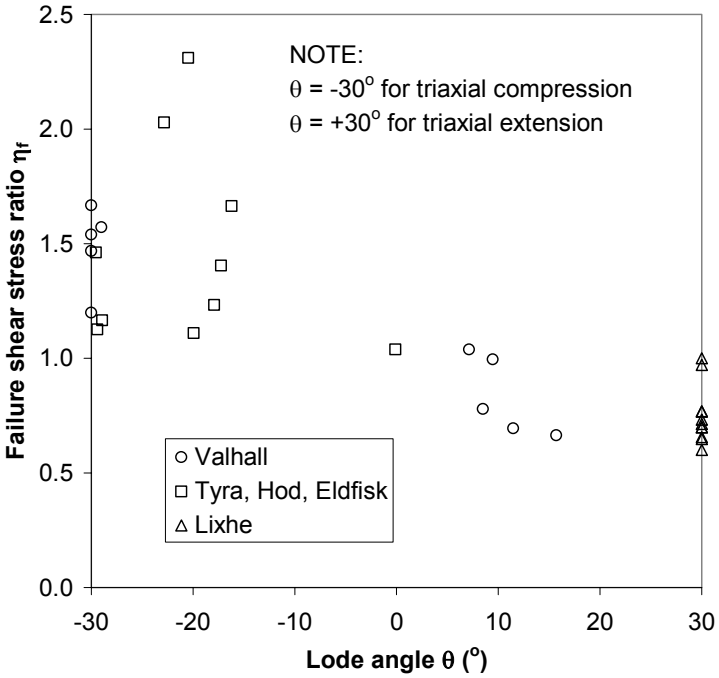

(a)

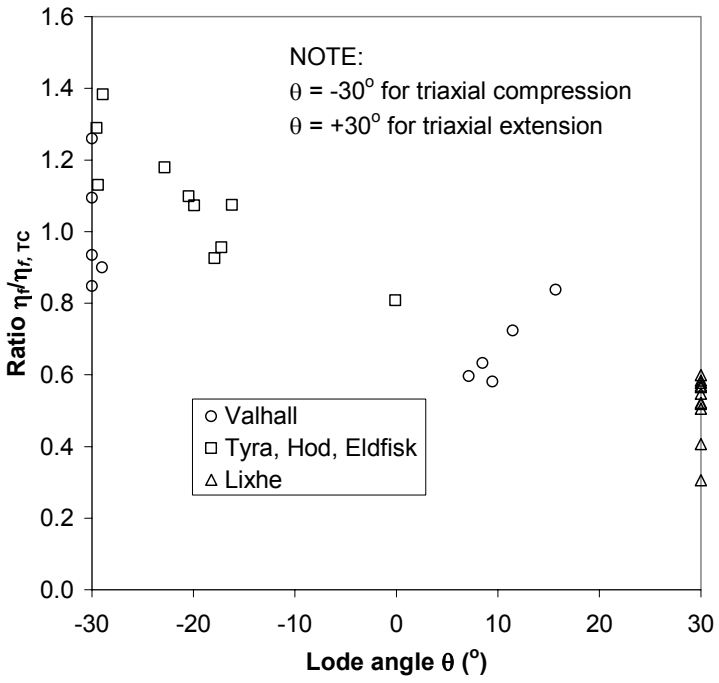

(b)

Figure 3.34. True triaxial test results and triaxial extension test results from multiple chalk fields and outcrops indicate that chalk strength decreases continuously as Lode angle θ increases. Plots show (a) uncorrected data; (b) data corrected for porosity variation in shear strength. Data shown is from DGI (2000).

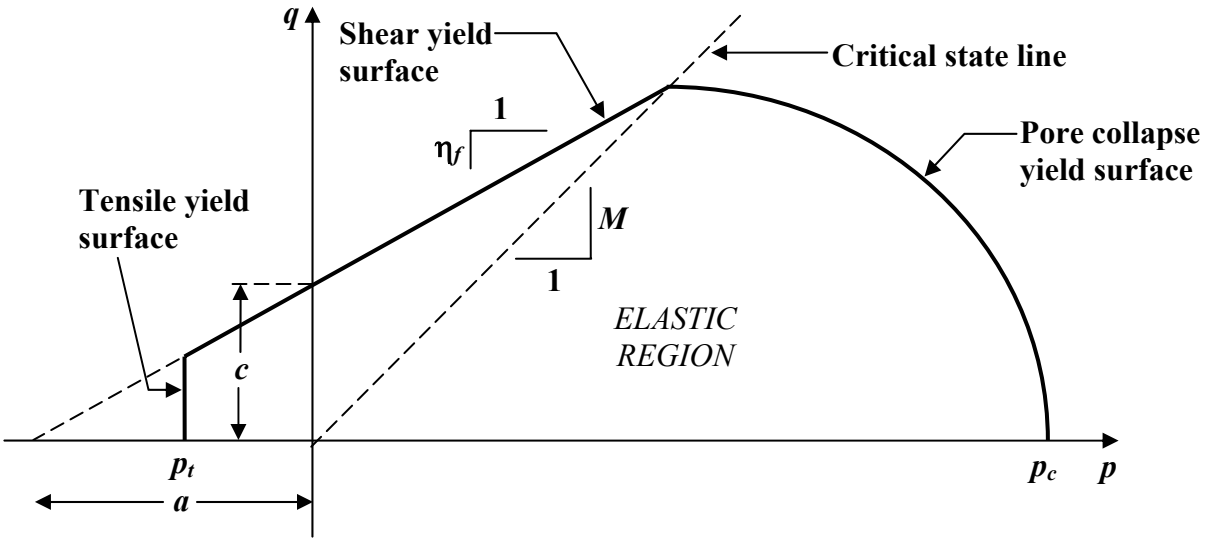

Figure 3.35 Multiple yield mechanisms and yield surfaces for chalk in *p-q* space.

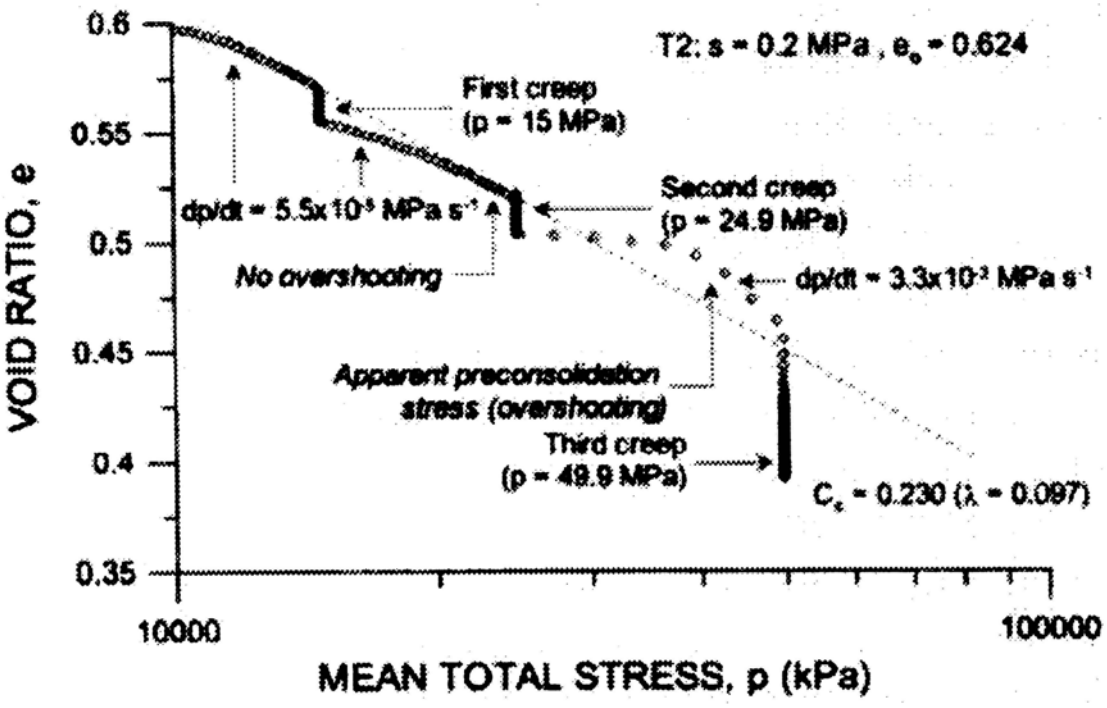

(a)

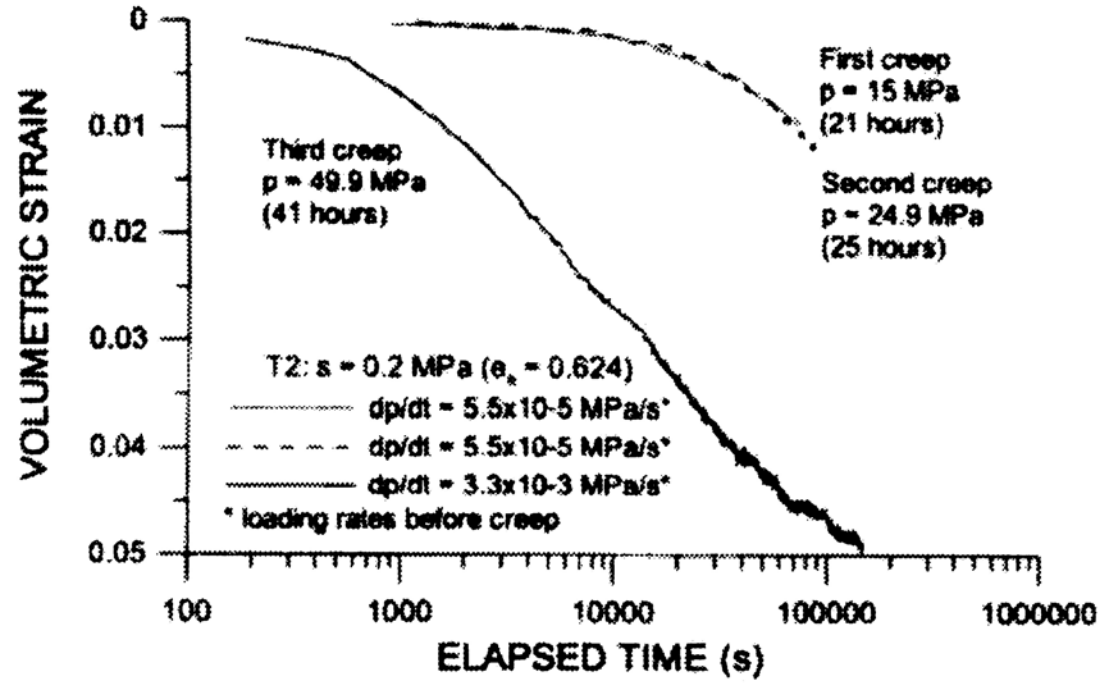

(b)

Figure 3.36. Creep phases of hydrostatic compression tests performed on Lixhe chalk indicate that creep behavior depends on the loading history. Plots show creep behavior in (a) stress-strain space; (b) time-strain space. Although tangent slopes in (b) are parallel, the creep rate depends on prior loading history (DeGennaro et al., 2003).

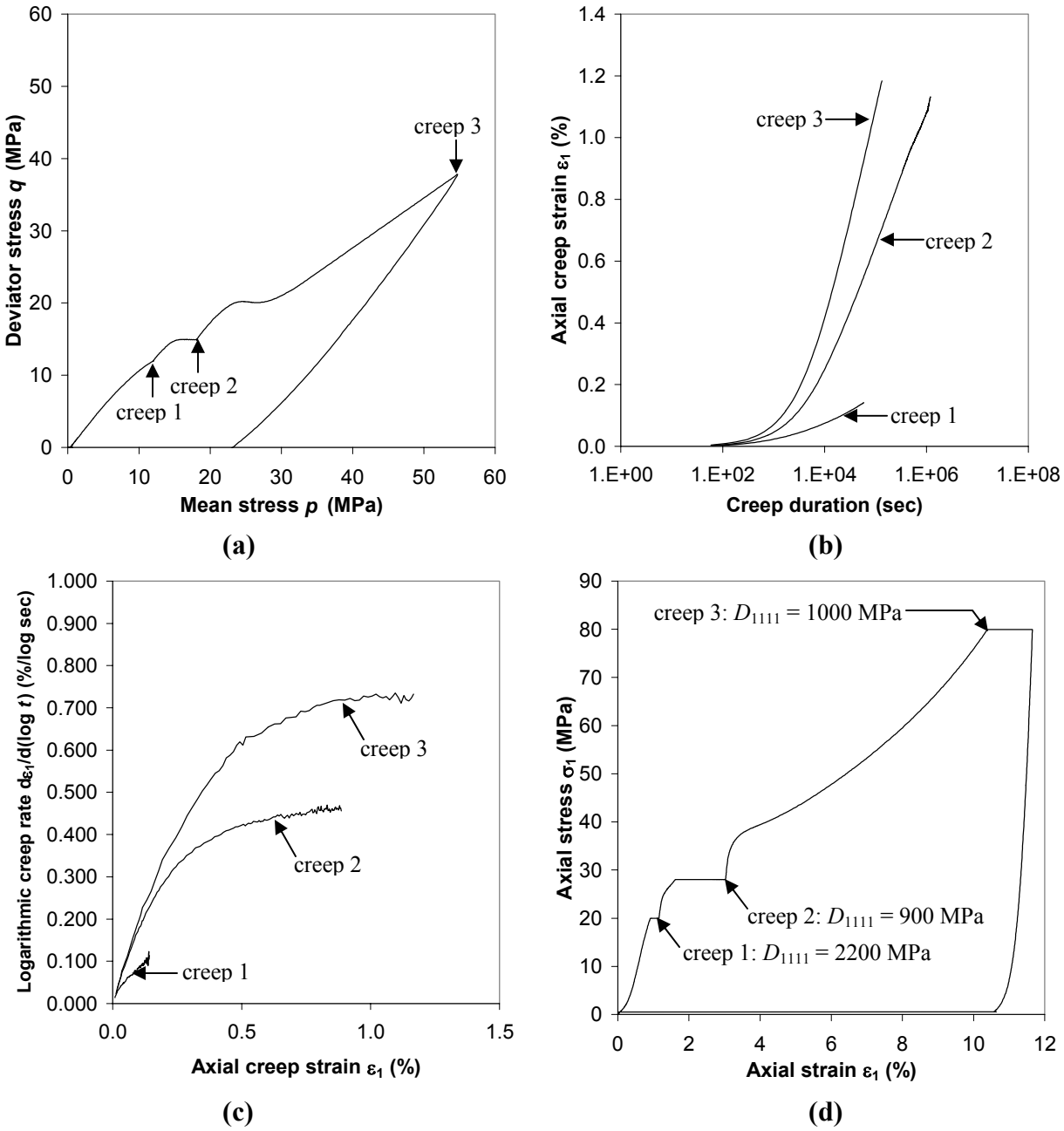

Figure 3.37. K_0 compression tests with creep phases reveals variability in creep behavior. Three creep phases performed at different positions in (a) stress space result in different logarithmic strain rates, as shown in (b) and (c). The creep behavior may be the result of previous loading history, as shown by the different stiffnesses D_{1111} present when creep is initiated, as shown in (d). Data shown is for Tyra field (File 454). Data shown is from DGI (2000).

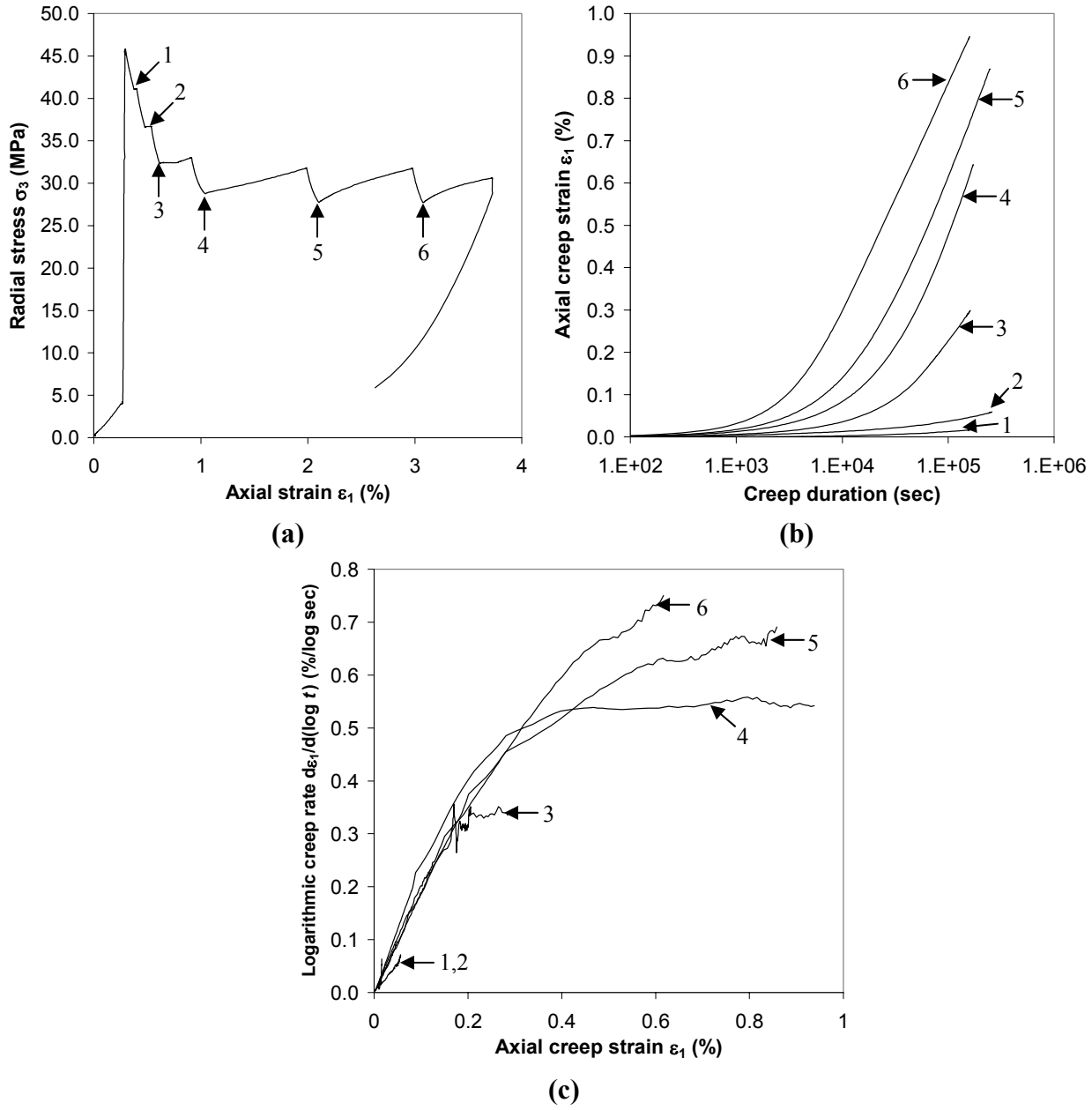

Figure 3.38. K_0 compression tests with σ_1-constant creep phases reveals variability in creep behavior. Six creep phases performed under the same axial stress and different radial stresses indicate that radial stresses increase during creep as shown in (a). Each phase results in a different logarithmic strain rate, as shown in (b) and (c). Data shown is for South Arne field (File 407). Data shown is from DGI (2000).

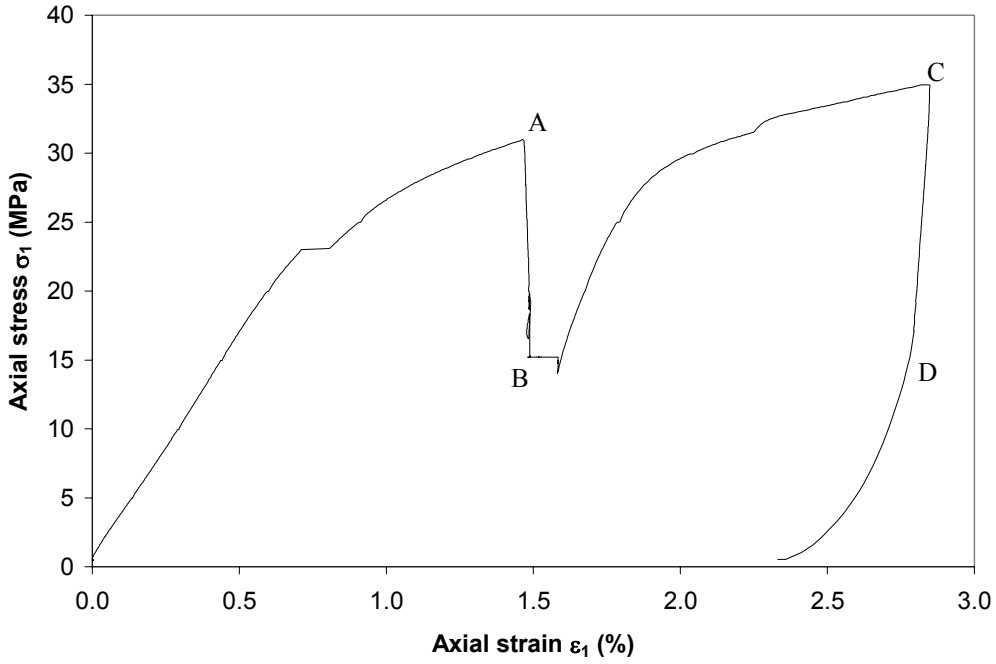

(a)

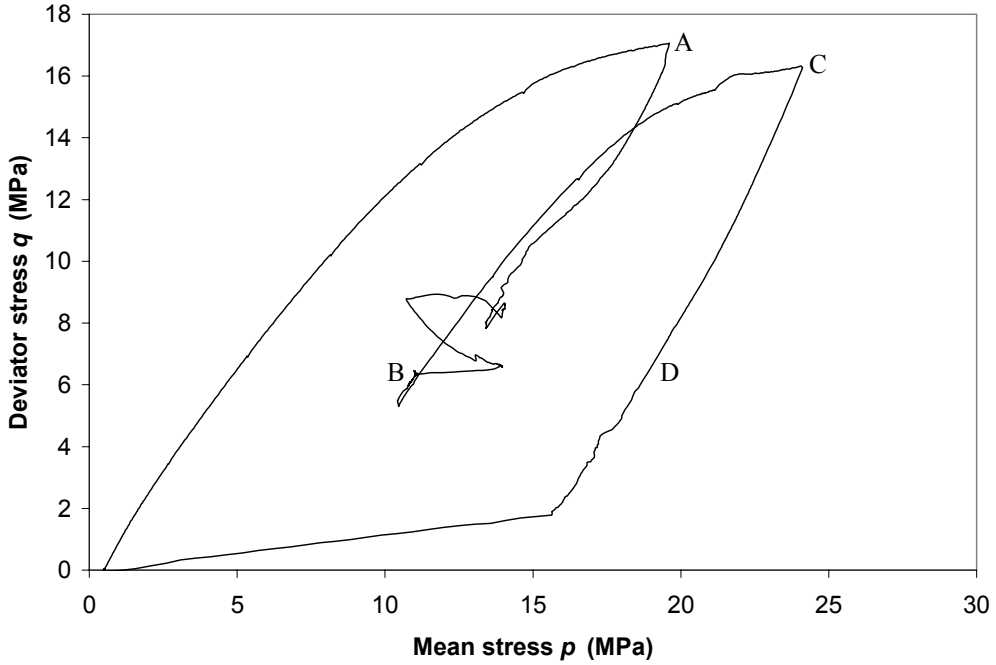

(b)

Figure 3.39. K_0 compression tests with stress relaxation phases shows aspects of creep behavior. Segments A-B and C-D are stress relaxation phases. During these test phases, the axial stresses decrease, resulting in the stress-strain behavior shown in (a) and the stress path behavior shown in (b). Data shown is for Valhall chalk (File 500). Data shown is from DGI (2003).

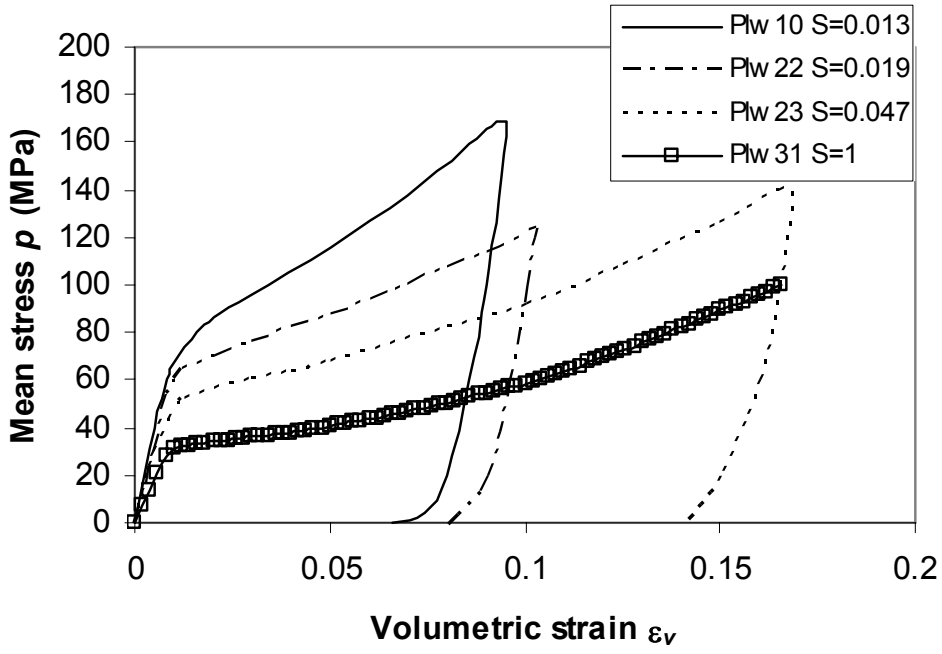

Figure 3.40. Stress-strain curves for hydrostatic compression tests performed on Pietra Lecesse outcrop chalks with different degrees of water saturation show that isotropic preconsolidation stress and elastic modulus decrease as water saturation increases (Papamichos et al., 1997).

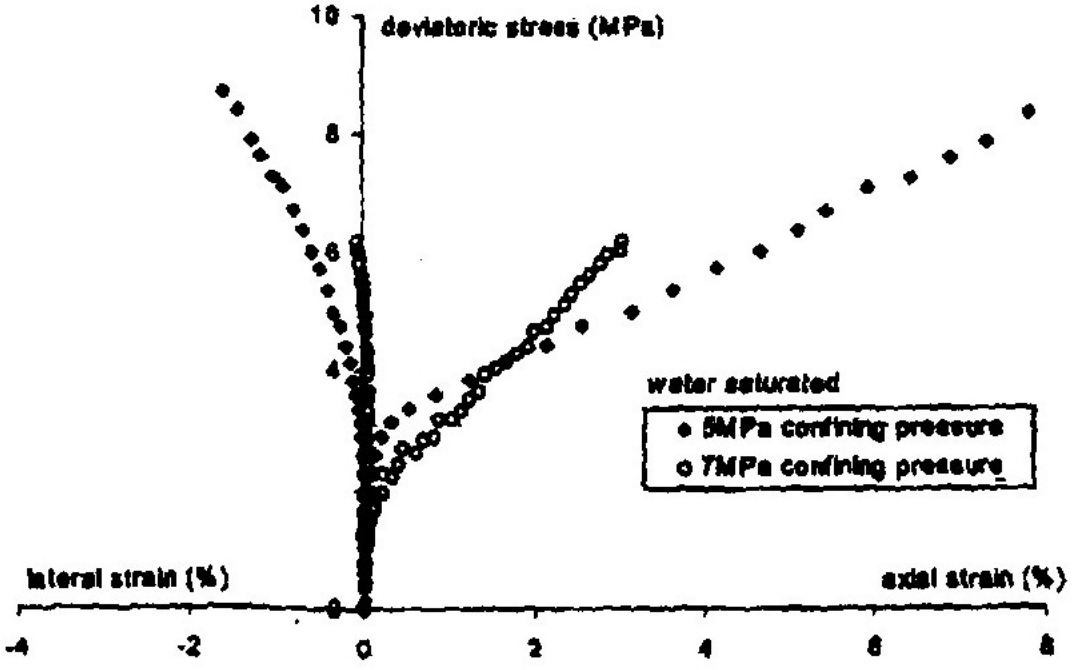

Figure 3.41. Stress-strain curves for water-saturated chalks subjected to triaxial compression at high mean stress *p* exhibit similar behavior to oil-saturated chalk, but yield stress and elastic modulus decrease; compare with Figure 3.14 (Homand and Shao, 2000).

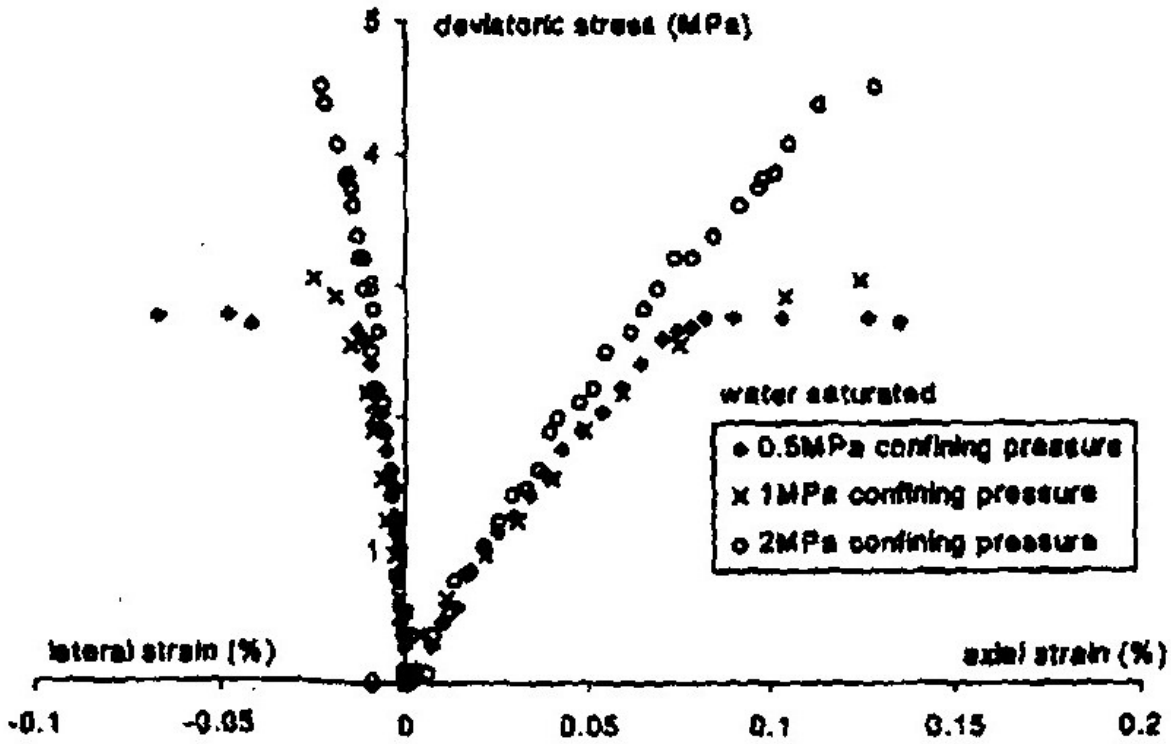

Figure 3.42. Stress-strain curves for water-saturated chalks subjected to triaxial compression at low mean stress *p* exhibit similar behavior to oil-saturated chalk, but yield stress and elastic modulus decrease; compare with Figure 3.23 (Homand and Shao, 2000).

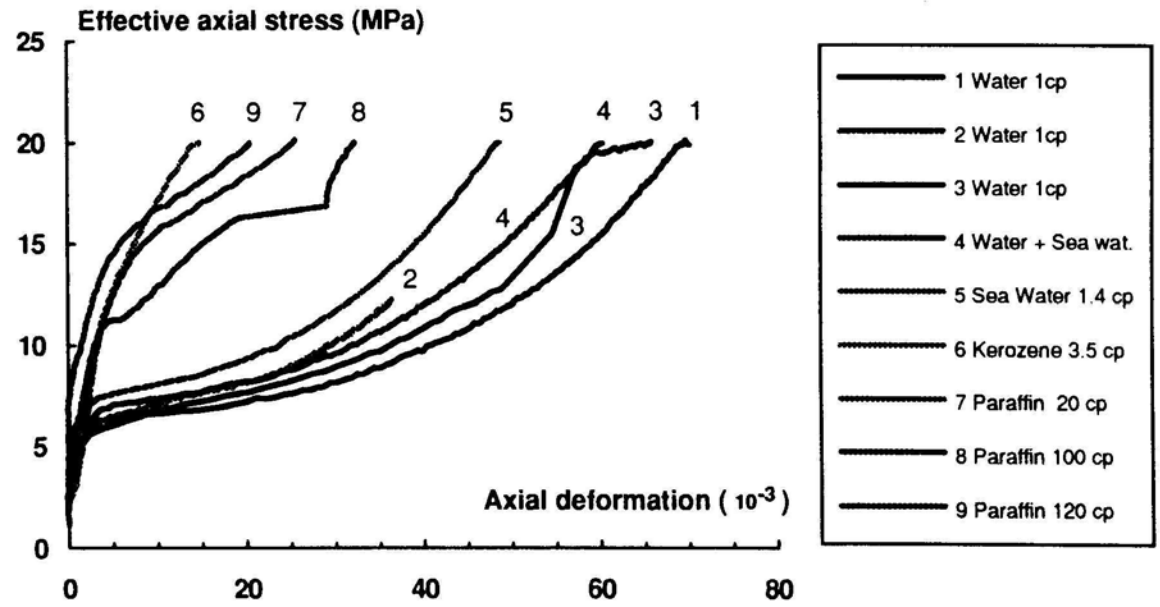

(a)

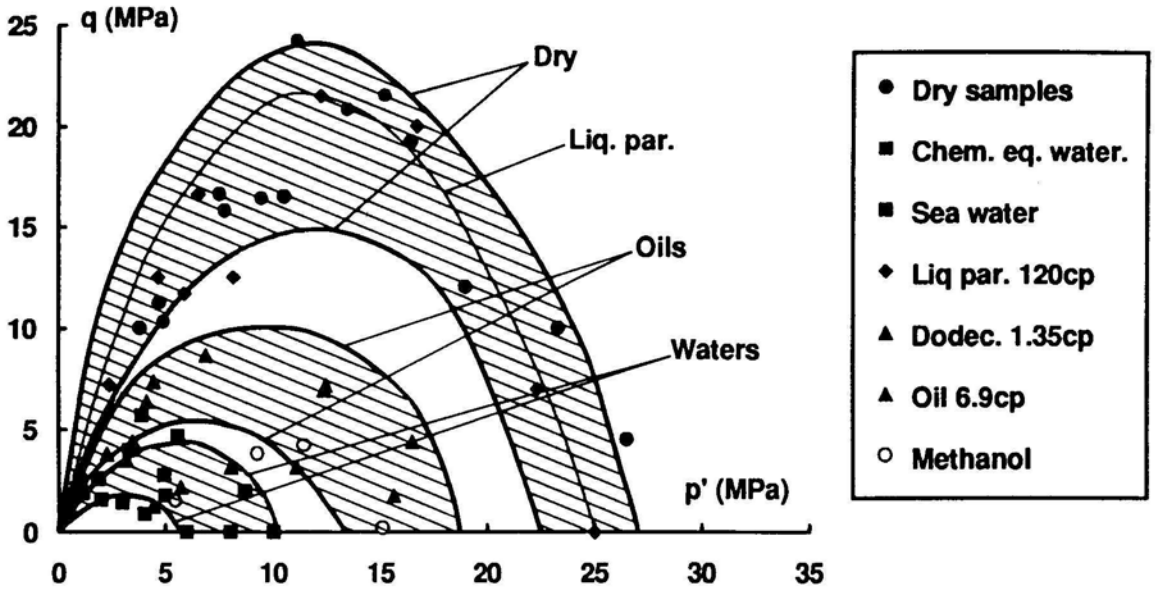

(b)

Figure 3.43. Water-saturated samples of Haubourdin chalk are weaker than oil-saturated samples, as shown in (a) stress-strain curves; (b) stress space. Figure (b) also shows that dry chalk is strongest of all in both shear and pore collapse (Schroeder and Shao, 1996).

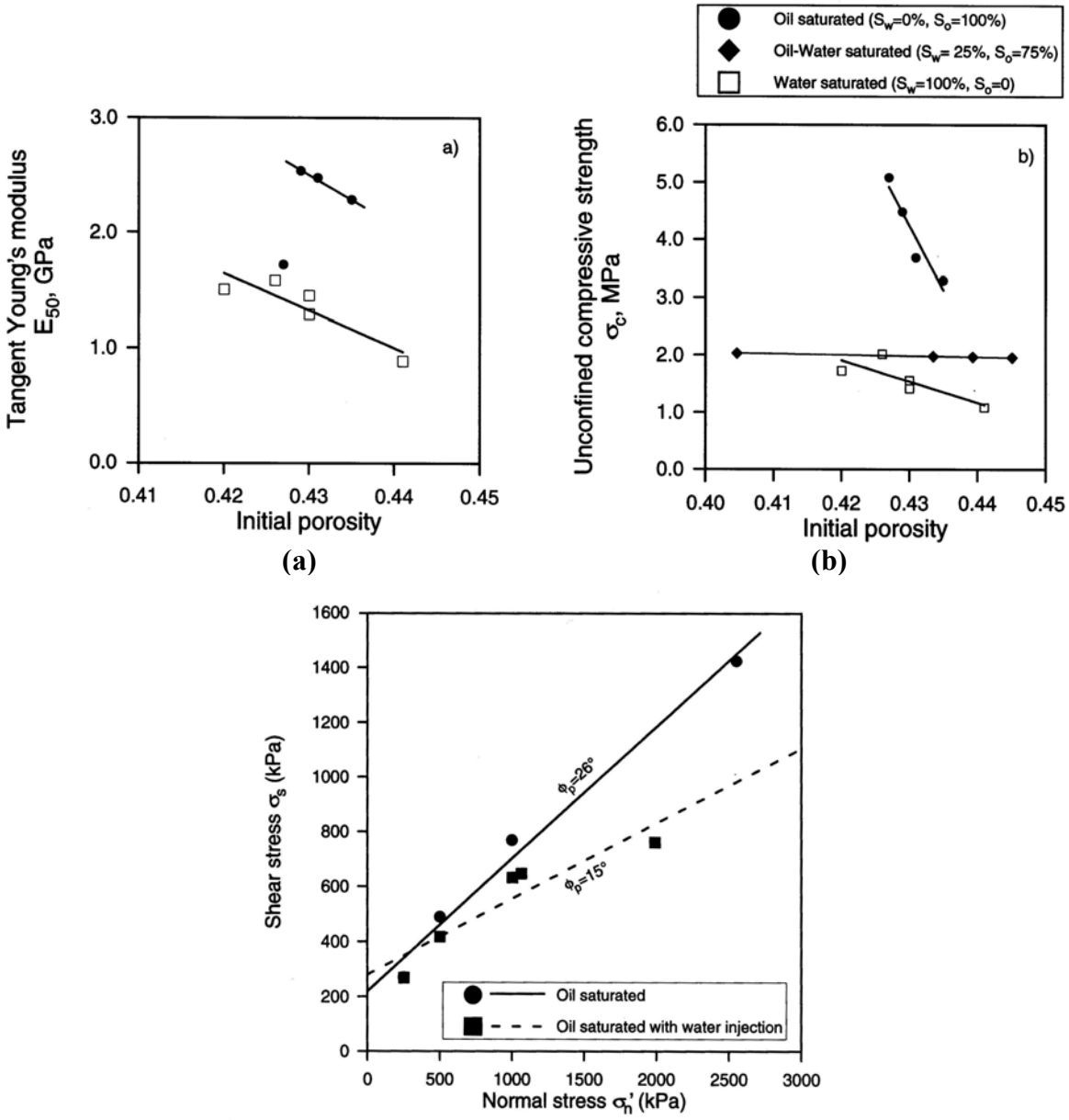

Figure 3.44. Fracture surfaces on Lagerdorf chalk are stiffer and stronger when oil-saturated than when water-saturated, as shown by difference in (a) elastic modulus; (b) unconfined compressive strength; (c) shear strength (Gutierrez et al., 2000).

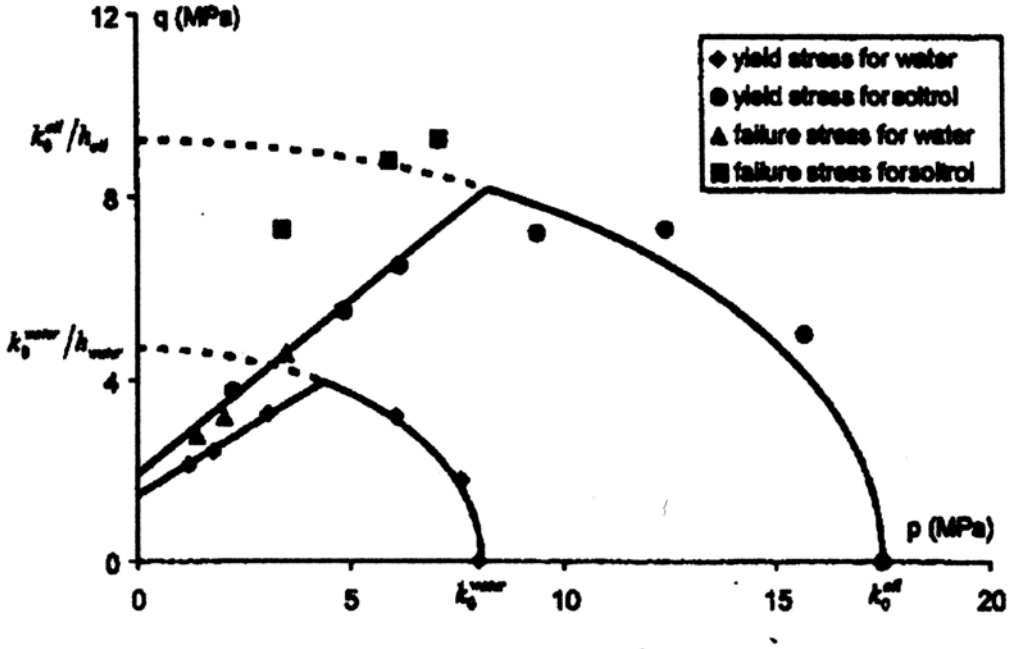

Figure 3.45. Initial yield surface for oil-saturated Lixhe chalk shows much greater initial strength than that for water-saturated chalk, in pore collapse and in shear (Homand and Shao, 2000).

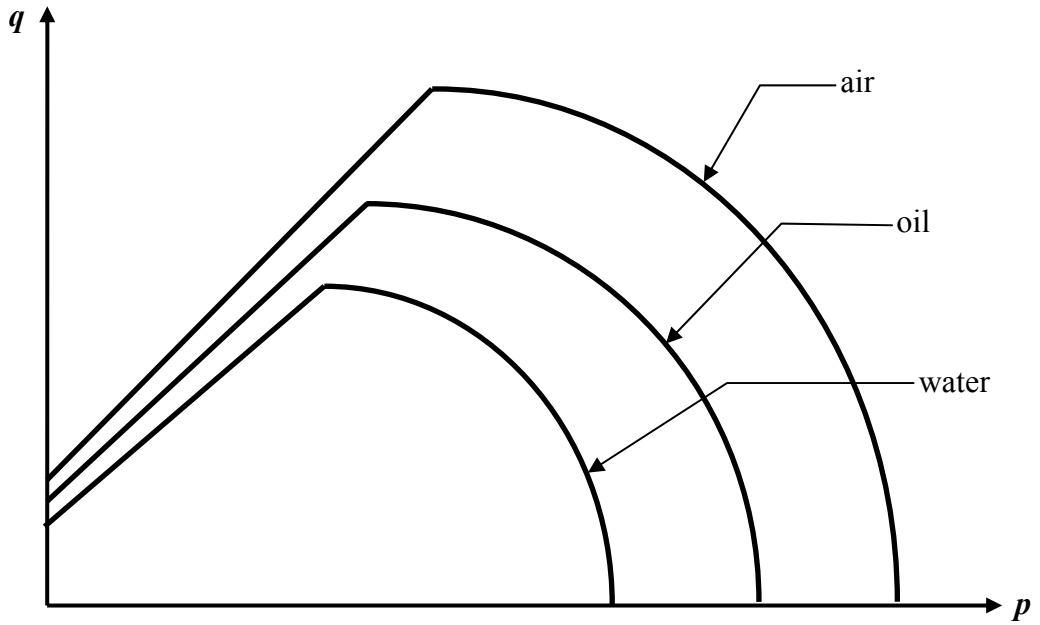

Figure 3.46. Typical initial yield surfaces for chalk with various saturating fluids: air, oil, and water indicate relative strengths.

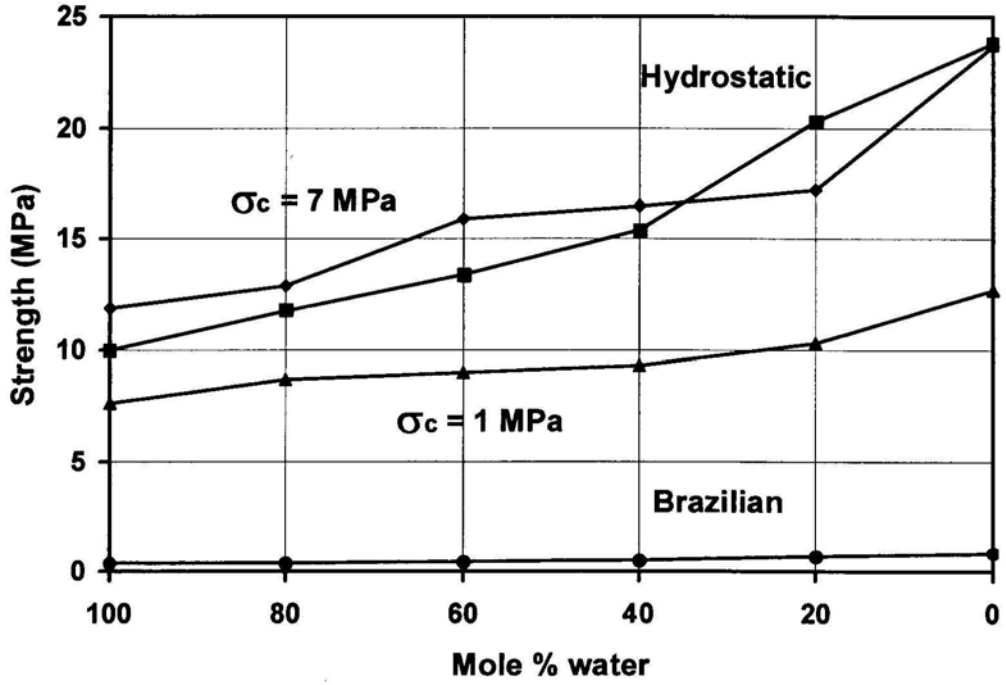

(a)

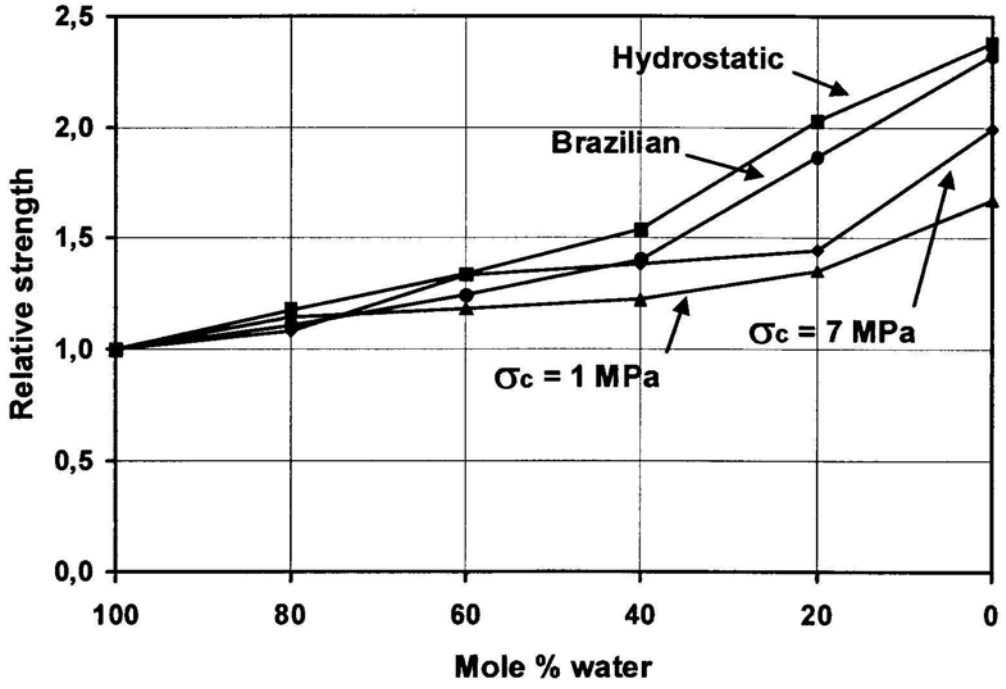

(b)

Figure 3.47. Dependence of chalk strength on pore fluid may be related to water content of pore fluid or to water activity. Lixhe chalk shows strength dependence for all yield mechanisms from results of hydrostatic compression, triaxial compression, and Brazilian tests. Raw strengths shown in (a); normalized strengths shown in (b) (Risnes et al., 2004).

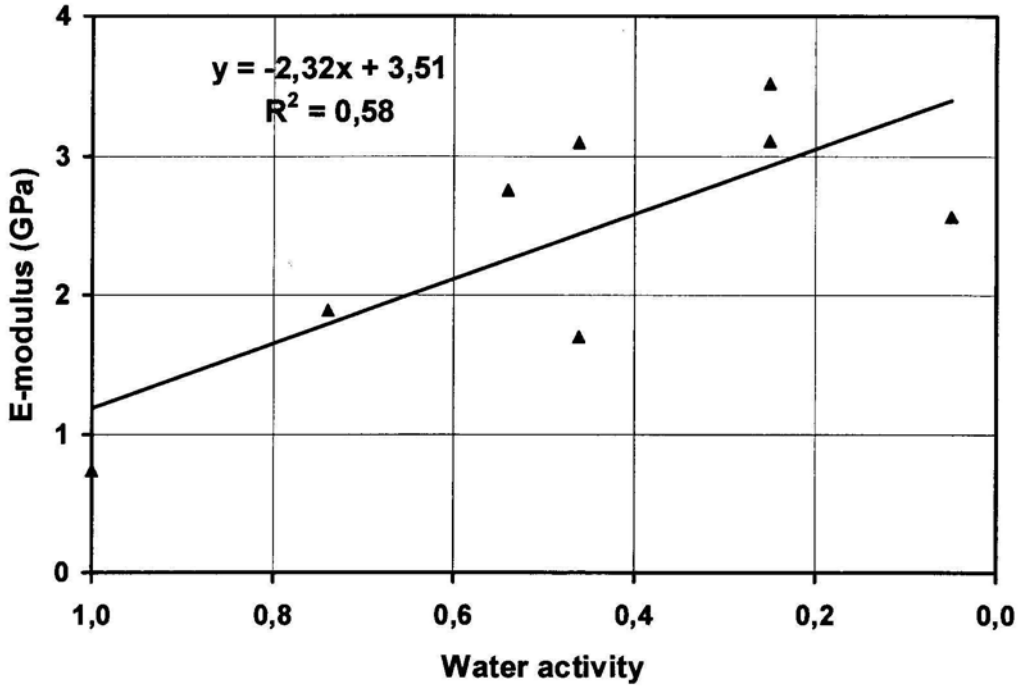

(c)

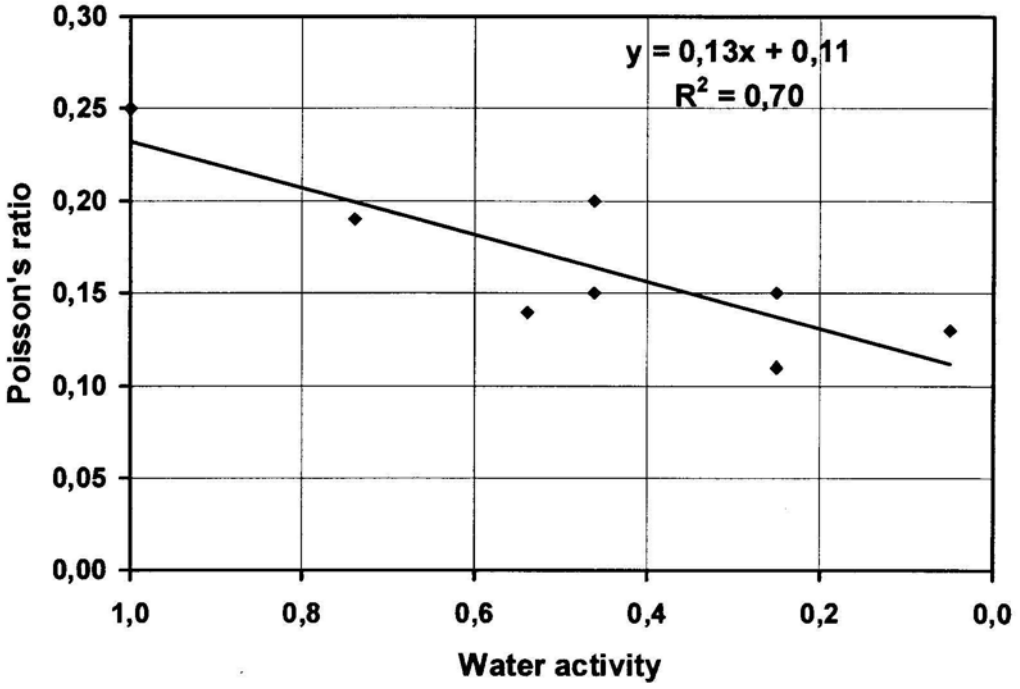

(d)

Figure 3.47(continued). Lixhe chalk also shows stiffness dependence on pore fluid, as shown by variability in (a) elastic modulus; (b) Poisson's ratio (Risnes et al., 2004).

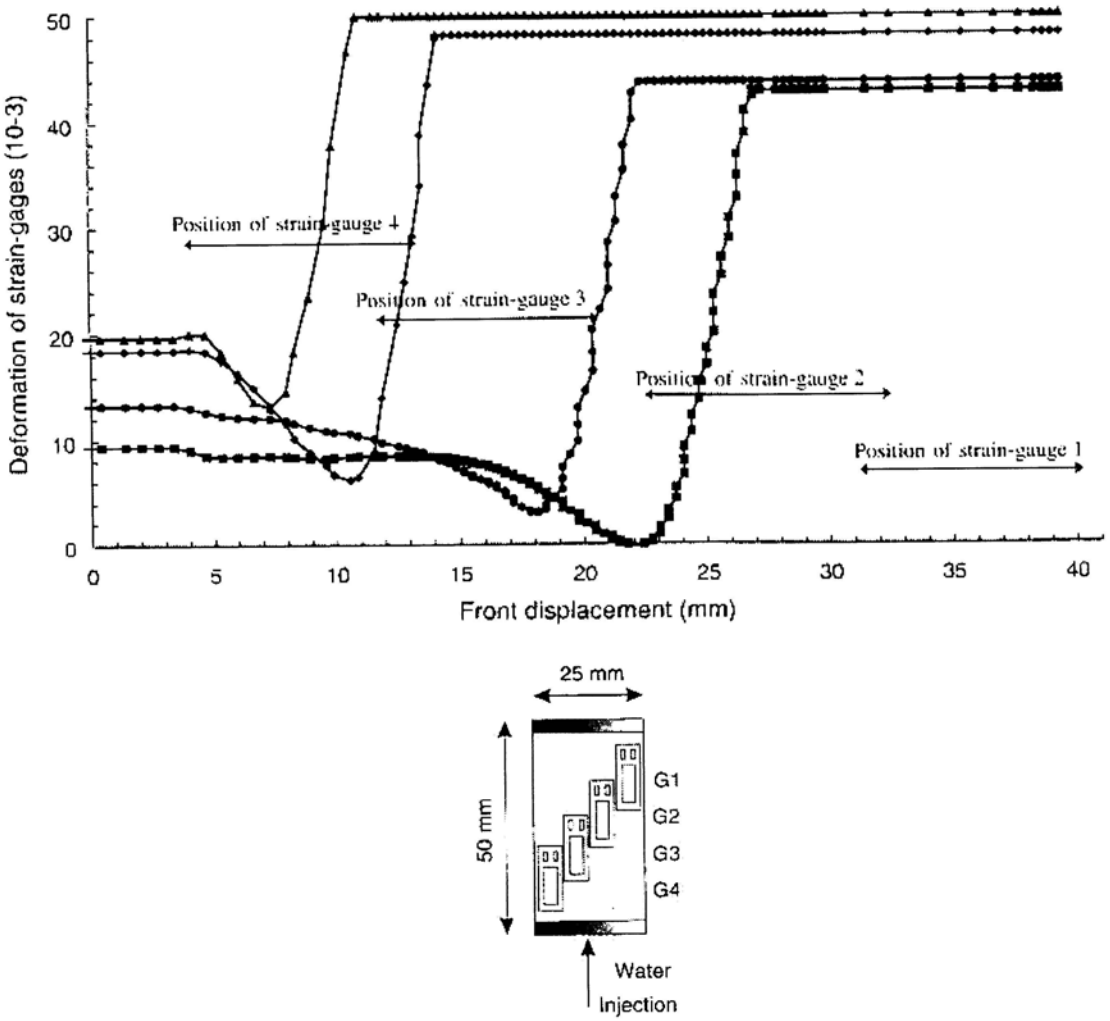

Figure 3.48. Strain gauges move in sequence as water front advances, indicating that axial strains and plastic behavior are affected immediately by change in pore fluid. Strain gauge positions shown in lower figure (Schroeder et al., 1998).

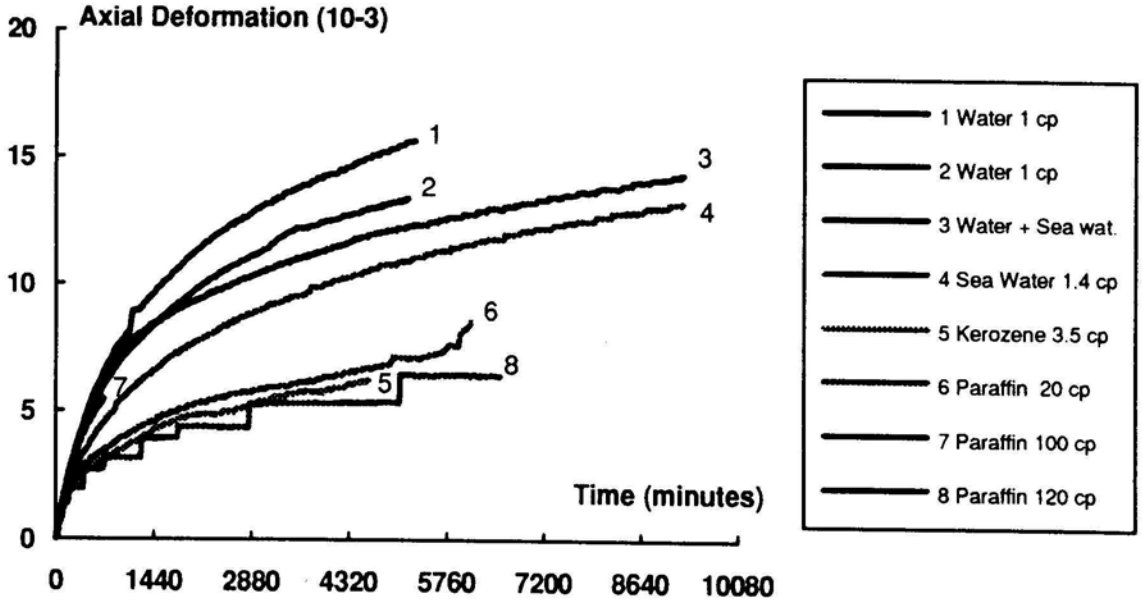

Figure 3.49. Creep testing of Haubourdin chalk shows that time-dependent behavior is also dependent on pore fluid. Creep rate of water-saturated chalk is greater than that of oil-saturated chalk (Schroeder and Shao, 1996).

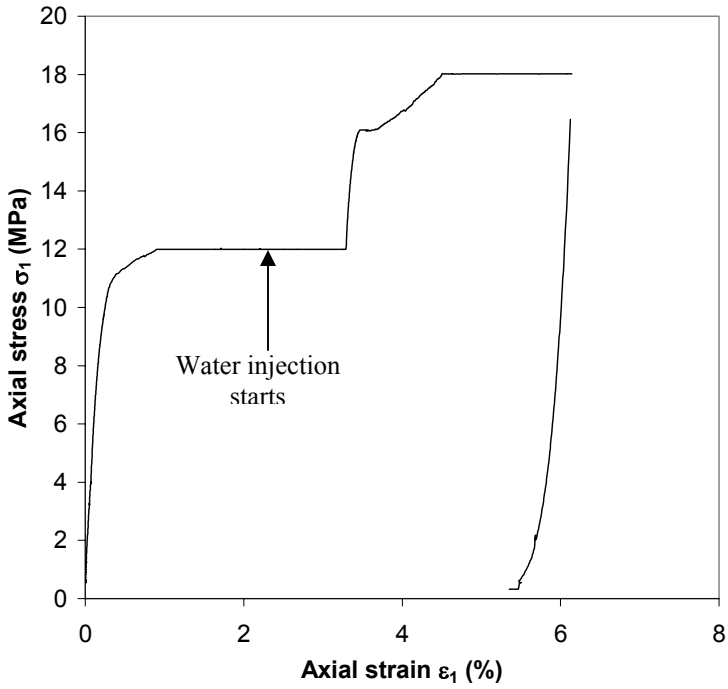

(a)

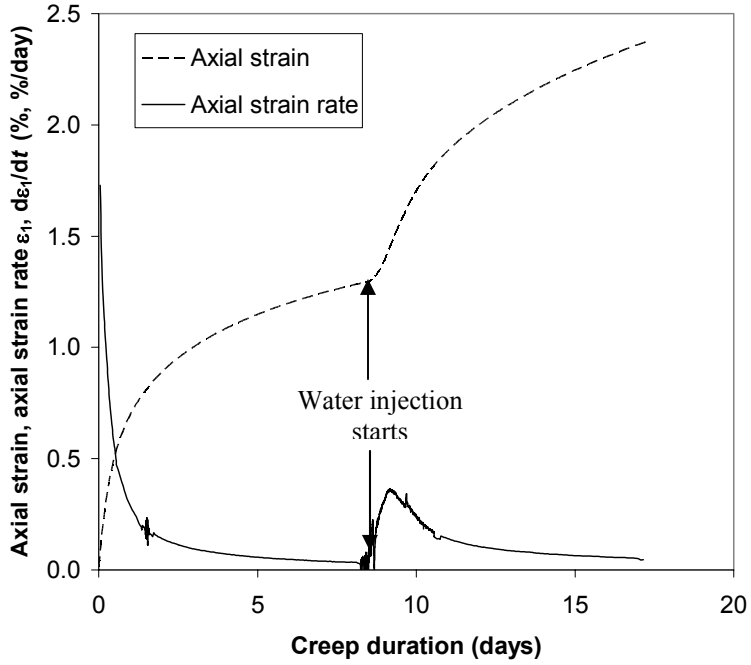

(b)

Figure 3.50. Replacement of oil as pore fluid by water (a) during creep phase of K_0 compression test changes time-dependent behavior of chalk. (b) Creep rate increases suddenly when water injection starts. Data shown is for Stevns Klint chalk (File 461).

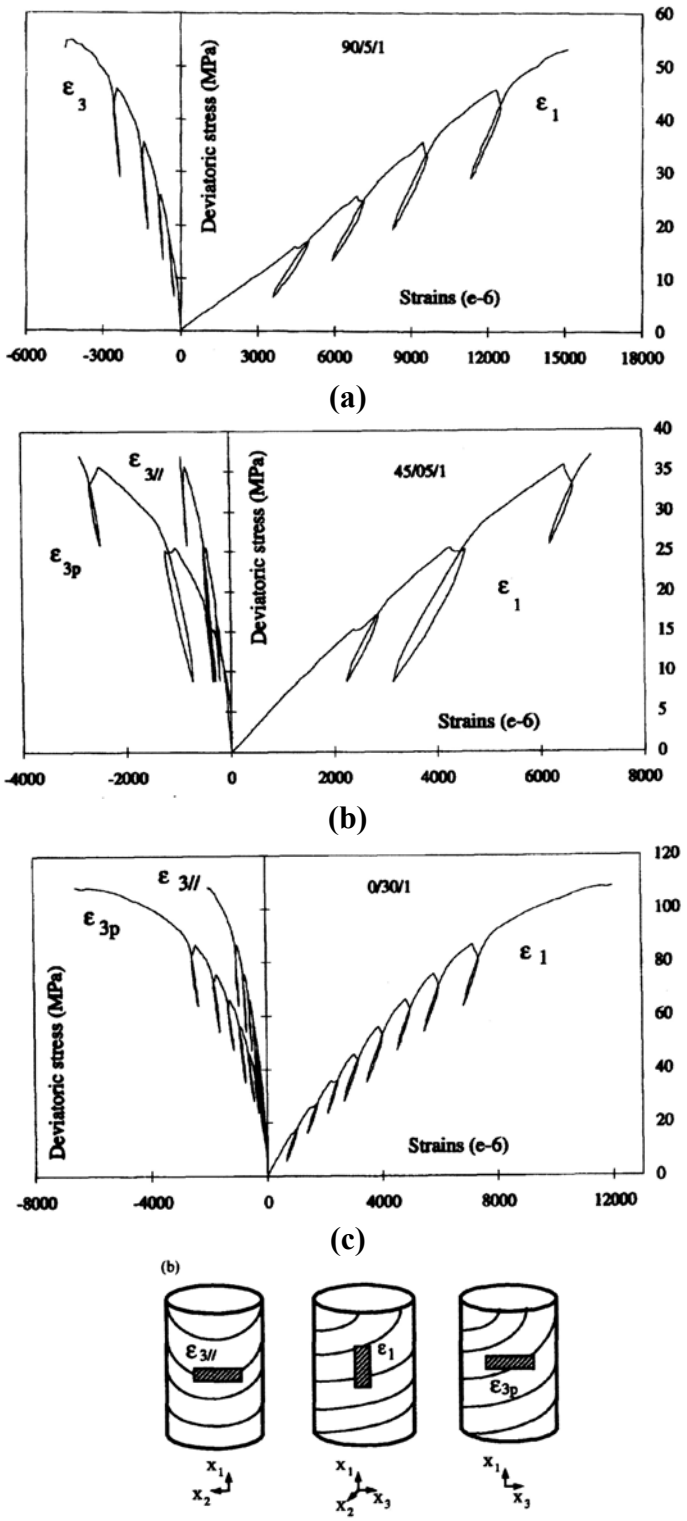

Figure 3.51. Orientation of major compressive stress relative to bedding planes in triaxial compression influences stress-strain behavior for Tournemire shale. Stress-strain curves are shown for (a) σ_1 perpendicular to bedding; (b) σ_1 oblique to bedding; (c) σ_1 parallel to bedding. Figure (d) shows position of strain gauges (Niandou et al., 1997).

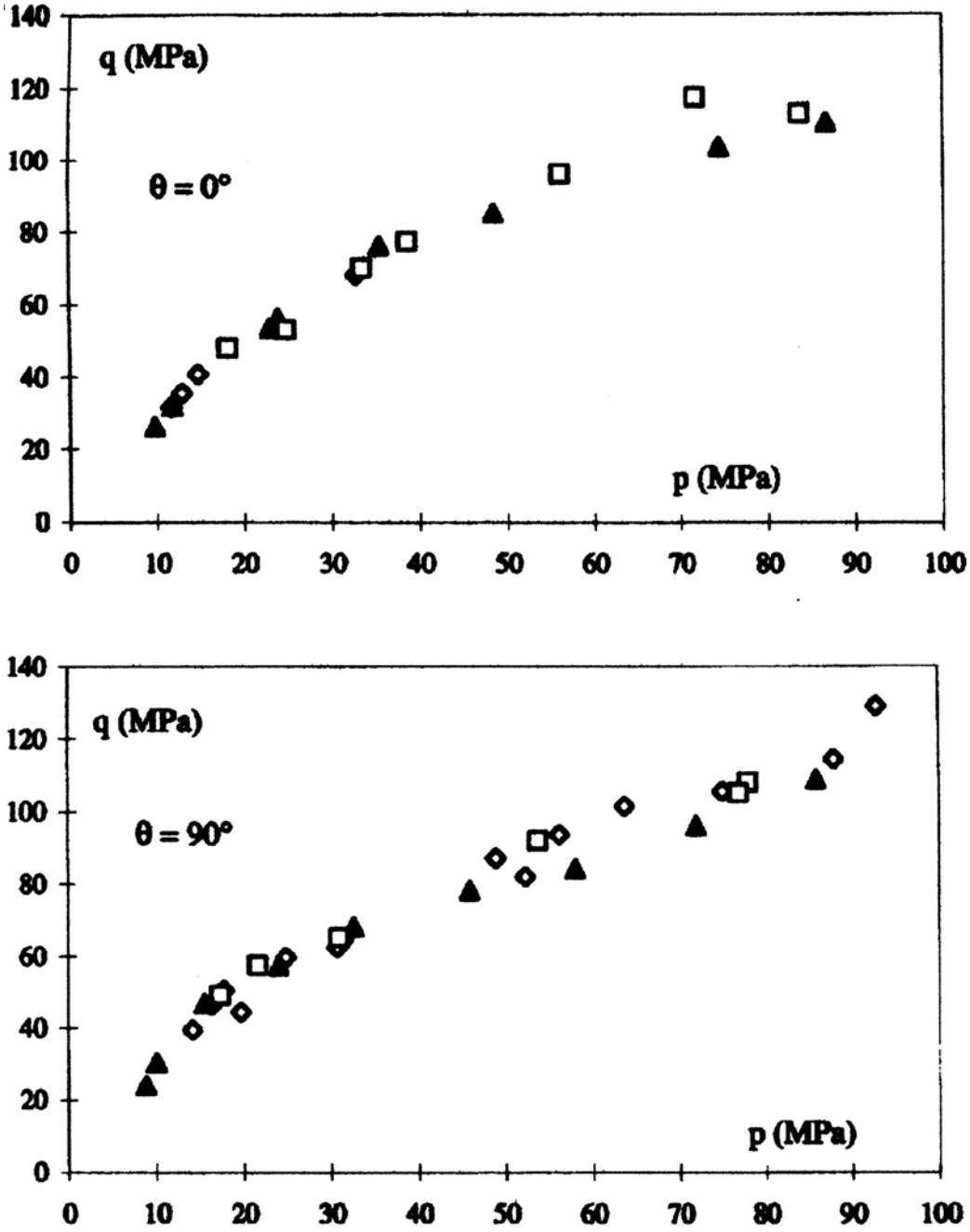

Figure 3.52. Shear strength in triaxial compression is relatively independent of bedding direction for Tournemire shale under high confining stress. The same failure shear stress ratio is observed if σ_1 is (a) perpendicular to bedding; (b) parallel to bedding (Niandou et al., 1997).

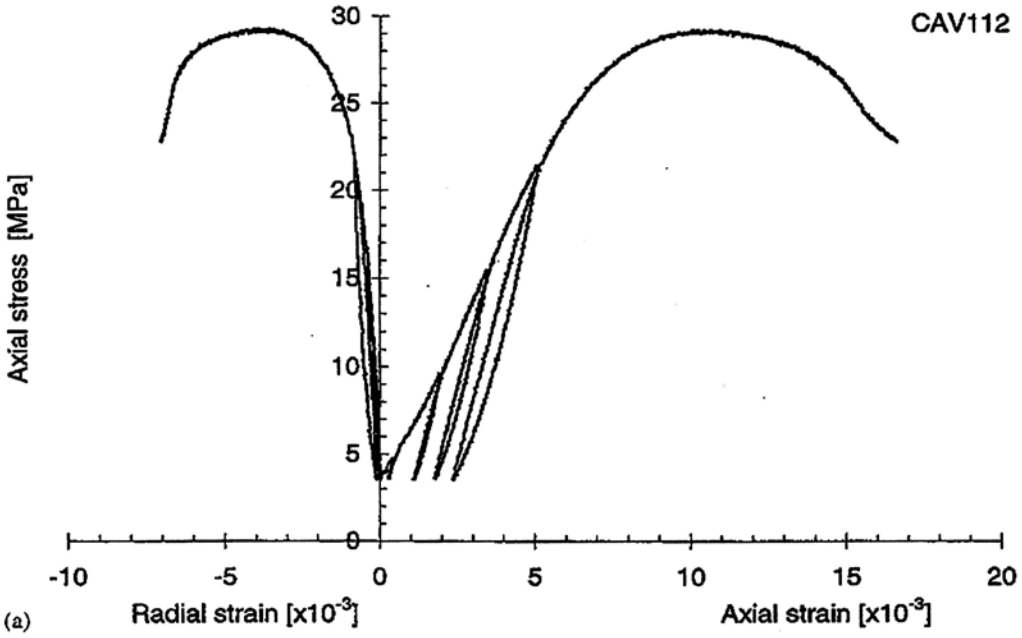

(a)

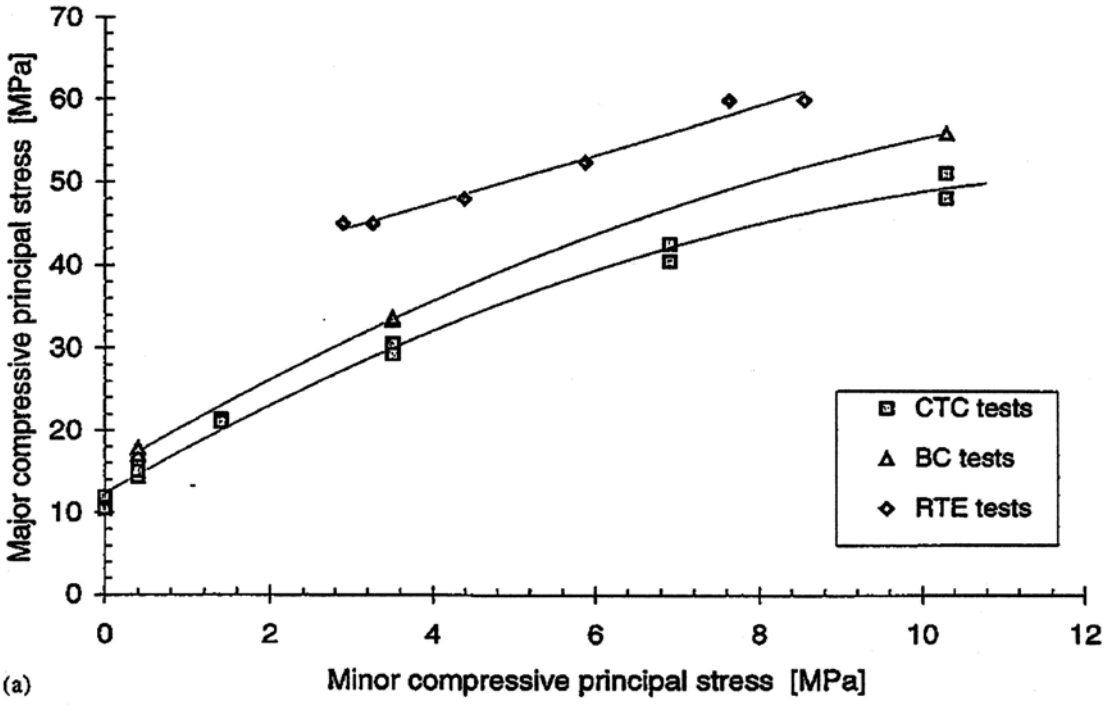

(b)

Figure 3.53. (a) Repeated loading-unloading cycles indicate that inelastic strains accumulate in Red Wildmoor sandstone long before shear failure. (b) Magnitude of intermediate principal stress influences shear strength, as shown by relative principal stress ratios at failure in triaxial compression, triaxial extension, and biaxial plane strain compression (Papamichos et al., 2000).

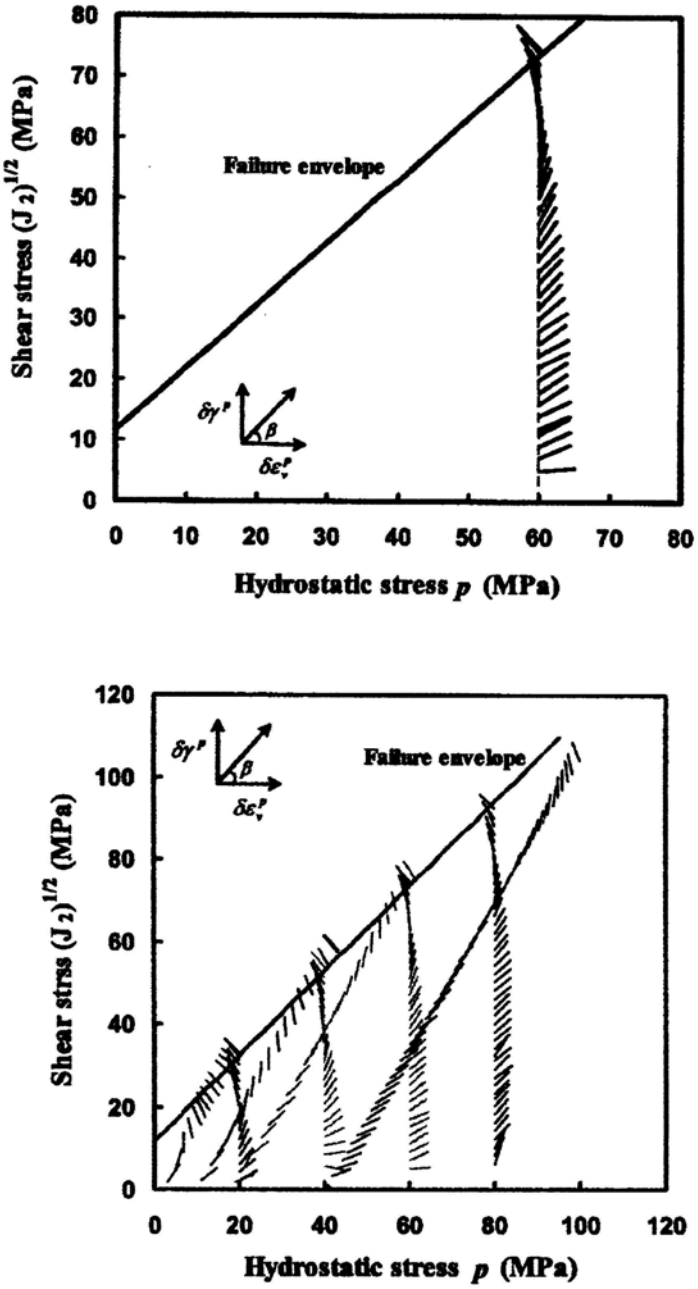

Figure 3.54. Plastic flow direction in Mushan sandstone varies as shearing proceeds. Plastic flow is initially contractant, but becomes less contractant and eventually dilatant as shear strength is mobilized. Results are shown for (a) a single pure shear test; (b) a suite of pure shear and drained triaxial compression tests (Jeng et al., 2002).

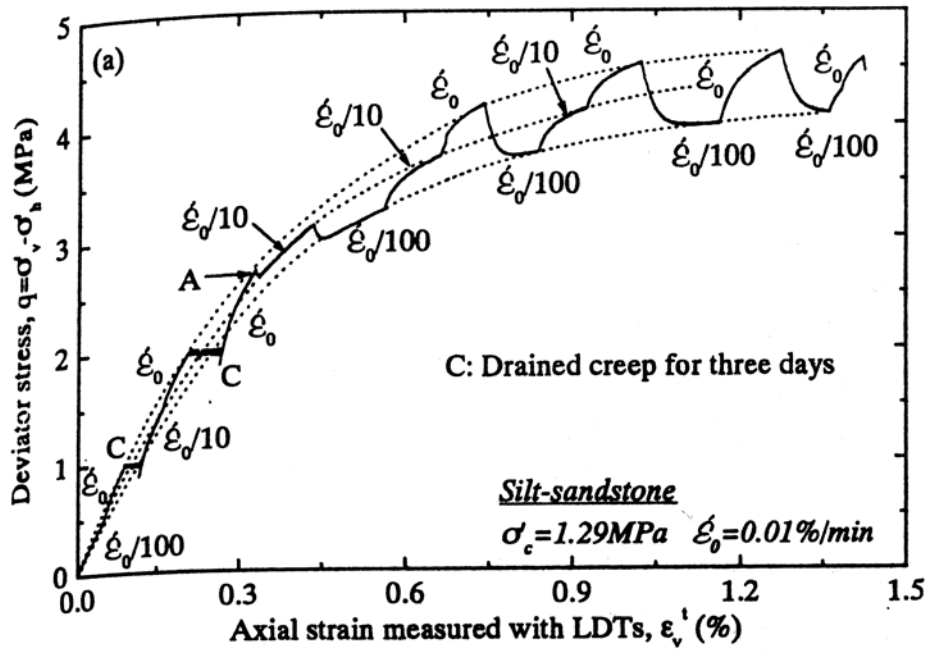

(a)

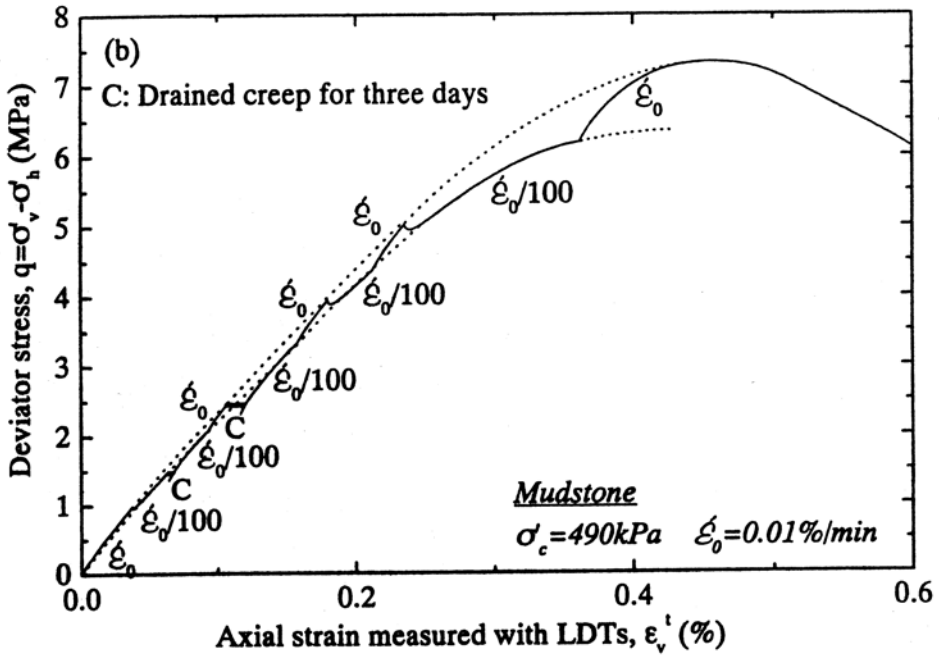

(b)

Figure 3.55. Soft rocks exhibit regular behavior under various strain rates including creep phases. A "backbone" stress-strain curve exists for each independent loading rate. Upon changing the loading rate, the stress-strain behavior quickly approaches the backbone curve corresponding to the new loading rate. Results for (a) silt-sandstone and (b) mudstone members of the Kazusa group show this trend (Hayano et al., 2001).

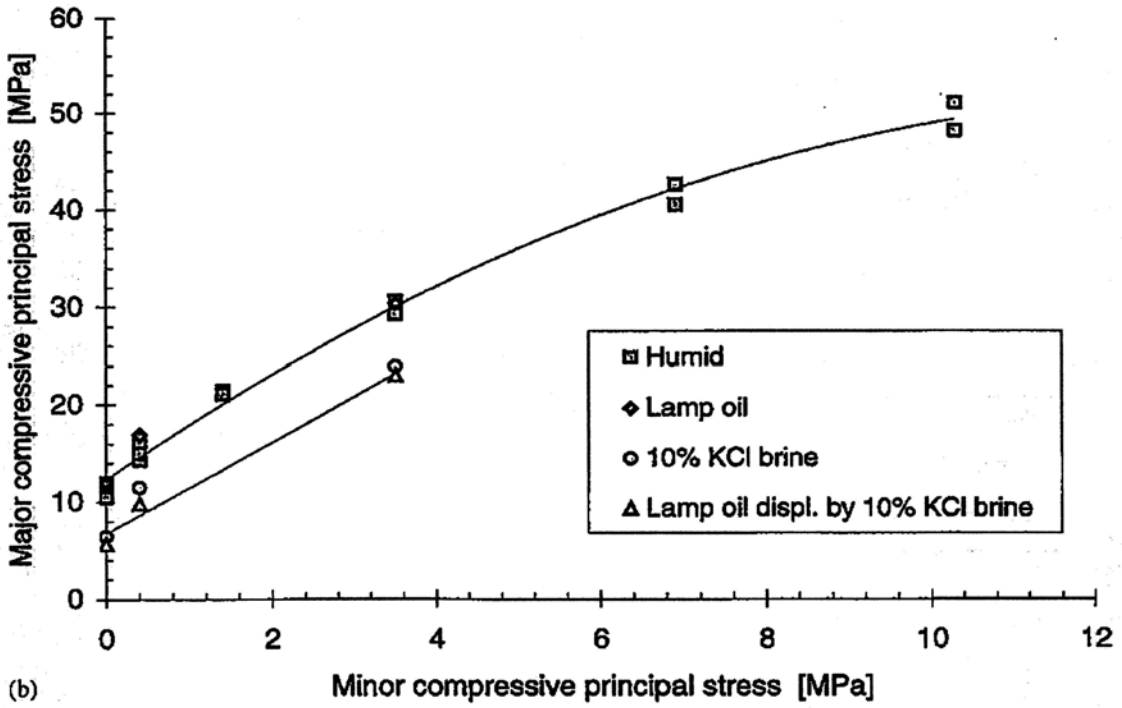

Figure 3.56. Oil-saturated Red Wildmoor sandstone exhibits higher shear strength than water-saturated sandstone in triaxial compression (Papamichos et al., 2000).